DEVELOPMENT OF 2D MOLYBDENUM DISULFIDE BASED NO_2 GAS SENSOR

A Thesis Submitted

In Partial Fulfilment of the Requirements
for the Degree of

DOCTOR OF PHILOSOPHY

by

RAMESH KUMAR
(2K20/PHDAP/504)

Under the Supervision of

PROF. VINOD SINGH	**PROF. MAHESH KUMAR**
Professor	**Professor**
Department of Applied Physics	**Department of Electrical Engineering**
Delhi Technological University	**Indian Institute of Technology Jodhpur**
(Supervisor)	**(Joint-Supervisor)**

Department of Applied Physics
DELHI TECHNOLOGICAL UNIVERSITY
(Formerly Delhi College of Engineering)
Shahbad Daulatpur, Main Bawana Road, Delhi-110042, India

MAY, 2026

With deep love & gratitude, I dedicate this work to my beloved family

Acknowledgements

I would like to express my sincere gratitude to all those whose support, guidance, and encouragement have played a vital role in shaping my Ph.D. journey and in the completion of this work.

Foremost, I extend my deepest respect and heartfelt appreciation to my supervisor, Head of the Department of Applied Physics and DRC Chairperson, ***Prof. Vinod Singh***, for his exceptional mentorship, insightful scientific guidance, and constant encouragement. His patience, clarity of thought, and unwavering confidence in my abilities have been pivotal in my development as a researcher. I remain truly grateful for his continuous support at every stage of this thesis.

I am equally thankful to my co-supervisor, ***Prof. Mahesh Kumar***, for his valuable insights, constructive suggestions, and academic rigor, which have greatly enhanced the quality of this research.

I also express my sincere respect to ***Prof. Prateek Sharma***, Vice-Chancellor of DTU. I am grateful to the experts and members of the SRC and DRC for their time, careful evaluation, and constructive feedback, which significantly strengthened the direction and depth of my research.

I am deeply indebted to my father ***Mr. Daleep Singh*** and mother ***Mrs. Saroj Devi*** for their unconditional love, constant support, and invaluable guidance at every stage of my life. Their blessings have always been my greatest strength and have shaped me into the person I am today.

I would also like to extend my heartfelt thanks to my wife ***Mrs. Maya***, whose patience, understanding, and endless encouragement have been a pillar of strength during this journey. Her support has helped me overcome many challenges and stay focused on my goals. My loving daughter ***Jaahanvi*** and son ***Dhurav Kulriya*** have been a constant source of happiness and inspiration, bringing balance and joy to my life even during the most demanding times.

I am equally grateful to my father-in-law ***Mr. Mahender Singh*** and mother-in-law ***Mrs. Krishna Devi*** for their continuous encouragement, care, and belief in my abilities. Their moral support has played a significant role in helping me stay motivated throughout this work.

I would like to thank my brothers ***Aaryan and Aarav*** for his unwavering support, encouragement, and for always standing by me in times of need.

A special and heartfelt thanks to ***Prof. Pawan Kulriya*** for his invaluable guidance, insightful suggestions, and constant encouragement throughout this research work. His depth of knowledge, willingness to help, and constructive feedback have greatly enriched the quality of this thesis. I am especially grateful for his patience, for always

being available to discuss ideas, and for providing clarity whenever I faced difficulties. His motivation and belief in my work gave me the confidence to move forward during challenging phases. I truly appreciate the time and effort he invested in guiding me, which has been instrumental in shaping this research and bringing it to successful completion.

I gratefully acknowledge ***Delhi Technological University (DTU)*** for providing the financial assistance and academic environment necessary to carry out this work. I extend my gratitude to all faculty and staff members of the Department for their cooperation and support.

I would like to express my sincere gratitude to my seniors ***Dr. Priya Pardeep Kumar, Dr. Umang, Dr. Kailash Garg, and Dr. Naima Tyagi*** for their constant support, insightful scientific discussions, and valuable guidance. Their encouragement has played a significant role in shaping my academic journey.

I extend my heartfelt thanks to my current lab group ***Mr. Ashok Kumar, Mr. Jasveer, Mr. Hemant Kumar Arora, Mr. Bharat Bhushan, Mr. Praveen Kumar, Mr. Surya Partap Singh, Mr. Hemendra Singh, Ms. Nisha and Mr. Aditya*** for their cooperation, shared responsibilities, and for fostering a positive environment that made the laboratory a space of learning and camaraderie.

I would like to gratefully acknowledge the wonderful companionship and invaluable support of my dear friends ***Mr. Harendra Mor, Dr. Sunil Kumar, Mr. Aditya Sharma, Mr. Subham Sharma, Dr. Priyanka, Dr. Aneesha, Mr. Anurag Sharma, Mr. Lokesh Ahalawat, Dr. Vikas Sangwan, and Dr. Ramesh Bishnoi***. Their constant encourage ment, thoughtful discussions, and readiness to help have been a great source of strength throughout my journey.

I would also like to acknowledge all my teachers, mentors, and well-wishers who have directly or indirectly contributed to my academic journey. Their knowledge, advice, and encouragement have been invaluable.

Finally, I am thankful to everyone who has been a part of this journey, whether through support, guidance, or encouragement. This achievement would not have been possible without all of you.

Ramesh Kumar

2K20/PHDAP/504

DELHI TECHNOLOGICAL UNIVERSITY

(Formerly Delhi College of Engineering)
Shahbad Daulatpur, Main Bawana Road, Delhi-42

CANDIDATE’S DECLARATION

I **Ramesh Kumar (2K20/PHDAP/504)** hereby certify that the work which is being presented in the thesis entitled “**Development of 2D Molybdenum Disulfide Based NO_2 Gas Sensor**” in partial fulfillment of the requirements for the award of the Degree of Doctor of Philosophy, submitted in the Department of Applied Physics, Delhi Technological University is an authentic record of my own work carried out during the period from **January 2021** to **May 2026** under the supervision of **Prof. Vinod Singh**, Department of Applied Physics, Delhi Technological University and **Prof. Mahesh Kumar,** Dept. of Electrical Engineering, Indian Institute of Technology, Jodhpur**.**

The matter presented in the thesis has not been submitted by me for the award of any other degree of this or any other Institute.

Candidate's Signature

This is to certify that the student has incorporated all the corrections suggested by the examiners in the thesis and the statement made by the candidate is correct to the best of our knowledge.

Prof. Vinod Singh	**Prof. Mahesh Kumar**
(Supervisor)	(Joint-Supervisor)

……………………..

(External Examiner)

DELHI TECHNOLOGICAL UNIVERSITY
(Formerly Delhi College of Engineering)
Shahbad Daulatpur, Main Bawana Road, Delhi-42

CERTIFICATE BY THE SUPERVISOR(s)

Certified that **Ramesh Kumar (2K20/PHDAP/504)** has carried out his research work presented in this thesis entitled "**Development of 2D Molybdenum Disulfide Based NO_2 Gas Sensor**" for the award of **Doctor of Philosophy** from Department of Applied Physics, Delhi Technological University, Delhi, under our supervision. The thesis embodies results of original work, and studies are carried out by the student himself and the contents of the thesis do not form the basis for the award of any other degree to the candidate or to anybody else from this or any other University/Institution.

Prof. Vinod Singh	**Prof. Mahesh Kumar**
(Supervisor) Professor and Head of Department Department of Applied Physics Delhi Technological University	(Jt. Supervisor) Professor Department of Electrical Engineering Indian Institute of Technology Jodhpur

Date:

Abstract

The rapid increase in environmental pollution and industrial activities has led to a growing demand for efficient, reliable, and cost-effective gas sensing technologies. Toxic gases such as nitrogen dioxide (NO_2) and hydrogen (H_2) pose significant risks to human health, environmental safety, and industrial operations. In this context, the present thesis focuses on the development and investigation of nanostructured molybdenum disulfide (MoS_2) thin films for gas sensing applications, with particular emphasis on understanding their structural properties and sensing behavior toward NO_2 and H_2 gases.

The research begins with the synthesis of MoS_2 thin films using a combination of electron beam evaporation and chemical vapor deposition (CVD) techniques. Molybdenum (Mo) thin films of varying thicknesses were initially deposited on suitable substrates and subsequently sulfurized under controlled conditions to obtain high-quality MoS_2 layers. Systematic optimization of synthesis parameters such as film thickness, annealing temperature, and sulfurization temperature was carried out to achieve uniform, crystalline, and reproducible thin films. Among the different samples studied, the 20 nm thick MoS_2 films exhibited superior crystallinity, structural stability, and surface uniformity, making them suitable for gas sensing applications.

Comprehensive structural and morphological characterization was performed using X-ray diffraction (XRD), Raman spectroscopy, field emission scanning electron microscopy (FESEM), and atomic force microscopy (AFM). The XRD analysis confirmed the formation of polycrystalline hexagonal-phase MoS_2, while Raman studies validated the presence of characteristic vibrational modes corresponding to in-plane and out-of-plane lattice vibrations. Surface morphology analysis revealed the formation of nanosheet and flower-like structures, providing a high surface-to-volume ratio and abundant active sites for gas adsorption.

A significant contribution of this work is the investigation of MoS_2–hydrogen interaction using in-situ X-ray diffraction. This approach enabled real-time monitoring of structural changes in MoS_2 under controlled hydrogen gas environments, eliminating sample-to-sample variations. The study revealed that exposure to hydrogen gas leads to noticeable changes in diffraction peak intensity, indicating structural modifications and possible lattice strain effects. These findings provide deeper insights into the interaction mechanisms between hydrogen molecules and layered MoS_2 structures.

Furthermore, the gas sensing performance of MoS_2 thin films toward NO_2 gas was systematically investigated as a function of operating temperature and gas concentration. The fabricated sensor exhibited n-type semiconducting behavior, with an increase in electrical resistance upon exposure to the oxidizing NO_2 gas due to electron withdrawal. The sensing response improved significantly with increasing temperature, achieving optimal performance at 150 °C. The sensor demonstrated a

maximum response of approximately 14.2% at 20 ppm concentration, along with a response time of about 102 seconds and a recovery time of 94 seconds. Additionally, the sensor response increased with increasing NO_2 concentration, indicating strong adsorption and efficient charge transfer processes.

Despite the promising performance, certain limitations such as reduced recovery at higher gas concentrations and potential structural defects were observed. These findings highlight the need for further improvements in selectivity, stability, and environmental adaptability of MoS_2-based sensors.

Overall, this thesis establishes a strong correlation between synthesis conditions, structural properties, and gas sensing performance of MoS_2 thin films. The integration of advanced synthesis techniques with in-situ characterization provides a comprehensive understanding of gas–material interactions. The results demonstrate that nanostructured MoS_2 is a highly promising material for next-generation gas sensors, with potential applications in environmental monitoring, industrial safety, and clean energy systems.

List of Publications

List of Publications included in the thesis:

1. **Ramesh Kumar**, Nitesh K. Chourasia, Pawan K. Kulriya, Mahesh Kumar, and Vinod Singh, “Investigation of MoS_2-hydrogen interaction using in-situ X-ray diffraction studies”; Applied Physics A 131, no. 1 (2025): 14.

   Impact Factor – 2.8
2. **Ramesh Kumar**, Jitendra Singh, Pawan K. Kulriya, Mahesh Kumar, and Vinod Singh, “Influence of temperature and NO_2 concentration on the sensing performance of nanostructured MoS_2”; Journal of Materials Science: Materials in Electronics 37, no. 5 (2026): 383.

   Impact Factor – 2.8

List of Publications not included in the thesis:

1. Chourasia, Nitesh K., Ankita Rawat, Ritesh Kumar Chourasia, Hemant Singh, Ramesh Kumar Kulriya, Vinod Singh, and Pawan Kumar Kulriya, “Unveiling the potential of $Ti_3C_2T_x$ MXene for gas sensing: recent developments and future perspectives”, Materials Advances 4, no. 23 (2023): 5948-5973.

   Impact Factor – 4.7

2. Vinod Singh, Pawan K. Kulriya, Ashok Kumar, Ramesh Kumar, Priya Pradeep Kumar, Umang Berwal, Jasveer Singh, Kailash Chandra, and Kedar Singh, “Hydrogen induced structural modifications in size selected Pd-Carbon core-shell NPs: Effect of carbon shell thickness, size and pressure”; International Journal of Hydrogen Energy 47, no. 25 (2022):12642-12652.

   Impact Factor – 8.3

Conferences Contributions-Poster and Oral presentations

1. **Ramesh Kumar**, Vinod Singh, Mahesh Kumar, "Synthesis and Characterization of MoS_2 Thin Films for Gas Sensing", International Conference on Advanced Functional Materials and Devices (AFMD-2025), at Department of Physics, ARSD College, University of Delhi 3th– 5th March 2025. (Oral Talk)

2. **Ramesh Kumar**, Vinod Singh, Mahesh Kumar, "MoS_2 - hydrogen interaction using in-situ X-ray diffraction studies", International Conference on Atomic, Molecular, Material, Nano and Optical Physics with Applications (ICAMNOP-2023), Department of Applied Physics, Delhi Technological University, Delhi 20th – 22th Dec 2022. (POSTER)

Workshops and Webinars Attended:

1. Attended a one-day national seminar on "National Science Day (NSD-2023)" held at Delhi Technological University, Delhi, India on 28th Feb 2023.

2. Attended a one-day national seminar on "Implementation of NEP-2020 in Special Reference to Innovation and Entrepreneurship" organized by Department of Applied Physics at Delhi Technological University (DTU), Delhi on 24th Feb 2023.

3. Attended a one-day national workshop on "Ascertaining a Skill Centre for Glass and Glazing (ASCGG-2023) (Bringing Industry and Academia Together)" organized by the Department of Applied Physics at Delhi Technological University (DTU), Delhi on 11th Aug 2023.

4. Participated in the "National Science Day (NSD-2023)" Quiz, organized by Human Resource Development Centre (HRDC) in association with Institution", Innovation Council (IIC) & Department of Applied Physics, held at Delhi Technological University, Delhi, India on 28th Feb 2023.

5. Attended a one-day national seminar on "Recent Advancement in Semiconductor Devices and Materials (RASDM-2023)" organized by Department of Applied Physics at Delhi Technological University (DTU), Delhi on 30th Jan 2023.

6. Attended a one-day national seminar on “Recent Trends in Applied Physics and Engineering (RTAPE-2020)” by Shanti Swarup Bhatnagar (SSB) Awardees at Delhi Technological University (DTU), Delhi on 10th Feb 2020.

LIST OF TABLES

LIST OF FIGURES

LIST OF SYMBOLS

Quantity	**Symbol**
Volt	V
Centimetre	cm
Second	s
Watt	W
Kelvin	K
Temperature	T
Pascal	Pa
Angstrom	Å
Wavelength	λ
Angle	θ
Interplanar spacing	d-spacing
Crystallite Size	D
Kilovolt	kV
Kinetic Energy	E_k
Binding Energy	E_b

LIST OF ABBREVIATIONS

NS	Nanoscience
NT	Nanotechnology
NMs	Nanomaterials
nm	Nanometer
CNTs	Carbon nanotubes
QDs	Carbon quantum dots
DOS	Density of states
3D	Three-dimensional
2D	two dimensions
1D	one-dimensional
0D	zero-dimensional
TMDs	transition metal dichalcogenides
CVD	chemical vapor deposition
AMX	amoxicillin
XRD	X-ray diffraction
FESEM	Field Emission Scanning Electron Microscopy
DI	deionised

TABLE OF CONTENTS

CHAPTER 3: INVESTIGATION OF MOS_2-HYDROGEN INTERACTION USING *IN-SITU* X-RAY DIFFRACTION STUDIES 57-76

CHAPTER 4: INFLUENCE OF TEMPERATURE AND NO_2 CONCENTRATION ON THE SENSING PERFORMANCE OF NANOSTRUCTURED MOS_2 77-96

CHAPTER 5: CONCLUSION, FUTURE SCOPE, AND SOCIAL IMPACT 97-101

Chapter 1

Introduction

1.1 Need for Gas Sensing and Environmental Monitoring

Rapid industrialisation and urban development have significantly increased the emission of hazardous gases into the environment. Among these, toxic gases such as nitrogen dioxide (NO_2) and hydrogen (H_2) play a crucial role in environmental pollution, industrial safety risks, and human health hazards. NO_2 is a highly reactive oxidising gas primarily emitted from combustion processes, including vehicle exhaust, power plants, and industrial activities. Even at low concentrations, prolonged exposure to NO_2 can cause respiratory issues, lung inflammation, and reduced immune response. On the other hand, H_2 gas, although clean and widely used as an energy carrier, is highly flammable and explosive when mixed with air. Its colourless and odourless nature makes leak detection extremely difficult using human senses. Therefore, reliable sensing systems are essential to ensure safety in hydrogen storage, fuel cells, and chemical industries [1,2]. Traditional detection techniques, such as gas chromatography and mass spectrometry, provide high accuracy but suffer from limitations like bulky instrumentation, high cost, and the requirement of skilled operation. These drawbacks restrict their use in real-time and on-site monitoring. Hence, there is a growing demand for compact, cost-effective, and highly sensitive gas sensors capable of operating under varying environmental conditions.

Nanomaterial-based gas sensors have emerged as a promising solution due to their high surface-to-volume ratio, enhanced adsorption capability, and tunable electronic properties. Among these, two-dimensional (2D) materials such as molybdenum disulfide (MoS_2) have gained significant attention for gas sensing applications owing to their unique layered structure and excellent surface reactivity [3,4]. Nanomaterials have attracted significant attention for gas sensing applications due to their unique physicochemical properties. Their high surface-to-volume ratio provides a large number of active adsorption sites, thereby enhancing the interaction between gas molecules and the sensing material. Furthermore, tunable electronic structures, size-dependent properties, high carrier mobility, and the possibility of defect engineering facilitate efficient charge transfer processes and modulation of electrical conductivity upon gas adsorption. These characteristics collectively contribute to enhanced sensitivity, lower detection limits, and improved sensing performance, making nanomaterials promising candidates for next-generation gas sensors. Among the various nanostructures explored, materials with nanoscale dimensions exhibit significantly enhanced performance in sensing applications, making them highly suitable for the detection of toxic and environmentally hazardous gases.

One of the most critical advantages of nanomaterials is their exceptionally high surface-to-volume ratio. As the size of a material decreases to the nanoscale, a larger fraction of atoms resides on the surface rather than in the bulk. This increase in surface atom density provides a greater number of active sites for gas adsorption, which directly influences the sensitivity of the sensor. The interaction between gas molecules and the sensor surface is fundamentally a surface phenomenon; therefore, materials with a higher surface area tend to exhibit stronger adsorption and, consequently, more pronounced changes in their electrical or optical properties. This property is particularly beneficial for detecting low concentrations of gases, where even minor changes in adsorption can lead to measurable signals [5,6].

In addition to their high surface area, nanomaterials possess enhanced adsorption capabilities due to the presence of defects, vacancies, and unsaturated bonds. These features act as active sites that facilitate strong interactions with gas molecules. For instance, vacancies in the lattice structure can trap charge carriers or act as adsorption centers, thereby improving the sensitivity and responsiveness of the sensor. Moreover, the adsorption process can be tailored by engineering the surface chemistry of the nanomaterial, enabling selective detection of specific gases. This tunability provides a significant advantage over conventional materials, which often lack such flexibility.

Another important characteristic of nanomaterials is their tunable electronic properties. At the nanoscale, quantum confinement effects and reduced dimensionality lead to modifications in the electronic band structure of the material. This allows for precise control over properties such as band gap, conductivity, and carrier concentration.

1.2 Classification of Gas Sensors

Gas sensors are analytical devices designed to detect the presence, concentration, and nature of gaseous species in a given environment. Based on the transduction mechanism–i.e., how the interaction between gas molecules and the sensing material is converted into a measurable signal–gas sensors can be broadly classified into several categories, including electrical, optical, thermal, and mass-sensitive sensors (Fig. 1.1).

Figure 1.1: Diagram depicting the different Gas types of Sensors.

(i) Electrical Sensors

Electrical sensors are among the most widely used gas sensors due to their simple design, low cost, and ease of integration with electronic systems. These sensors operate by monitoring changes in electrical properties such as resistance, conductivity, or current upon exposure to target gases. A major subclass is chemiresistive sensors, where gas adsorption on the sensing layer causes a measurable change in resistance. 2D materials like MoS_2 are particularly suitable for such sensors due to their high surface sensitivity and charge transfer capability. Field-effect transistor (FET)-based sensors also fall under this category, offering high sensitivity through modulation of channel conductivity [5–7].

(ii) Optical Sensors

Optical gas sensors detect gases by measuring changes in optical properties such as absorption, reflection, fluorescence, or refractive index. Techniques such as infrared absorption spectroscopy and photoluminescence-based sensing are commonly employed. These sensors provide high selectivity and are often used in applications requiring non-contact and remote sensing. However, they typically require complex instrumentation and are relatively expensive compared to electrical sensors [8,9].

(iii) Thermal Sensors

Thermal gas sensors operate based on changes in temperature or heat generated during gas interaction or combustion. Catalytic sensors, for example, detect combustible gases like hydrogen by measuring the heat released during oxidation reactions. While these sensors are effective for detecting flammable gases, they usually require elevated operating temperatures, leading to higher energy consumption [10,11].

(iv) Mass-Sensitive Sensors

Mass-sensitive sensors detect gases by measuring the change in mass of the sensing layer due to adsorption of gas molecules. Common examples include quartz crystal microbalance (QCM) and surface acoustic wave (SAW) sensors. These sensors offer high sensitivity and can detect very low concentrations of gases. However, they are often sensitive to environmental factors such as humidity and temperature fluctuations [12,13].

In recent years, research has increasingly focused on electrical (chemiresistive) gas sensors based on nanostructured materials, particularly 2D materials like MoS_2. Their large surface area, tunable electronic properties, and strong interactions with gas molecules make them highly promising for detecting gases such as NO_2 and H_2 with improved sensitivity and faster response times.

1.2.1 Key Gas Sensing Performance Parameters

The performance of a gas sensor is evaluated using several fundamental parameters that describe its sensitivity, speed, reliability, and selectivity toward a target gas. These parameters are essential for determining the practical applicability of a sensor in real-world conditions such as environmental monitoring and industrial safety.

(i) Response

The sensing response is defined as the relative change in electrical resistance of the sensor upon exposure to the target gas. Since reducing and oxidising gases may induce opposite resistance variations in MoS_2, the response expressions adopted in this thesis are clearly specified and justified wherever necessary to ensure consistency and avoid ambiguity [14,15].

For reducing gases (such as H_2):

Response $= \frac{R_g}{R_a}$

For oxidising gases (such as NO_2):

Response = $\frac{R_g}{R_a}$

where,

R_a = sensor resistance in air

R_g = sensor resistance in the presence of target gas

Further, the relative response percentage (%) can be calculated as:

Relative response for reducing gases (%) = $\frac{(R_g-R_a)}{R_a} \times 100$

Relative response for oxidizing gases (%) = $\frac{(R_a-R_g)}{R_g} \times 100$

(ii) Sensitivity

Sensitivity defines how strongly the sensor responds to a change in gas concentration. It is generally expressed as the ratio of sensor response to the concentration of the analyte gas [16].

Sensitivity = $\frac{\text{Response}}{\text{Concentration of Gas}}$

Higher sensitivity means the sensor can detect even very low gas concentrations, which is crucial for toxic gases like NO_2.

(iii) Response Time

Response time is the time required for the sensor to reach approximately 90% of its maximum response after exposure to the target gas. A shorter response time indicates faster detection capability, which is essential for real-time monitoring.

(iv) Recovery Time

Recovery time is the time taken by the sensor to return to 10% above its original baseline value after the removal of the target gas. Fast recovery ensures reusability and continuous operation of the sensor.

(v) Selectivity

Selectivity refers to the ability of a sensor to distinguish a specific gas in the presence of other interfering gases. High selectivity is particularly important in complex environments where multiple gases coexist.

(vi) Stability

Stability indicates the consistency of sensor performance over an extended period. A stable sensor maintains its response characteristics under continuous or repeated operation without significant degradation.

(vii) Reproducibility

Reproducibility defines the ability of the sensor to produce similar responses under identical conditions over multiple sensing cycles. It ensures the reliability and repeatability of measurements.

Overall, an ideal gas sensor should exhibit high sensitivity, fast response and recovery times, excellent selectivity, and long-term stability. 2D materials such as MoS_2 have shown significant potential in achieving these performance characteristics due to their high surface activity and efficient charge transfer properties [10,17,18].

1.3 Choice of Gas Sensing Materials

The selection of an appropriate sensing material plays a crucial role in determining the overall performance of a gas sensor. The interaction between gas molecules and the sensing layer occurs at the surface; therefore, materials with high surface reactivity, large surface area, and suitable electronic properties are highly desirable for efficient gas detection [8,17].

In recent years, nanostructured materials have gained significant attention in gas sensing applications due to their unique physicochemical properties. Compared to bulk materials, nanomaterials offer a much higher surface-to-volume ratio, which enhances the adsorption of gas molecules and facilitates effective charge transfer. These characteristics directly contribute to improved sensitivity, faster response, and lower detection limits [3,19]. Since gas sensing is primarily governed by surface adsorption processes, the availability of a larger active surface directly enhances the interaction between the sensing material and the target analyte. Consequently, even small concentrations of gas molecules can induce measurable changes in the physical properties of the material, leading to enhanced sensitivity [2,3].

In addition to increased surface area, nanomaterials exhibit enhanced adsorption capability due to the presence of structural defects, grain boundaries, and unsaturated surface atoms. These features act as energetically favorable sites for gas adsorption, facilitating stronger binding between the gas molecules and the sensor surface. Defects such as vacancies or interstitials can significantly influence the electronic structure of the material, thereby promoting efficient charge transfer during gas adsorption. This improved interaction between the adsorbate and the sensing material is crucial for achieving high-performance gas sensing. Another important factor contributing to the superior sensing behavior of nanostructured materials is their tunable electronic properties. At the nanoscale, materials often exhibit quantum confinement effects, which lead to modifications in their band structure and electronic characteristics. These changes can be exploited to tailor the electrical conductivity and carrier concentration of the material, which are key parameters in gas sensing. When gas molecules adsorb onto the surface of a nanomaterial, they can either donate or withdraw electrons, resulting in a change in the charge carrier density. This change manifests as a variation in electrical resistance or conductivity, forming the basis of many gas sensing mechanisms. The enhanced charge transfer process in nanomaterials is particularly important for improving sensor performance. Due to their reduced dimensions and increased surface activity, nanomaterials enable faster and more efficient exchange of electrons between the adsorbed gas molecules and the sensing layer. This leads to rapid changes in electrical signals, resulting in faster response and recovery times. Such characteristics are highly desirable in real-time monitoring applications, where quick detection and response are critical [5-19].

Furthermore, nanostructured materials often exhibit improved diffusion characteristics, allowing gas molecules to penetrate easily into the sensing layer. This facilitates uniform interaction throughout the material and enhances the overall sensing efficiency. In contrast, bulk materials typically suffer from limited diffusion and reduced accessibility of active sites, which can negatively impact sensor performance. The ability of nanomaterials to operate at lower temperatures is another key advantage. Many conventional gas sensors, particularly those based on metal oxides, require high operating temperatures to activate surface reactions. This leads to increased power consumption and limits their practical applications. In contrast, nanomaterials, due to their high reactivity and active surface sites, can effectively interact with gas molecules at relatively lower temperatures, including room temperature in some cases. This not only reduces energy consumption but also enhances the stability and lifespan of the sensor.

Moreover, nanostructured materials provide excellent flexibility for surface modification and functionalization. By introducing dopants, forming composites, or creating heterostructures, the sensing properties of nanomaterials can be further enhanced. These modifications can improve selectivity toward specific gases, which is a major challenge in gas sensing applications. The ability to engineer material properties at the nanoscale offers a significant advantage in designing highly selective and sensitive sensors. The reduced size of nanomaterials also enables their integration into miniaturized and portable sensing devices. With the growing demand for compact and wearable sensing systems, nanomaterial-based sensors provide a viable solution due to their small size, lightweight nature, and compatibility with modern electronic platforms. This opens up new possibilities for applications in environmental monitoring, industrial safety, healthcare diagnostics, and smart sensing systems [18-20]. Additionally, nanomaterials exhibit improved signal-to-noise ratio due to their enhanced surface interactions and efficient charge transport. This results in more reliable and reproducible sensing signals, which are essential for accurate detection. The combination of high sensitivity, rapid response, and low detection limits makes nanostructured materials highly suitable for detecting trace levels of gases. In summary, nanostructured materials have revolutionized the field of gas sensing by offering a range of advantages over traditional bulk materials. Their high surface-to-volume ratio, enhanced adsorption capability, tunable electronic properties, and efficient charge transfer mechanisms collectively contribute to improved sensing performance. These features enable the development of gas sensors with higher sensitivity, faster response times, and lower detection limits. As research in this field continues to advance, nanomaterials are expected to play a crucial role in the development of next-generation gas sensing technologies with improved efficiency, reliability, and versatility [16,20].

Nanomaterials used for gas sensing are generally classified based on their dimensionality. D(E), which represents the number of available electronic states per unit energy, arises significantly with the dimensionality of a material and is a key factor governing its optical and electronic behaviour (Fig. 1.2).

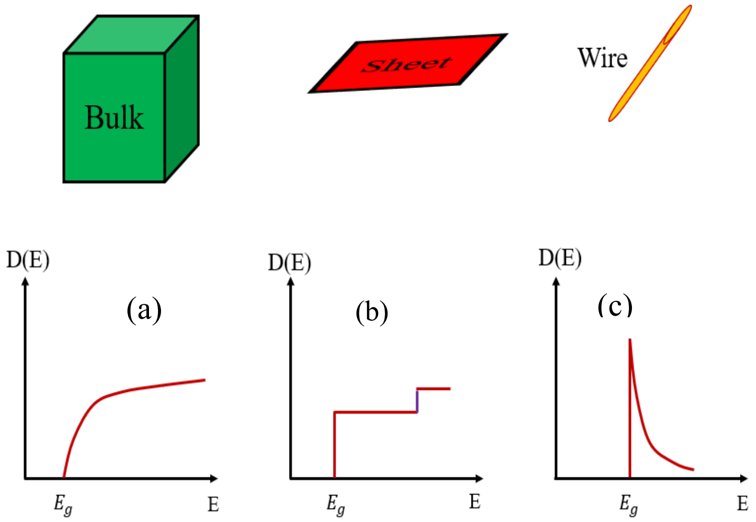

Figure 1.2: Diagram depicting the dependence of D(E) on energy for systems of varying dimensionality: 3D-bulk (a), 2D-sheet (b) and 1D-wire (c).

(i) Zero-Dimensional (0D) Nanomaterials

These materials, such as quantum dots and nanoparticles, are confined in all three spatial dimensions. Due to quantum confinement effects, they exhibit unique optical and electronic properties. However, issues such as aggregation and limited charge transport can sometimes restrict their sensing performance [1,19].

(ii) One-Dimensional (1D) Nanomaterials

Examples include nanowires, nanorods, and nanotubes. These structures provide efficient pathways for charge transport along one direction, leading to improved electrical conductivity. Their high aspect ratio also enhances surface interaction with gas molecules. In one-dimensional (1D) systems such as nanowires or nanotubes, the D(E) exhibits a series of singularities (Van Hove singularities) due to QC along two directions ($D_{1D}(E) \propto E^{-1/2}$) [20,21].

(iii) Two-Dimensional (2D) Nanomaterials

2D materials, such as graphene and TMDs, consist of atomically thin layers with large lateral dimensions. These materials have attracted tremendous interest due to their exceptionally high surface area, tunable bandgap, and strong interaction with adsorbed gas molecules. The presence of exposed active sites and weak van der Waals interactions between layers enables efficient gas adsorption and rapid charge transfer [18,21,22].

Among 2D materials, MoS_2 has emerged as a promising candidate for gas sensing applications. It exhibits a layered structure, good chemical stability, and semiconducting behaviour, making it suitable for detecting both oxidizing gases like NO_2 and reducing gases such as H_2. Additionally, MoS_2 can be synthesized in various nanostructured forms, including nanosheets and nanoflowers, which further enhance its sensing performance. In 2D, as in atomically thin layers, the D(E) becomes step-like, remaining constant within each sub-band and resulting in sharper optical transitions ($D_{2D}(E) \propto E^0$) [13,23].

(iv) Three-Dimensional (3D) Nanomaterials

These materials consist of interconnected nanostructures forming bulk architectures such as porous frameworks and nanocomposites. They provide mechanical stability and a high density of active sites, but their performance may be limited by reduced surface accessibility compared to lower-dimensional systems.In 3D bulk materials, the D(E) increases smoothly with the square root of energy ($D_{3D}(E) \propto E^{1/2}$), leading to continuous energy bands [24,25].

In modern gas sensing research, significant efforts have been directed toward improving the performance of sensing materials through strategies such as defect engineering, doping, surface functionalization, and heterostructure formation. These approaches help in enhancing adsorption sites, tuning electronic properties, and improving selectivity toward specific gases.

Among all material classes, 2D nanomaterials – particularly MoS_2–offer a balanced combination of sensitivity, stability, and scalability. Therefore, they are considered highly suitable for next-generation gas sensors designed for real-time and low-power applications [26,27].

1.3.1 Transition Metal Dichalcogenides (TMDs)

TMDs represent an important class of 2D layered materials that have attracted significant attention in recent years for gas sensing and other electronic applications. These materials generally follow the chemical formula MX_2, where M is a transition metal (such as Mo,W) and X is a chalcogen element (such as S, Se, or Te) [8,28]. TMDs possess a unique layered structure in which a layer of transition metal atoms is sandwiched between two layers of chalcogen atoms. These layers are held together by weak van der Waals forces, allowing easy exfoliation into few-layer or monolayer structures. This structural feature provides a large number of exposed surface sites, which are highly beneficial for gas adsorption and sensing applications [29,30].

One of the most attractive properties of TMDs is their tunable electronic behavior. Unlike graphene, which is a zero-bandgap material, TMDs exhibit semiconducting characteristics with a finite and adjustable bandgap. This property makes them highly suitable for gas sensing, as the interaction with gas molecules can effectively modulate their electrical conductivity. Among the TMD family, MoS_2 has been extensively studied due to its excellent physicochemical properties. MoS_2 exhibits a transition from an indirect bandgap in bulk form to a direct bandgap in monolayer form, which enhances its electronic and sensing performance. Its high surface-to-volume ratio, chemical stability, and strong interaction with gas molecules make it a promising material for detecting both oxidizing gases such as NO_2 and reducing gases like hydrogen H_2. The gas sensing performance of MoS_2 is primarily governed by surface adsorption and charge transfer mechanisms. When gas molecules interact with the surface, they either donate or withdraw electrons, leading to a change in carrier concentration and, consequently, the electrical resistance of the material. This makes MoS_2 highly responsive even at low gas concentrations [15]. The bandgap in TMDs is highly sensitive to factors such as layer thickness, strain, and external environment. As a result, their electronic properties can be engineered by controlling these parameters. This tunability enables precise optimization of sensing performance, including sensitivity and selectivity. When gas molecules interact with the surface of TMDs, they induce changes in charge carrier concentration through electron transfer processes. Because of the semiconducting nature of these materials, even small variations in carrier density can lead to significant changes in electrical conductivity, which can be readily detected [16,19].

Among the various TMDs, MoS_2 has emerged as one of the most extensively studied and promising materials for gas sensing applications. This is primarily due to its unique combination of structural, electronic, and chemical properties. MoS_2 possesses a layered structure in which a layer of molybdenum atoms is sandwiched between two layers of sulfur atoms. These layers are held together by weak van der Waals forces, allowing easy exfoliation into few-layer or monolayer forms. This structural characteristic not only enhances its surface area but also exposes a large number of active sites for interaction with gas molecules. A particularly important property of MoS_2 is the transition in its band structure as the material thickness is reduced. In its bulk form, MoS_2 exhibits an indirect bandgap of approximately 1.2 eV. However, when thinned down to a monolayer, it undergoes a transition to a direct bandgap of about 1.8 eV. This change significantly enhances its optical and electronic properties, including carrier mobility and light–matter interaction. The direct bandgap in monolayer MoS_2

leads to improved charge carrier dynamics, which is beneficial for sensing applications where rapid and efficient charge transfer is required. The high surface-to-volume ratio of MoS_2 further enhances its gas sensing capabilities. Since a large fraction of atoms are located at or near the surface, the material exhibits increased sensitivity to adsorbed species. Gas sensing in MoS_2 is primarily a surface-driven phenomenon, where the adsorption of gas molecules leads to charge transfer between the adsorbate and the sensing material. This interaction modifies the carrier concentration within the material, resulting in measurable changes in electrical resistance or conductivity. In addition to its structural advantages, MoS_2 exhibits excellent chemical stability, which is crucial for reliable sensor performance. It can maintain its structural integrity and functional properties even under varying environmental conditions, including exposure to reactive gases. This stability ensures consistent sensor response over prolonged periods, making it suitable for practical applications. The interaction between MoS_2 and gas molecules is strongly influenced by the presence of defects, particularly sulfur vacancies. These vacancies act as active sites for gas adsorption and significantly enhance the sensitivity of the material. They facilitate stronger binding of gas molecules and promote efficient charge transfer processes. As a result, defect engineering has become an important strategy for improving the performance of MoS_2-based gas sensors. MoS_2 has demonstrated excellent capability for detecting both oxidizing and reducing gases. In the presence of oxidizing gases such as nitrogen dioxide (NO_2), electrons are withdrawn from the MoS_2 surface, leading to a decrease in electron concentration. For n-type MoS_2, this results in an increase in electrical resistance. Conversely, when exposed to reducing gases such as hydrogen (H_2), electrons are donated to the material, increasing the carrier concentration and decreasing the resistance. This bidirectional response enables MoS_2 to function effectively as a versatile gas sensing material. The sensing mechanism in MoS_2 is predominantly governed by surface adsorption and charge transfer processes. When gas molecules come into contact with the surface, they interact with the available active sites and either donate or accept electrons depending on their chemical nature. This interaction alters the electronic structure of the material and modulates its conductivity. Because of the high sensitivity of MoS_2 to changes in carrier concentration, even low concentrations of gas molecules can produce a detectable signal.

Another advantage of MoS_2 is its potential for low-temperature or room-temperature operation. Unlike conventional metal oxide sensors that require elevated temperatures to activate surface reactions, MoS_2 can effectively interact with gas molecules at relatively lower temperatures.

This reduces power consumption and enhances the practicality of the sensor for portable and wearable applications [31,32].

Furthermore, MoS_2 can be integrated with other materials to form heterostructures or composites, further enhancing its sensing performance. Such hybrid systems can exhibit improved selectivity, faster response times, and better stability due to synergistic effects between different materials. In summary, TMDs, particularly MoS_2, provide a versatile platform for developing high-performance gas sensors due to their unique structural, electronic, and surface properties. Their ability to operate under relatively low temperatures and their compatibility with nanofabrication techniques make them strong candidates for next-generation sensing devices.

1.4 Gas Sensing Mechanism

The gas sensing mechanism in semiconductor-based materials is primarily governed by the interaction between gas molecules and the surface of the sensing layer. This interaction leads to charge transfer processes that ultimately result in measurable changes in the electrical properties of the material, such as resistance or conductivity [31,32]

In 2D nanomaterials like MoS_2, the sensing behavior is strongly influenced by their high surface-to-volume ratio and the availability of active sites for gas adsorption. When the sensor is exposed to ambient air, oxygen molecules are first adsorbed onto the surface of the material. The nature and chemical state of oxygen species adsorbed on the surface of semiconductor materials are strongly influenced by the operating temperature. At lower temperatures, molecular oxygen is adsorbed on the surface by capturing electrons from the conduction band, forming superoxide ions. As the temperature increases, these species undergo further ionization, leading to the formation of more reactive oxygen ions. The temperature-dependent adsorption behavior can be represented by the following equilibria [33–35]:

$$\mathrm{O_2(gas) + e^{-1} \leftrightarrow O^{2-}(ads)\ when\ T < 200℃}$$

$$\mathrm{\frac{1}{2}O_2(gas) + e^{-1} \leftrightarrow O^{-}(ads)\ when\ T > 250℃}$$

$$\mathrm{\frac{1}{2}O_2(gas) + 2e^{-1} \leftrightarrow O^{2-}(ads)\ when\ T > 250℃}$$

These ionized oxygen species play a crucial role in gas sensing, as they participate in surface reactions with target gas molecules, thereby modulating the electrical properties of the sensing material [36,37].

Further, the sensing response occurs when the sensor is exposed to target gases, which can be broadly classified into **oxidizing gases** (e.g., NO_2) and **reducing gases** (e.g., H_2).

(i) Interaction with Oxidizing Gases (NO_2)

Nitrogen dioxide is a strong oxidizing gas that tends to accept electrons from the sensing material. When NO_2 molecules interact with the surface of MoS_2, they capture electrons directly from the material or from the adsorbed oxygen species. This leads to a further reduction in electron concentration.

In n-type materials like MoS_2, this process results in an increase in resistance, as the number of charge carriers decreases. The adsorption of NO_2 also enhances the depletion layer at the surface, which further contributes to the resistance change [38].

(ii) Interaction with Reducing Gases (H_2)

Reducing gases such as hydrogen behave in the opposite manner. When H_2 molecules come into contact with the sensor surface, they react with the adsorbed oxygen ions. This reaction releases the trapped electrons back into the conduction band of the material [33,39].

As a result, the electron concentration increases, leading to a decrease in resistance in n-type materials like MoS_2. This change in resistance is used as the sensing signal for hydrogen detection.

(iii) Role of Surface Adsorption and Charge Transfer

The efficiency of gas sensing largely depends on the adsorption-desorption dynamics and the extent of charge transfer between the gas molecules and the sensing material. Strong adsorption enhances sensitivity, while fast desorption ensures quick recovery. These processes are influenced by factors such as surface defects, morphology, and operating temperature [40,41].

(iv) Influence of Temperature and Structural Changes

Temperature plays a crucial role in gas sensing performance. At higher temperatures, adsorption and reaction kinetics are enhanced, leading to faster response and recovery times.

However, excessive temperature may also cause desorption of gas molecules, reducing sensitivity [15,42,43].

Advanced characterization techniques such as in-situ X-ray diffraction (XRD) provide valuable insights into structural changes occurring in the sensing material during gas exposure. These studies reveal that interaction with gases like hydrogen can induce lattice modifications, phase changes, or strain variations in MoS_2, which directly affect its sensing behaviour. Such structural evolution highlights the dynamic nature of gas-material interaction beyond simple surface adsorption.

These processes collectively determine the sensitivity, selectivity, and response characteristics of the gas sensor [23,44].

1.5 Challenges and Strategies

Despite significant advancements in gas sensing technologies, the development of highly efficient, reliable, and practical gas sensors remains a challenging task. Although materials such as MoS_2 and other 2D nanostructures have demonstrated promising sensing performance, several limitations still hinder their large-scale application in real-world environments.

(i) Key Challenges in Gas Sensing

a) Low Selectivity

One of the major challenges in gas sensing is poor selectivity. Many sensing materials respond similarly to different gases, making it difficult to distinguish a specific target gas such as NO_2 or H_2 in the presence of other interfering gases.

b) Slow Response and Recovery

Pristine sensing materials often exhibit slow adsorption and desorption kinetics, leading to longer response and recovery times. This limits their use in real-time monitoring applications.

c) Operating Temperature Requirement

Several conventional gas sensors require high operating temperatures to achieve optimal performance. This results in increased power consumption and reduces the feasibility of portable or low-power devices.

d) Long-Term Stability Issues

Over time, the sensing performance may degrade due to environmental factors, surface contamination, or structural changes in the material. Maintaining consistent performance over extended periods is a significant challenge.

e) Humidity Interference

Environmental humidity can strongly influence sensor response by competing with gas molecules for adsorption sites, thereby affecting accuracy and reliability.

(ii) Strategies to Overcome Challenges

To address these limitations, various material engineering and design strategies have been explored:

a) Nanostructuring and Morphology Control

The design and engineering of materials with well-controlled nanostructures play a crucial role in enhancing gas sensing performance. Morphologies such as nanosheets, nanoflowers, and porous architectures significantly increase the effective surface area of the sensing material, thereby providing a larger number of active sites for gas adsorption. This structural advantage facilitates stronger interaction between the gas molecules and the material surface, which is essential for efficient sensing. In particular, porous and hierarchical nanostructures enable easy diffusion of gas molecules throughout the material, ensuring uniform interaction and improved accessibility of active sites. As a result, the adsorption–desorption dynamics become more efficient, leading to faster response and recovery characteristics. Furthermore, the enhanced surface reactivity associated with such nanostructures promotes effective charge transfer between the adsorbed gas species and the sensing layer, resulting in a more pronounced change in electrical properties. Consequently, materials with controlled nanostructured morphologies exhibit significantly improved sensitivity, rapid response times, and lower detection limits, making them highly suitable for advanced gas sensing applications.

b) Defect Engineering

Introducing defects such as vacancies or edge sites creates additional active sites for gas interaction. In MoS_2, sulfur vacancies significantly enhance adsorption strength and charge transfer, thereby improving sensing performance. In the case of molybdenum disulfide (MoS_2), sulfur vacancies are among the most commonly observed and functionally important defects.

These vacancies arise due to the absence of sulfur atoms in the lattice, leading to the formation of localized electronic states. As a result, these sites exhibit higher chemical reactivity and serve as preferential adsorption centers for gas molecules. The presence of sulfur vacancies enhances the binding strength between the gas molecules and the MoS_2 surface, which in turn promotes efficient charge transfer during adsorption [6-7].

c) Doping and Functionalization

Doping of sensing materials with suitable metal or non-metal elements is an effective strategy for tuning their electronic and chemical properties, thereby enhancing gas sensing performance. The introduction of dopant atoms into the host lattice alters the electronic structure by modifying parameters such as band gap, carrier concentration, and defect states. These changes directly influence the interaction between the sensing material and gas molecules, leading to improved sensitivity and selectivity. For instance, dopants can act as electron donors or acceptors, facilitating charge transfer processes during gas adsorption and resulting in more pronounced variations in electrical conductivity [4,5]. Additionally, doping can create new active sites or modify existing ones, thereby enhancing the adsorption strength of specific gases. This enhanced charge transfer process leads to a significant modulation in the carrier concentration of the material, resulting in a more pronounced change in electrical resistance or conductivity. Consequently, the sensitivity of the sensor is greatly improved, even at low gas concentrations. Additionally, defect sites can influence the adsorption–desorption kinetics, contributing to faster response and recovery characteristics. Therefore, controlled introduction of defects, particularly sulfur vacancies in MoS_2, provides a powerful strategy for optimizing gas sensing performance by increasing adsorption efficiency and strengthening the charge transfer mechanism [7,8].

d) Heterostructure Formation

Constructing heterostructures by combining different materials enhances charge transfer and creates built-in electric fields at the interface. This significantly improves response speed, selectivity, and overall sensing efficiency. In gas sensing applications, heterostructures provide multiple advantages over single-component materials. The presence of an interface increases the number of active sites available for gas adsorption and enhances the interaction between the sensing layer and the target gas molecules. When gas molecules adsorb onto the surface, the built-in electric field at the interface accelerates the charge transfer process, resulting in a more rapid and pronounced change in electrical conductivity. This leads to improved sensitivity and significantly faster response and recovery times [6-9]. Moreover, heterostructures can be engineered to achieve enhanced selectivity by carefully choosing materials with complementary properties. For instance, combining a material with strong adsorption capability with another material having high charge mobility can create a synergistic effect that optimizes sensing performance. Additionally, the interface can act as a barrier or junction (such as p–n or n–n junctions), further influencing carrier transport and amplifying the sensing signal.

e) Temperature Optimization and Room Temperature Operation

Efforts are being made to develop sensors that can operate efficiently at or near room temperature. This reduces power consumption and enables integration into portable and wearable devices. Traditional gas sensors, particularly those based on metal oxide semiconductors, often require elevated operating temperatures to activate surface reactions between the sensing material and target gas molecules. This high-temperature requirement leads to increased power consumption, reduced device lifespan, and limited applicability in portable systems. In contrast, room-temperature sensing offers a more energy-efficient and practical solution for real-world applications. Operating at or near ambient conditions significantly reduces the energy requirements of the sensing device, making it highly suitable for battery-powered and low-power electronic systems. This is particularly important for applications such as environmental monitoring, indoor air quality assessment, and healthcare diagnostics, where continuous operation over extended periods is essential. Lower power consumption also minimizes heat generation, thereby improving the stability and reliability of the sensor. The development of room-temperature gas sensors is closely linked to the use of advanced materials such as nanostructured semiconductors and two-dimensional (2D) materials. These materials exhibit high surface reactivity and enhanced adsorption properties, enabling effective interaction with gas molecules even at lower temperatures. As a result, sufficient charge transfer can occur without the need for thermal activation, allowing the sensor to produce a measurable response under ambient conditions [6,12].

f) Advanced Characterization Techniques

Techniques such as in-situ XRD and other real-time analysis methods help in understanding the dynamic interaction between gas molecules and sensing materials. This knowledge aids in designing more efficient and stable sensors. In gas sensing applications, the interaction between the sensing material and target gas is a highly dynamic process involving adsorption, desorption, charge transfer, and possible structural modifications. Traditional characterization methods often fail to capture these transient processes, as they analyze the material either before or after gas exposure. In contrast, in-situ XRD allows direct observation of changes in crystal structure, phase composition, and lattice parameters during gas exposure. This provides valuable information about how the material responds to different gas environments at the atomic and crystallographic levels [5,19].

Overall, overcoming these challenges requires a combination of material design, structural engineering, and deeper understanding of gas–surface interactions. 2D materials like MoS_2, when modified through advanced strategies such as doping, defect engineering, and heterostructure formation, offer a promising pathway toward the development of high-performance gas sensors suitable for practical applications [16,32,45].

1.6 Thesis Problem

The increasing demand for efficient gas sensing systems has driven extensive research toward the development of advanced materials capable of detecting hazardous gases with high sensitivity, selectivity, and stability. Among various target gases, NO_2 and H_2 are of particular importance due to their significant environmental and industrial impact. While NO_2 poses serious health and environmental risks even at low concentrations, hydrogen, being highly flammable and explosive, requires reliable detection systems to ensure safety in energy and industrial applications.

Although 2D materials such as MoS_2 have shown promising potential for gas sensing, several limitations still persist. Pristine MoS_2 often suffers from relatively slow response and recovery characteristics, limited selectivity toward specific gases, and performance instability under varying environmental conditions. Furthermore, the influence of operating parameters such as temperature and gas concentration on sensing behavior is not yet fully understood.

Another important aspect that requires deeper investigation is the structural evolution of sensing materials during gas interaction. Conventional sensing studies primarily focus on electrical response, while the real-time structural changes occurring within the material during gas exposure are often overlooked. Understanding these changes is crucial for establishing a direct correlation between material properties and sensing performance.

Therefore, the present research is focused on addressing these critical challenges by investigating the gas-sensing behaviour of nanostructured MoS_2 under different environmental conditions. Special emphasis is placed on:

a) Understanding the interaction of MoS_2 with hydrogen gas through advanced characterization techniques such as in-situ XRD

b) Studying the influence of temperature and NO_2 concentration on sensing performance

c) Improving the overall sensing characteristics in terms of sensitivity, response, and stability

This work aims to provide deeper insight into the structure-property-performance relationship of MoS_2-based gas sensors, thereby contributing to the development of more efficient and reliable sensing devices for real-world applications.

1.7 Objectives of the Thesis

The present research is designed to systematically explore the gas sensing behavior of 2D MoS_2-based materials through controlled synthesis, detailed characterization, and performance evaluation. The primary objectives of the proposed work are as follows:

1. Extensive literature survey on 2D nanomaterials for gas sensing application.
2. Synthesize MoS_2 thin films with controlled morphology using CVD and sulfurization methods.
3. Characterization of 2D Molybdenum Disulfide.
4. Perform in-situ XRD studies of MoS_2 under hydrogen exposure to understand structural stability.
5. Investigate NO_2 sensing performance as a function of temperature and concentration.

The outcomes of this research, aimed at achieving the aforementioned objectives, are organized into six chapters, each summarized below. This structure reflects the comprehensive optimization of synthesis parameters carried out based on the findings from characterization studies and gas-sensing performance evaluations.

1.8 Layout of Thesis

The present thesis is systematically organized into five chapters, each addressing a distinct aspect of the research work with a logical progression from fundamental concepts to experimental investigations and final outcomes. The overall structure has been carefully designed to provide a comprehensive understanding of the synthesis, characterization, and gas sensing performance of MoS_2-based systems. This organization ensures a coherent flow of information, allowing the reader to clearly follow the development of the study from conceptual background to detailed analysis and interpretation. Additionally, the structured approach enhances clarity, consistency, and continuity throughout the thesis, facilitating a deeper understanding of the material properties and their relevance to gas sensing applications.

Chapter 1: Introduction and Background of Gas Sensing Using 2D Nanomaterials

This chapter provides a comprehensive introduction to gas sensing technologies, covering the detection of both oxidizing gases (such as NO_2) and reducing gases (such as H_2). The increasing demand for energy-efficient sensors capable of operating at or near room temperature, with high sensitivity, selectivity, and stability, is critically discussed. Fundamental concepts of chemiresistive sensing, including surface adsorption and charge transfer mechanisms, are elaborated in detail.

Furthermore, the chapter highlights the significance of nanostructured materials, particularly 2D materials, in enhancing gas sensing performance. Among these, MoS_2 is emphasized due to its unique structural, electronic, and surface properties, making it a promising candidate for gas sensing applications. Finally, existing limitations in current sensing technologies are identified, and the motivation and objectives of the present research work are clearly outlined.

Chapter 2: Experimental Methodology – Synthesis, Characterization Techniques, and Gas Sensing Measurements

This chapter describes the experimental procedures adopted for the synthesis and analysis of MoS_2 thin films. TMDs, especially MoS_2, are introduced due to their unique electrical, optical, and structural properties. Thin films are synthesized using electron beam (e-beam) deposition followed by sulfurization via chemical vapor deposition (CVD). Various characterization techniques such as XRD, Raman spectroscopy, atomic force microscopy (AFM), scanning electron microscopy (SEM), and energy-dispersive X-ray spectroscopy (EDX) are discussed in detail. Additionally, gas sensing measurement techniques are explained.

Chapter 3: Investigation of MoS_2-Hydrogen Interaction using In-situ X-ray Diffraction Studies

In this chapter, we have examined those significant effects of hydrogen (H_2) exposure on the structural properties of molybdenum disulfide (MoS_2) thin films through in-situ X-ray diffraction (XRD) analysis. Molybdenum (Mo) thin films were initially deposited using the electron beam (e-beam) deposition method and subsequently sulfurized via chemical vapor deposition (CVD) to obtain MoS_2 thin films. The quality of the MoS_2 films was optimized by varying the thickness of the Mo layer, sulfurization temperature, and the temperature of the Mo film. It was determined that crystalline MoS_2 thin films with an optimal thickness of 20 nm can be achieved through sulfurization at 220 °C, while maintaining the Mo thin film at 600 °C. Pressure-dependent hydrogenation of the MoS_2 thin films, as investigated by in-situ XRD, reveals an increase in crystallite size accompanied by a decrease in the relative intensity of the diffraction peaks with rising hydrogen pressure. Furthermore, a micro-strain of approximately 6.3% is induced in the MoS_2 films upon exposure to 1% and 10% hydrogen. Notably, the MoS_2 thin films remain predominantly stable up to a hydrogen pressure of 400 mbar; however, they undergo abrupt transformations and become entirely amorphous when the hydrogen gas pressure is subsequently elevated to 800 mbar. These observations of hydrogen-induced crystalline-amorphous phase transformation in MoS_2 not only enhance the understanding of the interactions between MoS_2 and hydrogen but also have critical implications for the application of MoS_2 thin films in various devices.

This work is published as Ramesh Kumar, Nitesh K. Chourasia, Pawan K. Kulriya, Mahesh Kumar, and Vinod Singh. "Investigation of MoS_2-hydrogen interaction using in-situ X-ray diffraction studies." *Applied Physics A* 131, no. 1 (2025): 14.

Chapter 4: Influence of Temperature and NO_2 Concentration on the Sensing Performance of Nanostructured MoS_2

This chapter investigates the gas sensing behavior of nanostructured MoS_2 thin films toward NO_2 under varying temperature and concentration conditions. The films are fabricated using chemical vapor deposition and deposited on suitable substrates with optimized electrode configurations. Structural and morphological studies confirm the formation of uniform and crystalline MoS_2 nanosheets. Gas sensing measurements show that the resistance of the sensor increases upon exposure to NO_2, indicating n-type semiconducting behavior. The sensor exhibits enhanced response at elevated temperatures, along with good selectivity and reasonable response-recovery characteristics. The influence of temperature on sensing performance and defect formation is also discussed.

This work is published as Ramesh Kumar, Jitendra Singh, Pawan K. Kulriya, Mahesh Kumar, and Vinod Singh. "Influence of temperature and NO_2 concentration on the sensing performance of nanostructured MoS_2." *Journal of Materials Science: Materials in Electronics* 37, no. 5 (2026): 383.

Chapter 5: Conclusions, Future Scope, and Social Impact

5.1 Conclusions

This research work focused on the development and performance optimization of 2D MoS_2-based gas sensors for NO_2 detection. The study systematically investigated synthesis strategies, structural stability, and sensing performance to address the limitations of conventional metal oxide gas sensors, particularly high operating temperature and high-power consumption.

MoS_2 thin films were successfully synthesized using e-beam deposition followed by sulfurization via CVD. Structural and morphological characterizations confirmed the formation of highly crystalline, uniform, and continuous MoS_2 thin films with optimized thickness (~20 nm). Raman spectroscopy, XRD, SEM, EDEX, AFM, and analysis verified phase purity and nanosheet morphology suitable for gas sensing applications.

In-situ XRD studies under hydrogen exposure revealed important insights into the structural stability of MoS_2. The films remained stable up to 400 mbar hydrogen pressure but exhibited crystalline-to-amorphous transformation at higher pressures (800 mbar), indicating pressure-dependent structural evolution. These findings contribute to the understanding of gas-material interaction mechanisms and device reliability under reactive environments.

Gas sensing investigations demonstrated that nanostructured MoS_2 exhibits strong sensitivity toward NO_2 gas. The sensor resistance increased upon exposure to NO_2, confirming n-type semiconducting behaviour. The optimal sensing response (~14.2%) was achieved at 20 ppm NO_2 concentration at 150 °C, with fast response and recovery times. The study further confirmed improved selectivity toward NO_2 compared to other interfering gases.

Overall, this work establishes MoS_2 thin films as promising candidates for selective and efficient NO_2 gas detection. The results highlight that careful optimization of synthesis parameters, thickness control, and operating temperature significantly enhances sensor performance.

5.2 Future Scope

a) Enhancement of room-temperature sensing performance through heterostructure formation and surface modification.

b) Investigation of long-term stability and humidity effects for practical applications.

c) Theoretical studies to understand gas adsorption and charge transfer mechanisms.

d) Integration of MoS_2 sensors into portable and IoT-based environmental monitoring devices.

5.3 Social Impact

The development of high-performance NO_2 gas sensors has significant societal and environmental implications:

a) **Environmental Monitoring:** NO_2 is a major air pollutant emitted from automobiles and industrial processes. Reliable detection systems contribute to pollution control and environmental safety.

b) **Public Health Protection:** Exposure to NO_2 even at low concentrations can cause severe respiratory diseases. Early detection systems can help prevent health hazards in urban and industrial environments.

c) **Industrial Safety:** Real-time gas monitoring enhances workplace safety in chemical plants, refineries, and manufacturing industries.

d) **Sustainable Development:** The development of low-power, room-temperature gas sensors supports energy-efficient technologies aligned with sustainable and green engineering practices.

e) **Smart Cities and IoT Integration:** Advanced gas sensors can be integrated into smart city infrastructure for continuous air quality monitoring and automated pollution control systems.

1.9 References:

[1] B. Mekuye, B. Abera, Nanomaterials: An overview of synthesis, classification, characterization, and applications, Nano Sel. 4 (2023) 486–501.

[2] F. Faez, F.M.A. Altalbawy, P. Kanjariya, B.R. Sampangi Rama Reddy, H.M. Albert, S. Ray, R. Kalia, S. Saydaxmetova, A. Sinha, Enhancing the H_2S and SO_2 sensing capabilities of WS_2 nanosheets by transition metal (Mo, Nb, Zr) adsorption: A DFT study, Comput. Theor. Chem. 1253 (2025) 115450.

[3] R.P. Sedhain, G.C. Kaphle, structural and electronic properties of transition metal di-chalcogenides (MX_2) M=(Mo, W) and X=(S, Se) in bulk state: a first-principles study, J. Inst. Sci. Technol. 22 (2017) 41–50.

[4] H.J. Lee, M. Choe, W. Yang, S.W. Lee, Y.J. Park, H. Hwang, M. Chhowalla, Z. Lee, H.S. Shin, Phase-Engineered WS_2 Monolayer Quantum Dots by Rhenium Doping, ACS Nano. 17 (2023) 25731–25738.

[5] Li, Guoqing, et al. "All the catalytic active sites of MoS_2 for hydrogen evolution." Journal of the American Chemical Society 138 (2016) 16632-16638.

[6] J. Chen, N. Kuriyama, H. Yuan, H. T. Takeshita, and T. Sakai, "Electrochemical hydrogen storage in MoS_2 nanotubes," Journal of the American Chemical Society, 123 (2001) 11813-11814.

[7] M. Bougouma, A. Batan, B. Guel, T. Segato, J.B. Legma, F. Reniers, M.P. Delplancke-Ogletree, C. Buess-Herman, T. Doneux, Growth and characterization of large, high quality $MoSe_2$ single crystals, J. Cryst. Growth. 363 (2013) 122–127.

[8] Aneesha, N. Ohta, M.S. Mehata, In situ synthesis of WS_2 QDs for sensing of H_2O_2: Quenching and recovery of absorption and photoluminescence, Mater. Today Commun. 34 (2023) 105013.

[9] M.S. Mehata, Aneesha, Selectively probing ferric ions in aqueous environments using protonated and neutral forms of 7-azaindole as a multiparametric chemosensor, Photochem. Photobiol. Sci. 22 (2023) 1505–1516.

[10] A.A. Adul-Rasool, D.M. Athair, H.K. Zaidan, A.M. Rheima, Z.T. Al-Sharify, S.H. Mohammed, E. kianfar, 0,1,2,3D nanostructures, types of bulk nanostructured materials, and drug nanocrystals: An overview, Cancer Treat. Res. Commun. 40 (2024) 100834.

[11] M. Kaur, S.K. Mehta, S.K. Kansal, Nitrogen doped graphene quantum dots: Efficient fluorescent chemosensor for the selective and sensitive detection of 2,4,6-trinitrophenol, Sensors Actuators, B Chem. 245 (2017) 938–945.

[12] F. Cai, X. Liu, S. Liu, H. Liu, Y. Huang, A simple one-pot synthesis of highly fluorescent nitrogen-doped graphene quantum dots for the detection of Cr(vi) in aqueous media, RSC Adv. 4 (2014) 52016–52022.

[13] H. Lee, J. Ahn, S. Im, J. Kim, W. Choi, High-Responsivity Multilayer $MoSe_2$ Phototransistors with Fast Response Time, Sci. Rep. 8 (2018) 1–7.

[14] I. Jain, "Hydrogen the fuel for 21st century," International journal of hydrogen energy, 34 (2009) 7368-7378.

[15] E. Lee, A. Vahidmohammadi, B.C. Prorok, Y.S. Yoon, M. Beidaghi, D.J. Kim, Room Temperature Gas Sensing of Two-Dimensional Titanium Carbide (MXene), ACS Appl. Mater. Interfaces. 9 (2017) 37184–37190.

[16] C.Y. Hsu, A.M. Rheima, Z. sabri Abbas, M.U. Faryad, M.M. Kadhim, U.S. Altimari, A.H. Dawood, A. dhari jawad al-bayati, Z.T. Abed, R.S. Radhi, A.S. Jaber, S.K. Hachim, F.K. Ali, Z.H. Mahmoud, G. Behzadi pour, E. Kianfar, Nanowires Properties and Applications: A Review Study, South African J. Chem. Eng. 46 (2023) 286–311.

[17] L. Jin, C. Wu, K. Wei, L. He, H. Gao, H. Zhang, K. Zhang, A.M. Asiri, K.A. Alamry, L. Yang, X. Chu, Polymeric Ti3C2T xMXene Composites for Room Temperature Ammonia Sensing, ACS Appl. Nano Mater. 3 (2020) 12071–12079.

[18] Aneesha, M.S. Mehata, Waterborne explosives: A rapid detection method using $MoSe_2$ quantum dots, Mater. Res. Bull. 185 (2025) 113287.

[19] Pataniya, Pratik M., and C. K. Sumesh. "MoS_2 nanosheets on Cu-foil for rapid electrocatalytic hydrogen evolution reaction." Journal of Electroanalytical Chemistry 912 (2022)116270.

[20] E.D. Hanson, L.M. Lilley, J.D. Cain, S. Hao, E. Palacios, K. Aydin, C. Wolverton, T. Meade, V.P. Dravid, Phase engineering and optical properties of 2D $MoSe_2$: Promise and pitfalls, Mater. Chem. Phys. 225 (2019) 219–226.

[21] M.S. Mehata, Reusable fluorescent WS_2 QDs sensor for ultralow-level detection of Cr^{6+} in real water samples, Mater. Today Commun. 49 (2025) 114183.

[22] X. Zhou, H. Sun, X. Bai, Two-Dimensional Transition Metal Dichalcogenides: Synthesis, Biomedical Applications and Biosafety Evaluation, Front. Bioeng. Biotechnol. 8 (2020) 1–13.

[23] M.O. Valappil, A. Anil, M. Shaijumon, V.K. Pillai, S. Alwarappan, A Single-Step Electrochemical Synthesis of Luminescent WS_2 Quantum Dots, Chem. - A Eur. J. 23

(2017) 9144–9148.

[24] S.M. Saleh, R. Ali, A. Algreiby, B. Alfeneekh, I.A.I. Ali, A novel organic chromo-fluorogenic optical sensor for detecting chromium ions, Heliyon. 10 (2024) 37480.

[25] S. Kumar, A. Mirzaei, A. Kumar, M. H. Lee, Z. Ghahremani, T.-U. Kim*, et al.*, "Nanoparticles anchored strategy to develop 2D MoS_2 and $MoSe_2$ based room temperature chemiresistive gas sensors," Coordination Chemistry Reviews, 503 (2024) 215657.

[26] R. Lv, J.A. Robinson, R.E. Schaak, D. Sun, Y. Sun, T.E. Mallouk, M. Terrones, Transition metal dichalcogenides and beyond: Synthesis, properties, and applications of single- and few-layer nanosheets, Acc. Chem. Res. 48 (2015) 56–64.

[27] Isha, Aneesha, M.S. Mehata, Synthesis of Graphene Quantum Dots (GQDs) from Paddy Straw for Bilirubin Detection Plasmonics 20 (2025), 2359–2366 .

[28] K. Kang, -Hyeok Yang, Synthesis of transition metal dichalcogenides, in: Synth. Model. Charact. 2D Mater. Their Heterostruct., Elsevier, 2020: pp. 247–264.

[29] Q. Zhang, L. Mei, X. Cao, Y. Tang, Z. Zeng, Intercalation and exfoliation chemistries of transition metal dichalcogenides, J. Mater. Chem. A. 8 (2020) 15417–15444.

[30] F. Creazzo, Engineering of $MoSe_2$ and WSe_2 Monolayers and Heterostructures by DFT-Molecular Dynamics Simulations, ACS Appl. Mater. Interfaces. 17 (2025) 39676–39693.

[31] Kapatel, Sanni, and C. K. Sumesh. "One pot sono-chemical synthesis of 2D layered MoS_2 nanosheets." AIP Conference Proceedings. 1 (2016) 1728.

[32] M. Choudhary, A. Shrivastav, A.K. Sinha, A.K. Chawla, D.K. Avasthi, K. Saravanan, S. Krishnamurthy, R. Chandra, S. Wadhwa, International Journal of Hydrogen Energy Emerging nanomaterials for hydrogen sensing : Mechanisms and prospects, Int. J. Hydrogen Energy. 77 (2024) 557–574.

[33] T. Fu, Sensing properties and mechanism of gas sensor for H_2S and NO_2 based on $[Cu_5(bipyO_2)_6Cl_8]Cl_2$, 123 (2007) 1113–1119.

[34] G. Eda, H. Yamaguchi, D. Voiry, T. Fujita, M. Chen, and M. Chhowalla, "Photoluminescence from chemically exfoliated MoS_2," Nano letters, 11 (2011) 5111-

5116.

[35] R. Kronberg, M. Hakala, N. Holmberg, and K. Laasonen, "Hydrogen adsorption on MoS $_2$-surfaces: A DFT study on preferential sites and the effect of sulfur and hydrogen coverage," Physical Chemistry Chemical Physics, 19 (2017), 16231-16241.

[36] A. Garcia-Miranda Ferrari, R.D. Crapnell, P.S. Adarakatti, B.P. Suma, C.E. Banks, Electroanalytical overview: The detection of chromium, Sensors and Actuators Reports. 4 (2022) 100116.

[37] P. Sharma, M.S. Mehata, Colloidal MoS_2 quantum dots based optical sensor for detection of 2,4,6-TNP explosive in an aqueous medium, Opt. Mater. (Amst). 100 (2020) 109646.

[38] L. Ma, D. N. Nath, E. W. Lee, C. H. Lee, M. Yu, A. Arehart*, et al.*, "Epitaxial growth of large area single-crystalline few-layer MoS_2 with high space charge mobility of 192 cm^2 V^{-1} s^{-1}," Applied Physics Letters, 105, 2014.

[39] A.K. Mia, M. Meyyappan, P.K. Giri, Two-Dimensional Transition Metal Dichalcogenide Based Biosensors: From Fundamentals to Healthcare Applications, Biosensors. 13 (2023) 1–28.

[40] V. Saini, A. Gupta, K. Rangan, B. Khungar, A selective turn-off fluorescence detection of nitroexplosive 2,4,6-trinitrophenol by pyridinium-based chemosensor in pure aqueous medium, Dye. Pigment. 180 (2020) 108447.

[41] R. Narciso Pedrosa, C.E.P. Villegas, A. Reily Rocha, R.G. Amorim, W. Scopel, Interlayer Excitons and Radiative Lifetimes in $MoSe_2$/SeWS Bilayers: Implications for Light-Emitting Diodes, ACS Appl. Nano Mater. 8 (2025) 5051–5058.

[42] C. Yim, M. O'Brien, N. McEvoy, S. Riazimehr, H. Schäfer-Eberwein, A. Bablich, et al., "Heterojunction hybrid devices from vapor phase grown MoS_2," Scientific reports, 4 (2014) 5458.

[43] I. Ijaz, E. Gilani, A. Nazir, A. Bukhari, Detail review on chemical, physical and green synthesis, classification, characterizations and applications of nanoparticles, Green Chem. Lett. Rev. 13 (2020) 59–81.

[44] D. Marinov, J.-F. de Marneffe, Q. Smets, G. Arutchelvan, K. M. Bal, E. Voronina*, et al.*, "Reactive plasma cleaning and restoration of transition metal dichalcogenide

monolayers," npj 2D Materials and Applications, vol. 5, 17, 2021.

[45] U. J. Cho, D. Jang, Y. Jeon, T. Kim, B. Jo, R. Kim, et al., "A Palladium-Deposited Molybdenum Disulfide-Based Hydrogen Sensor at Room Temperature," Applied Sciences 13 (2023)10594.

Chapter 2

Experimental Methodology – Synthesis and Characterization

This chapter describes the experimental procedures adopted for the synthesis of MoS_2 thin films, their subsequent sulfurization, and the detailed characterisation techniques used to analyse their structural and sensing properties. The methodology has been carefully designed to achieve high-quality, uniform, and reproducible films suitable for gas sensing applications.

2.1 Preparation of Mo films

The electron beam evaporation (e-beam) deposition method was employed for preparation of high-quality Mo thin films by using Mo target on Si/SiO_2 substrate. The key advantages of this technique lie in its ability to produce high-purity Mo films with excellent control over thickness and microstructure, making it indispensable in various industries ranging from electronics to thin-film coatings and beyond [1,2]. At first, the substrates were cleaned with trichloroethylene followed by acetone, and alcohol to remove contaminations and native oxide. The base vacuum of the order of 2×10^{-6} mbar was maintained with the help of rotary vane and turbo-molecular pump. The deposition rate is kept at a slow rate of 0.7 – 0.8 nm/sec for the uniformed and to achieve desired thickness. Three different thicknesses (5 nm, 10 nm, 20 nm) of Mo film were obtained by keeping the same deposition rate. The film deposited at the RT having black color which may be due to oxygen deficiency and a large number of defects. Therefore, these films were further annealed in oxygen ambient at temperature of 400 °C for duration of 1 hour. After annealing, the color of films changed and they become totally transparent [3-5].

2.2 Sulfurization of Mo films

Sulfurization of Mo films is a fundamental process to transform deposited molybdenum (Mo) thin films into two-dimensional molybdenum disulfide (MoS_2) layers. For this purpose, a double zone chemical vapor deposition (CVD) method was employed for the sulfurization. The sulfurization of thin film of 20 nm thickness were grown on Si/SiO_2 substrates via double zone sulfurization using an ambient-pressure CVD technique as shown in Fig. 2.1. Flushing of the quartz tube using Argon gas stream, followed by continuous Ar flow for 15 min, was performed. This reduces the oxygen content in the reactor prior to the sulfurization process. Before the experiment, a quartz boat containing 1.0 gm Sulphur powder (Sigma Aldrich, 99.999%) was placed upstream in the heating ring, and the Si/SiO_2 substrate covered with pre-exfoliated Mo film was placed face up on another quartz boat and located in the middle of the tubular furnace, as shown in Fig. 2.1. The distance between the two quartz boats is about 150 mm.

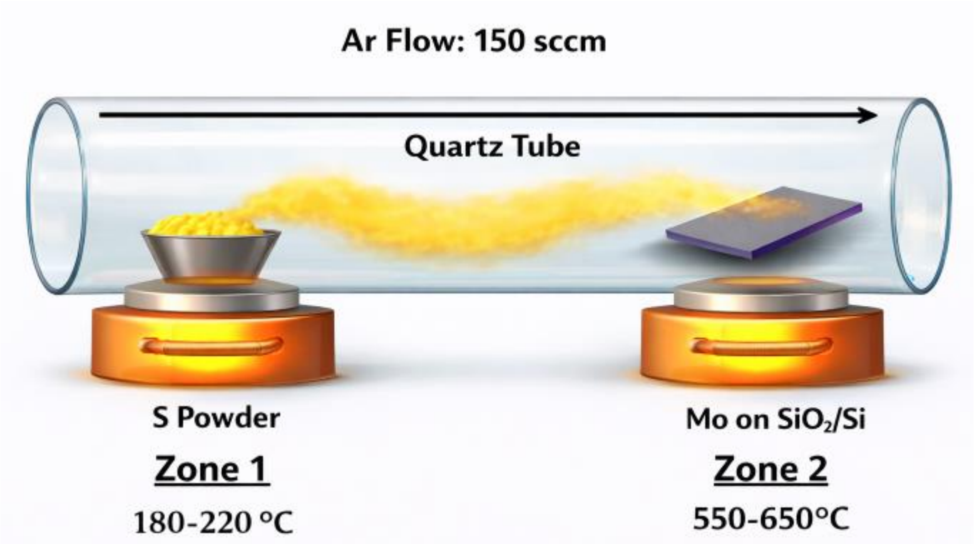

Figure 2.1: Sulfurization of Mo films using double zone CVD technique.

After that, the tubular furnace was heated to 600 °C at a rate of 20 °C/min. When the temperature of the tubular furnace rose to 470 °C, the Sulphur powder was heated to 200 °C through the heating ring at a rate of 20 °C/min. During this process, the Ar flow rate remained at 80 SCCM. After the growth time of 30 min, the furnace was cooled down naturally to room temperature with Ar flow of 100 SCCM.

2.3 Designing and Fabrication of Gas Sensor Platform

The 0.5 mm thick alumina substrate was used to create the gas sensor platform. The electrode pattern was made of metallic Molybdenum (Mo) with a layer thickness of 200 nm. Sputter deposition was used to deposit a thin layer of molybdenum (Mo). The electrode pattern was defined using a physical mask. The spacing was kept at 300 μm, and the electrode line width was 300 μm. The heating element (resistor) and gas sensor electrode were combined into a single device platform. The dimensions of the sensor die were 3.0 mm by 3.0 mm. For gas sensing, the sensor was installed on the header of the customised transistor outline (TO) packages. After process parameters optimization, gas sensing layer (MoS_2) was coated on the interdigital transducer electrodes (IDT). Humidity strongly influences Chemiresistive gas sensing by competing with target gas molecules for surface adsorption sites. In this study, sensing measurements were conducted under controlled dry air conditions to suppress humidity-related interference and to isolate the intrinsic interaction between NO_2 molecules and the MoS_2 sensing layer, thereby enabling clear evaluation of temperature-dependent sensing behaviour. The schematic and optical image of the MoS_2 gas sensor device shown in Fig. 2.2.

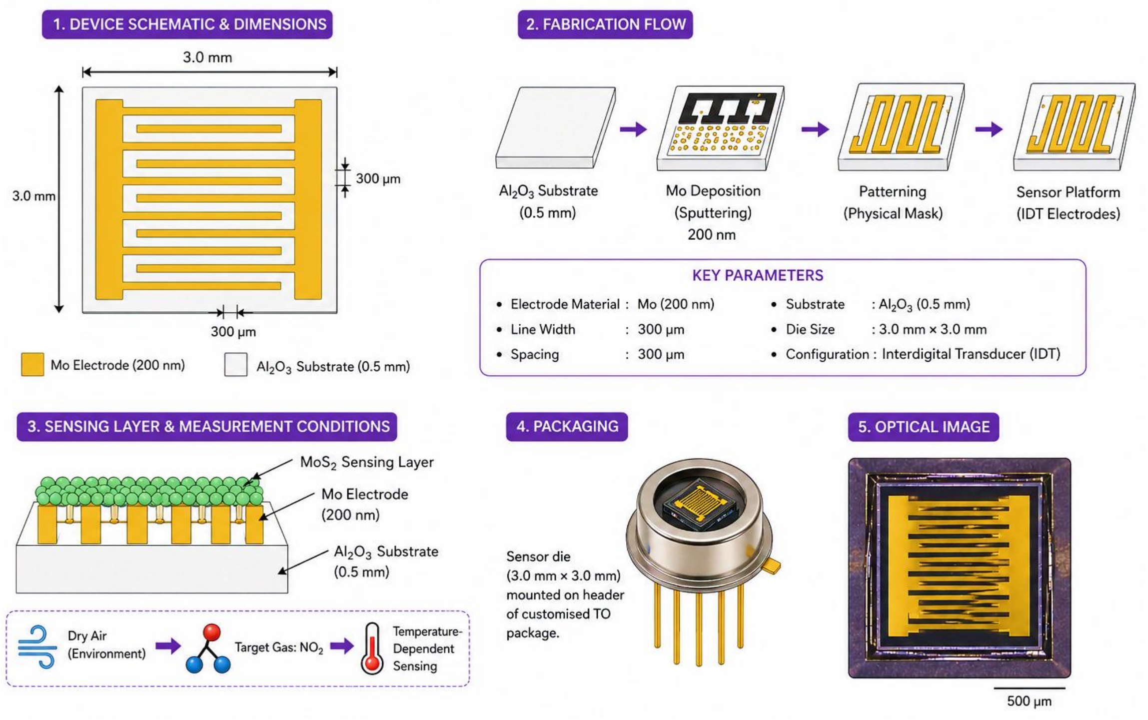

Figure 2.2: Schematic and optical image of the MoS_2 gas sensor device showing the interdigitated electrodes used for resistance measurements and the integrated micro-heater for temperature control.

2.4 Preparation of MoS_2 films:

Fig. 2.3 shows the schematic of three-zone tubular chemical vapour deposition furnace used to deposit the MoS_2 thin film on the alumina substrate having dimensions of 3.0 mm by 3.0 mm. The thickness of MoS_2 film was kept ~20 nm to ensure continuous film coverage, high crystallinity, and stable electrical contact with the interdigitated electrodes, while maintaining reliable controllability of the CVD growth process. We have also deposited thinner films (5 nm and 10 nm) which displayed discontinuity and increased contact resistance that were not found suitable for sensing applications. Similarly, thicker films can reduce surface sensitivity due to dominant bulk conduction pathways. Before deposition, the alumina substrate was first ultrasonically cleaned with acetone and isopropyl alcohol (IPA), and then gaseous nitrogen was used to dry it. An extra cleaning procedure was performed prior to the alumina substrate being put into the CVD furnace's middle zone. The quartz boat was filled with high purity (99.999 %) of molybdenum trioxide (MoO_3) and the alumina boat was filled with high purity (99.995 %) sulfur procured from the Sigma Aldrich. The three zones for alumina are kept at 800 °C for the substrate, 650 °C for MoO_3, and 200 °C for sulfur. High-purity Ar gas flowed with a mass flow controller (MFC) at 200 sccm during the growth process [6-8].

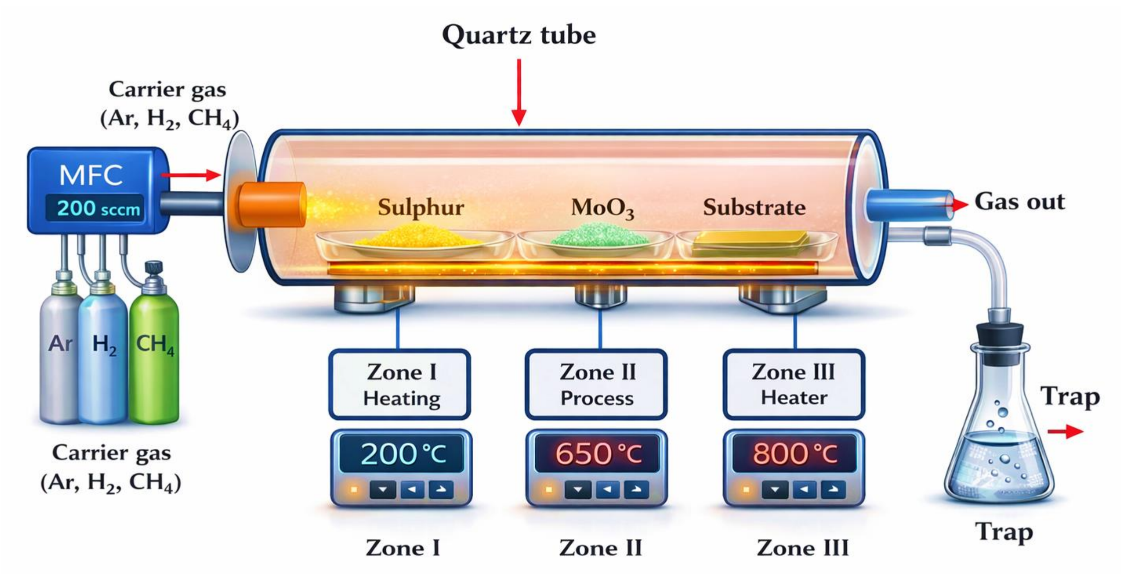

Figure 2.3: Synthesis of MoS_2 films using the three-zone chemical vapour deposition technique.

2.5 X-ray Diffraction (XRD) Technique

XRD is one of the most widely used and powerful characterisation techniques for analysing the structural properties of crystalline materials. It provides detailed information about crystal structure, phase composition, crystallite size, lattice parameters, strain, and degree of crystallinity. Due to its non-destructive nature and high accuracy, XRD has become an essential tool in materials science, nanotechnology, and solid-state physics. The origin of XRD can be traced back to the early 20th century, when pioneering contributions by scientists such as Debye, Scherrer, and Hull established the foundation of powder diffraction techniques. These early developments enabled the understanding of diffraction patterns obtained from polycrystalline materials and laid the groundwork for modern crystallographic analysis. Over the years, XRD has undergone significant advancements, particularly with the integration of computational methods. A major breakthrough in this field was the introduction of the Rietveld refinement method, which allows full-pattern fitting of diffraction data using computer-based algorithms. This approach has greatly enhanced the accuracy of structural analysis and made it possible to interpret complex diffraction patterns with high precision. In contemporary research, XRD is not only used for basic phase identification but also for advanced structural investigations, including the analysis of nanoscale materials, defect structures, and microstrain [9,10]. The evolution of X-ray diffraction from its early use in simple diffraction experiments to its current role in sophisticated structural modeling reflects the remarkable advancements achieved in this technique over the past century. Initially, XRD was primarily employed for basic phase identification and determination of crystal structures using relatively simple analytical approaches. However, with the development of advanced instrumentation, improved detectors, and powerful computational methods, XRD has transformed into a highly precise and versatile tool for detailed structural analysis. Modern techniques, such as Rietveld refinement and whole-pattern fitting, allow accurate modeling of complex crystal systems, including nanostructured and multi-phase materials. These advancements have significantly enhanced the ability to extract detailed information about lattice parameters, crystallite size, strain, and atomic arrangements. Consequently, X-ray diffraction has become an indispensable technique in materials science, enabling comprehensive understanding and precise characterization of a wide range of materials [8-10].

2.5.1 Generation of X-rays

X-rays used in diffraction studies are generated using a specially designed X-ray tube, which operates under high vacuum conditions. These electromagnetic radiations typically lie in the wavelength range of 0.1 Å to 100 Å, however, for crystallographic investigations, X-rays in the range of ~0.5 Å to 2.5 Å are most suitable, as they are comparable to the interatomic spacing in crystalline materials. The X-ray tube primarily consists of two main components: a cathode and an anode, enclosed within a vacuum chamber. The cathode generally comprises a tungsten filament, which emits electrons when heated through the process of thermionic emission. When a high potential difference (typically 30–60 kV) is applied between the cathode and the anode, these emitted electrons are accelerated toward the anode target with high kinetic energy. The anode is usually made of copper, and when the high-energy electrons strike its surface, they transfer their energy to the atoms of the target material. This interaction leads to the ejection of inner-shell electrons (K-shell) from the copper atoms, creating vacancies. Electrons from higher energy levels (such as L or M shells) subsequently transition to fill these vacancies, resulting in the emission of characteristic X-rays [11-13,14].

The emitted X-rays consist mainly of two prominent lines, namely CuK_{α} and CuK_{β}, with wavelengths of approximately 1.54 Å and 1.39 Å, respectively. For diffraction analysis, it is essential to obtain monochromatic radiation. This ensures accurate and reliable diffraction measurements. For precise X-ray diffraction analysis, it is therefore essential to utilize monochromatic radiation, which ensures that the diffraction peaks correspond to a single wavelength. To achieve this, a nickel filter is commonly incorporated into the XRD setup. The nickel filter selectively absorbs the higher-energy CuKβ radiation due to its suitable absorption edge, while allowing the CuKα radiation to pass through with minimal attenuation. As a result, the incident X-ray beam becomes effectively monochromatic, consisting predominantly of CuKα radiation with a wavelength of approximately 1.5406 Å [3-9].

The use of monochromatic radiation significantly improves the accuracy and reliability of diffraction measurements. It enhances peak sharpness and resolution, enabling precise determination of diffraction angles and interplanar spacings. Furthermore, it minimizes errors in peak indexing and phase identification, which are critical for structural analysis. The elimination of unwanted spectral components also ensures better signal-to-noise ratio, leading to more consistent and reproducible results. Therefore, the use of a nickel filter to isolate the CuKα line is a crucial step in obtaining high-quality diffraction data for detailed crystallographic investigations.

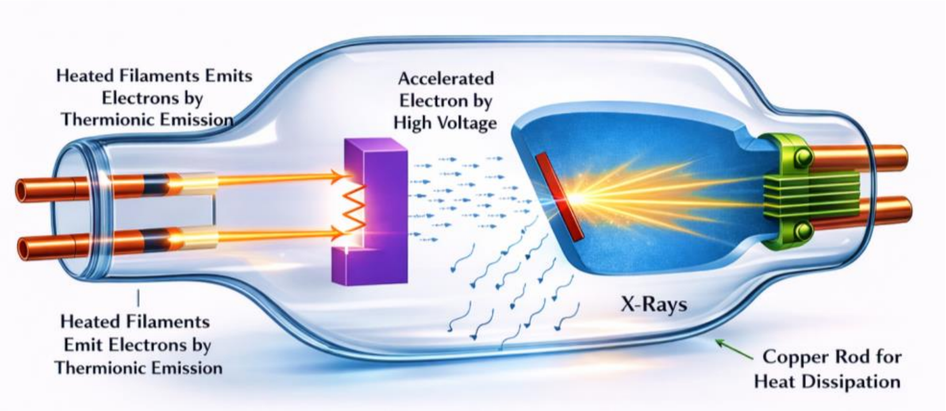

Figure 2.4: Schematic representation of the generation of X-rays in an X-ray tube.

The generated X-ray beam is then directed toward the sample, where it interacts with the crystal lattice and produces diffraction patterns that can be analysed to extract structural information as represented by Fig. 2.4.

2.5.2 Principle of X-ray Diffraction and Bragg's Law

The fundamental principle of X-ray diffraction is based on the interaction of incident X-rays with the periodic arrangement of atoms in a crystalline material. When a monochromatic X-ray beam is directed onto a crystal, it is scattered by the electrons present in the atoms. Due to the regular arrangement of atoms in the crystal lattice, these scattered waves can interfere with each other, leading to the formation of a diffraction pattern. In a crystalline solid, atoms are arranged in parallel planes separated by a definite interplanar spacing denoted by d. When X-rays strike these planes at a specific angle, they are reflected from successive atomic layers. The path difference between the reflected waves determines whether the interference will be constructive or destructive [16,17]. Constructive interference occurs when the path difference between the reflected X-rays is equal to an integral multiple of the wavelength of the incident radiation. This condition gives rise to intense diffraction peaks and is mathematically expressed by Bragg's Law (Fig. 2.5):

$2d\mathrm{Sin}\theta = n\lambda$ where,

d = interplanar spacing

θ = angle of incidence (Bragg angle)

λ = wavelength of incident X-rays

n = order of diffraction (integer)

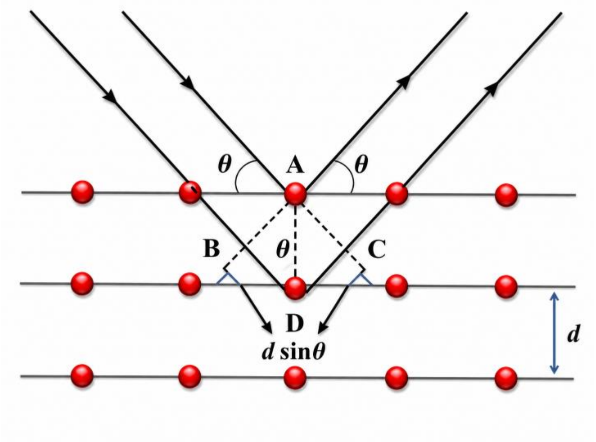

Figure 2.5: Schematic representation of the diffraction of X-rays obeying Bragg's law.

This relationship defines the condition under which diffraction maxima are observed. Only those planes that satisfy Bragg’s condition contribute to the diffraction pattern, resulting in peaks at specific angular positions.

It is important to note that X-ray diffraction can occur only when the wavelength of the incident radiation is comparable to or smaller than twice the interplanar spacing of the crystal lattice, satisfying the condition $\lambda \leq 2$ d. This requirement ensures that the incident X-rays are capable of interacting effectively with the periodic arrangement of atoms within the crystal. When this condition is fulfilled, constructive interference takes place at specific angles, leading to the formation of well-defined diffraction peaks. The angular positions of these diffraction peaks are directly related to the spacing between crystallographic planes and are governed by Bragg’s law. Therefore, analysis of peak positions allows precise determination of lattice parameters, crystal structure, and phase identification of the material. In addition to peak positions, the intensity of the diffraction peaks carries significant information about the internal arrangement of atoms within the crystal. Factors such as atomic scattering power, distribution of atoms within the unit cell, and crystal symmetry influence the observed intensity patterns. Moreover, variations in peak intensity and shape can also provide insights into crystallinity, preferred orientation (texture), and the presence of defects or strain within the material. By carefully analyzing both the angular positions and intensities of the diffraction peaks, a comprehensive understanding of the structural characteristics of the material can be achieved. Thus, X-ray diffraction serves as a powerful tool for extracting detailed crystallographic information, enabling accurate evaluation of material properties at the atomic level [4,5].

2.5.3 Data Acquisition and Analysis

In the present work, XRD measurements were performed using a Bruker D8 Advance diffractometer equipped with a CuK_α radiation source ($\lambda \approx 1.5406$ Å). The data were collected at room temperature using a step scanning method over a 2θ range of 10°-60°, with a step size of 0.02° and an appropriate scan rate. The obtained diffraction patterns were analyzed by comparing the peak positions with standard reference data available in the JCPDS (Joint Committee on Powder Diffraction Standards) database. This comparison enabled phase identification and confirmation of the formation of MoS_2 structures. Furthermore, peak positions, intensities, and widths were carefully analyzed to evaluate crystallinity, structural quality, and possible lattice distortions in the synthesized films.

2.5.4 In situ XRD setup

It was used to probe the structural properties of the as prepared and hydrogenated MoS_2 films. XRD patterns have been recorded using Bruker AXS D8 Advanced in-situ XRD facility equipped with Cu K_α source with wavelength 1.54 Å (40 kV and 40 mA power). The *in-situ* XRD setup has provision for creation of high vacuum using rotary vane pump and turbo-molecular pump [4]. A gas injection facility is also integrated to injection the H_2 gas in the controlled manner which allows us to record diffraction pattern in the controlled gas atmosphere. A schematic diagram of the *in-situ* XRD setup is shown in the Fig. 2.6. First, the MoS_2 films were mounted on sample holder and a high vacuum order of $1x10^{-5}$ mbar was created. After that, diffraction pattern of the MoS_2 films was recorded in the vacuum. Now, MoS_2 films was exposed to different concentrations of H_2 gas (3 %) mixed with noble gas Argon (Ar), one by one after different intervals of pressure ranging from 50 mbar to 900 mbar and diffraction pattern of the same sample is recorded after each pressure without changing position of sample. Since, all diffraction patterns are recorded on the same sample so effect of the sample-to-sample variation is ruled out [19,20]. This process also allows us to compare of intensity of the diffraction peaks with change in the pressure of the H_2 gas. The data were recorded in locked coupled mode in the scan range of 2θ from 10° to 60° with step size of 0.02° at a scan speed of 0.25°/min.

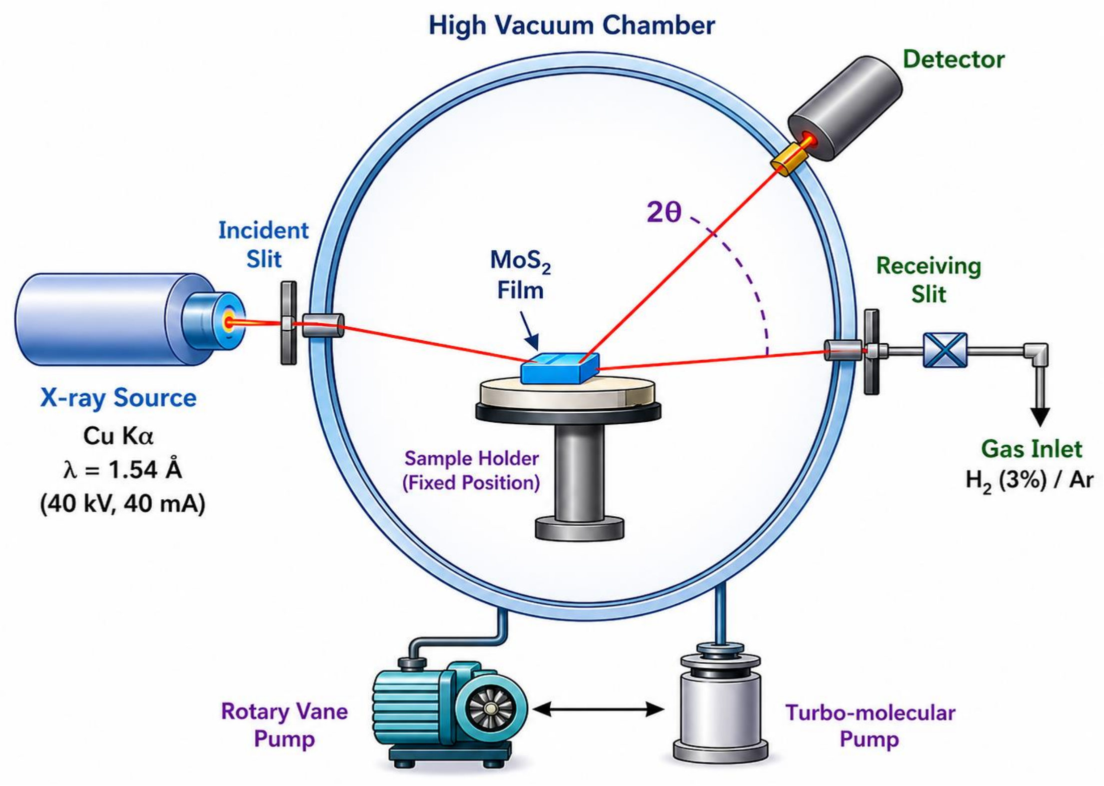

Figure 2.6: Schematic representation of the in-situ XRD setup.

2.6 Field Emission Scanning Electron Microscopy (FESEM)

Field Emission Scanning Electron Microscopy (FESEM) is a highly advanced surface characterization technique that is extensively utilized for examining the morphology and microstructural features of materials at the nanoscale. It enables the acquisition of high-resolution images by employing a finely focused beam of high-energy electrons instead of visible light, thereby overcoming the resolution limitations associated with optical microscopy. The interaction of this electron beam with the sample surface generates various signals that can be used to construct detailed images, allowing precise visualization of surface topography, grain boundaries, particle size distribution, and nanoscale features. One of the key advantages of FESEM over conventional scanning electron microscopy (SEM) lies in the use of a field emission electron source, which produces a highly coherent and intense electron beam with a very narrow energy distribution. This results in superior spatial resolution, improved depth of field, and enhanced image contrast. The finely focused electron probe enables the observation of extremely small features, often down to sub-nanometer scales, making FESEM particularly suitable for the analysis of nanostructured materials. In addition, the reduced beam divergence minimizes electrostatic distortions, leading to sharper and more accurate imaging of delicate structures. FESEM is especially effective for studying a wide range of advanced materials, including thin films, nanocomposites, quantum dots, and two-dimensional layered materials such as MoS_2. These materials often exhibit complex surface morphologies and nanoscale features that require high-resolution imaging techniques for proper characterization. The ability of FESEM to provide detailed surface information makes it an indispensable tool for understanding growth mechanisms, surface roughness, defect formation, and structural uniformity. Furthermore, FESEM is considered a non-destructive technique, as it requires minimal sample preparation and does not significantly alter the intrinsic properties of the material under investigation. This allows repeated measurements and reliable analysis without compromising sample integrity. Due to its versatility and high performance, FESEM is widely employed across various scientific disciplines, including materials science, nanotechnology, and semiconductor research. It plays a crucial role in analyzing surface features, evaluating film quality, identifying microstructural defects, and correlating morphological characteristics with functional properties of materials [21-23].

2.6.1 Working Principle of FESEM

The working principle of Field Emission Scanning Electron Microscopy (FESEM) is fundamentally based on the interaction of a highly energetic and finely focused electron beam with the surface of a specimen. In this technique, electrons are generated from a field emission gun (FEG), which operates under a strong electric field to extract electrons from a sharp metallic tip through quantum tunneling. These emitted electrons are then accelerated toward the sample surface under a high potential difference, typically in the range of several kilovolts, resulting in a high-energy electron beam. The accelerated electron beam is subsequently directed and focused into an extremely fine probe using a series of electromagnetic lenses and apertures. These lenses precisely control the trajectory and convergence of the electron beam, enabling it to achieve a very small spot size with high brightness and coherence. The focused beam is then scanned systematically across the surface of the specimen in a raster pattern using scanning coils, allowing point-by-point interaction with the material. When the incident electron beam interacts with the atoms present on the sample surface, a variety of signals are generated as a result of complex electron–matter interactions. These signals include secondary electrons, backscattered electrons, and characteristic X-rays, each providing unique and complementary information about the sample. Secondary electrons, which are low-energy electrons emitted from the near-surface region, are primarily used for imaging surface morphology with high spatial resolution. Backscattered electrons, produced due to elastic scattering with atomic nuclei, provide compositional contrast based on the atomic number of the elements present. Characteristic X-rays, generated through electronic transitions within atoms, enable elemental analysis when detected using energy-dispersive spectroscopy (EDX). The combined analysis of these emitted signals allows FESEM to provide detailed insights into both the surface structure and compositional characteristics of the material. This makes FESEM an indispensable tool for high-resolution imaging and microstructural analysis of advanced materials. Among these, secondary electrons (SE) are most commonly used for imaging surface morphology because they originate from the top few nanometers of the sample and provide high-resolution surface details. The intensity of these emitted electrons is collected by detectors and converted into an image, which reflects the surface structure of the material. The entire system operates under high vacuum conditions to prevent scattering of electrons by air molecules and to ensure accurate signal detection [24,25]. The resolution of FESEM is mainly governed by the diameter of the electron beam and the efficiency of electron emission, which is significantly enhanced in field emission sources (Fig. 2.7).

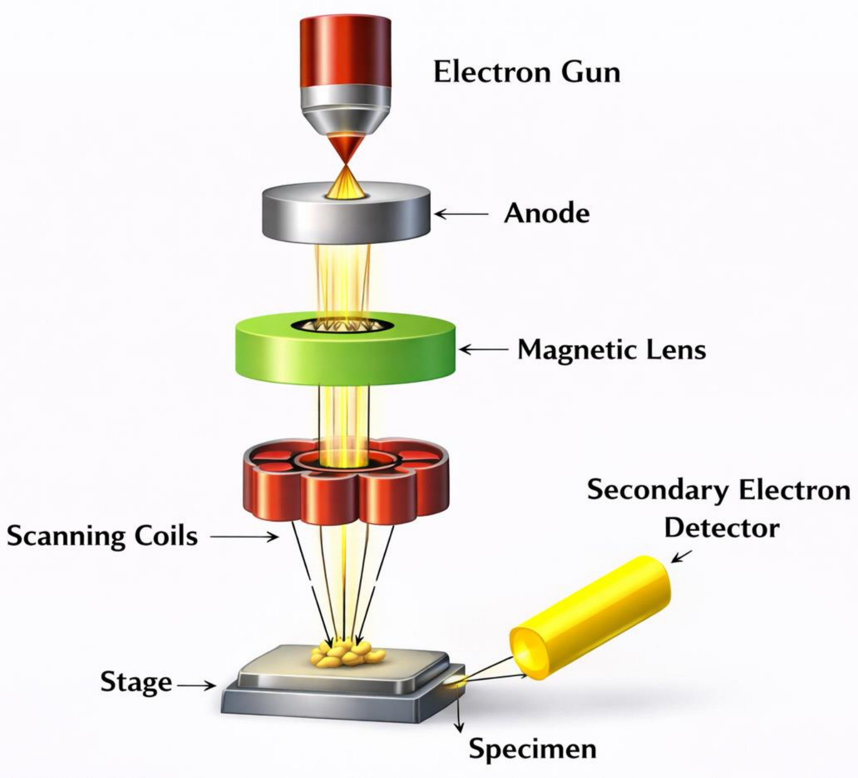

Figure 2.7: Schematic representation of FESEM instrumentation setup.

2.6.2 Electron-Matter Interaction in FESEM

The interaction between the incident electron beam and the specimen in FESEM is a complex process that results in the generation of multiple types of signals. Each of these signals carries distinct information about the surface and compositional characteristics of the material. As illustrated in Fig. 2.X, the primary interaction leads to the emission of secondary electrons, backscattered electrons, characteristic X-rays, and Auger electrons. When the high-energy primary electron beam strikes the sample surface, it transfers energy to the loosely bound outer-shell electrons of the atoms. If this transferred energy exceeds the binding energy, these electrons are ejected from the surface and are known as secondary electrons (SE). Due to their low kinetic energy and limited escape depth, secondary electrons originate from the near-surface region of the specimen. As a result, they provide highly detailed information about surface morphology and are primarily used for high-resolution topographical imaging [26,27].

In addition to secondary electrons, backscattered electrons (BSE) are also generated as a result of elastic interactions between the incident electrons and the atomic nuclei of the specimen. These electrons are scattered back toward the detector with relatively higher energy. The intensity of the backscattered electron signal strongly depends on the atomic number (Z) of the elements present in the sample. Materials with higher atomic numbers produce a stronger BSE signal, enabling compositional contrast imaging. This makes BSE imaging particularly useful for distinguishing different phases in multi-component or heterogeneous materials.

Another important signal generated during electron–matter interaction is characteristic X-ray radiation. This occurs when primary electrons displace inner-shell electrons from atoms in the specimen, creating vacancies. Electrons from higher energy levels subsequently fill these vacancies, releasing energy in the form of X-ray photons with element-specific energies. These characteristic X-rays are analyzed using energy-dispersive X-ray spectroscopy (EDX), allowing both qualitative and quantitative elemental analysis of the material (Fig. 2.8).

In addition, Auger electrons are produced through a process similar to X-ray emission. However, instead of emitting an X-ray photon, the energy released during electronic transitions is transferred to another electron, which is then emitted from the atom. Auger electrons are highly surface-sensitive and provide valuable information about the elemental composition of the topmost atomic layers [28-30]. When combined with X-ray analysis, they enhance the overall accuracy of compositional characterization.

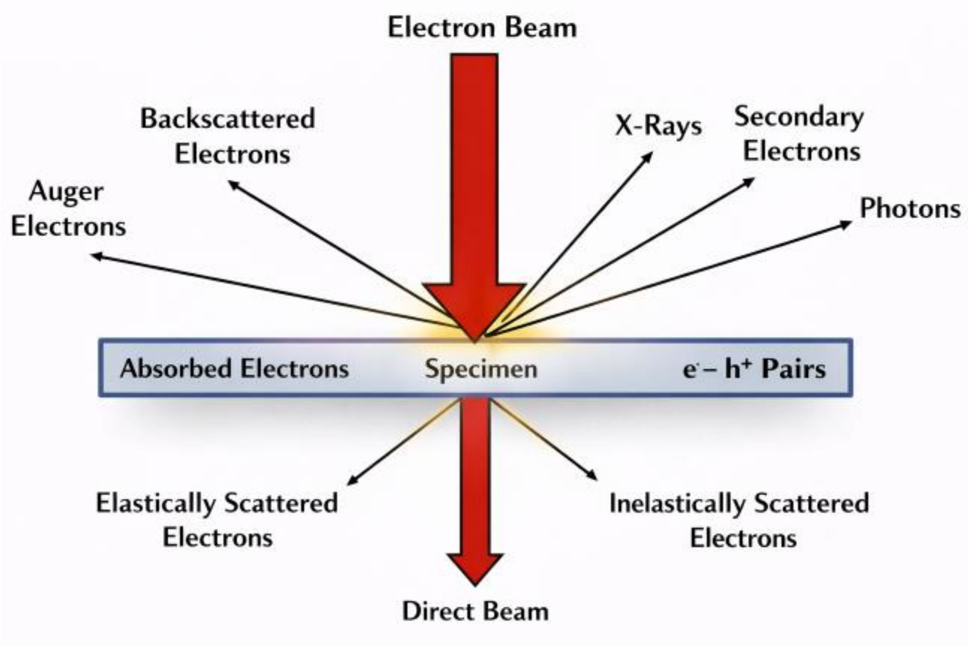

Figure 2.8: Interaction of electrons with the specimen in FESEM.

2.6.3 Advantages and Applications of FESEM

Field Emission Scanning Electron Microscopy (FESEM) is a highly advanced and versatile characterization technique that enables detailed investigation of surface morphology and elemental composition at extremely high magnifications. It provides high-resolution imaging by utilizing a finely focused electron beam, allowing precise visualization of nanoscale features such as grain boundaries, particle distribution, and surface irregularities. One of the most significant advantages of FESEM is its ability to achieve exceptionally high spatial resolution, often reaching values as fine as ~0.5 nm, which makes it particularly suitable for studying nanostructured materials.

In addition to its superior resolution, FESEM offers an almost unlimited depth of field, which ensures that a larger portion of the sample surface remains in focus simultaneously. This feature is especially beneficial when analyzing samples with complex or uneven topographies, as it provides clear and well-defined images across varying surface heights. The enhanced depth of field, combined with high brightness and contrast, enables accurate interpretation of surface features without the need for extensive sample preparation. Furthermore, FESEM not only provides morphological information but also allows compositional analysis when integrated with detectors such as energy-dispersive X-ray spectroscopy (EDX). This capability makes it a powerful tool for correlating structural and elemental characteristics of materials. Due to these advantages, FESEM has become an indispensable technique in fields such as materials science, nanotechnology, and semiconductor research, where precise analysis of surface features at the nanoscale is essential. Compared to conventional scanning electron microscopy, FESEM offers superior imaging performance due to the use of a field emission source, which produces a highly focused and stable electron beam. This results in sharper images with enhanced contrast and significantly reduced electrostatic distortions. These features make FESEM particularly suitable for investigating nanoscale structures and surface characteristics with high precision. Due to its versatility, FESEM finds wide applications across various scientific and engineering disciplines. It is extensively used in physics for structural analysis of materials, in chemistry for studying surface reactions, in biology for high-resolution imaging of cellular structures, and in materials science for examining the morphology of advanced nanomaterials. Additionally, it plays a crucial role in electronics for microchip inspection and failure analysis. The combination of high resolution, compositional sensitivity, and imaging accuracy makes FESEM an indispensable tool in both academic research and industrial applications, where detailed understanding of micro- and nanoscale structures is essential.

2.6.4 FESEM Analysis in the Present Work

In the present study, the surface morphology of the synthesized nanomaterials was examined using a Zeiss Gemini SEM 500. This analysis provided valuable insights into the surface features, morphology, and structural uniformity of the prepared samples.

2.7 Atomic Force Microscopy (AFM)

AFM is a high-resolution surface characterization technique widely used to study the topography and surface properties of materials at the nanometer scale. Unlike electron microscopy techniques, AFM does not rely on electron beams but instead uses a sharp probe to scan the surface of a specimen. This makes it particularly suitable for analyzing both conductive and non-conductive materials without requiring complex sample preparation [31,32].

Atomic Force Microscopy (AFM) provides three-dimensional surface information with exceptionally high spatial resolution, enabling detailed investigation of surface roughness, grain size, and various nanoscale features. By scanning a sharp probe across the surface of a material, AFM can generate precise topographical maps that reveal subtle variations in height and texture at the nanometer or even sub-nanometer level. This capability makes it particularly useful for studying thin films, nanostructures, and layered materials, where surface characteristics play a critical role in determining functional properties.

In addition to topographical imaging, AFM can also provide quantitative information about surface parameters such as roughness, particle distribution, and grain boundaries. These measurements are essential for understanding growth mechanisms, surface uniformity, and the influence of morphology on material performance. Furthermore, AFM operates under ambient or controlled environmental conditions and does not require conductive coatings or extensive sample preparation, which preserves the intrinsic properties of the material. Due to its versatility and non-destructive nature, AFM has become an indispensable tool in nanoscience, materials research, and surface engineering. It is widely employed for characterizing a broad range of materials, including semiconductors, polymers, biological samples, and two-dimensional materials. Its ability to provide high-resolution, three-dimensional imaging along with quantitative surface analysis makes AFM a powerful technique for correlating surface morphology with physical and chemical properties in nanoscale materials research, and thin-film characterization, especially for studying layered materials such as MoS_2.

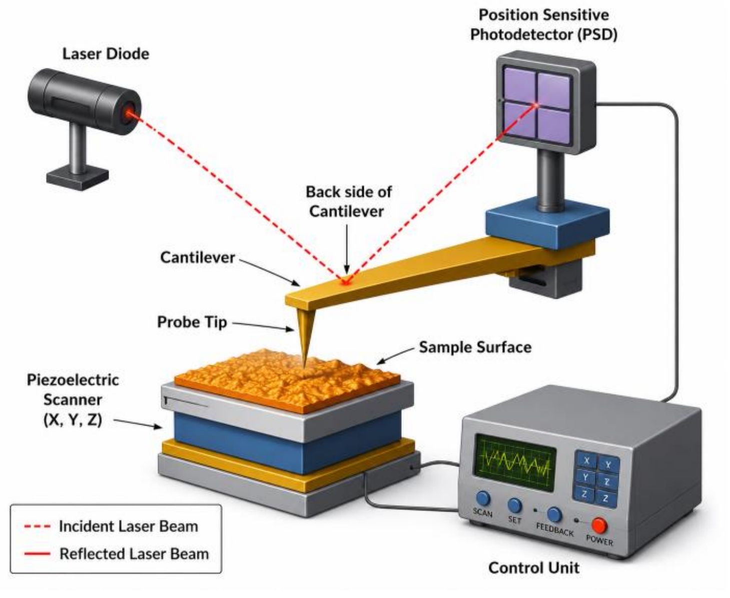

Figure 2.9: Instrumental set of Atomic Force Microscopy.

2.7.1 Working Principle of AFM

The working principle of Atomic Force Microscopy (AFM) is based on the interaction forces between a sharp probe tip and the surface of the sample. The core component of the AFM system is a microfabricated cantilever with an extremely sharp tip, typically having a radius of curvature in the nanometer range, positioned at its free end. This tip is brought very close to the sample surface and scanned across it in a controlled manner to probe surface features at the nanoscale. As the tip approaches the sample surface, various intermolecular forces come into play, including van der Waals forces, electrostatic interactions, capillary forces, and short-range repulsive forces. The nature and magnitude of these forces depend strongly on the distance between the tip and the sample. At relatively larger distances, attractive forces dominate, while at very small separations, repulsive forces become significant due to the overlap of electron clouds. These interaction forces cause the cantilever to deflect either upward or downward depending on whether the force is attractive or repulsive. The deflection of the cantilever is detected with high precision using an optical detection system. A laser beam is focused onto the back surface of the cantilever, and the reflected beam is directed onto a position-sensitive photodetector. Any minute deflection in the cantilever results in a corresponding shift in the position of the reflected laser spot on the detector. This shift is converted into an electrical signal, which is then processed to determine the surface profile of the sample. As the tip scans the surface in a raster pattern, the variations in cantilever deflection are continuously recorded and translated into a high-resolution three-dimensional image of the surface. This enables detailed mapping of surface morphology, roughness, and nanoscale features with exceptional accuracy. The precise control of tip–sample interaction, combined with sensitive detection of cantilever deflection, allows AFM to provide reliable and quantitative surface characterization.

As the probe tip scans the sample surface in a systematic raster pattern, the variations in cantilever deflection caused by tip–sample interactions are continuously monitored and recorded. These deflection signals are processed through a feedback control system, which adjusts the vertical position of the scanner to maintain a constant interaction force or oscillation amplitude, depending on the operating mode. The recorded data are then translated into a high-resolution topographical image that represents the three-dimensional surface profile of the sample. This imaging process enables precise mapping of surface features, including height variations, grain boundaries, and nanoscale structures, with exceptional accuracy. Due to its ability to detect extremely small changes in surface height, AFM can achieve spatial resolution at the nanometer and even sub-nanometer scale, making it a powerful tool for detailed surface characterization of advanced materials (Fig. 2.9).

Atomic Force Microscopy (AFM) can be operated in several distinct modes depending on the nature of the interaction between the probe tip and the sample surface, with each mode offering specific advantages for different types of materials and applications. In **contact mode**, the probe tip remains in continuous physical contact with the sample surface throughout the scanning process. The interaction forces between the tip and the surface cause deflections in the cantilever, which are directly translated into topographical information. While this mode provides high spatial resolution and is effective for hard surfaces, it can introduce significant lateral forces that may damage soft, fragile, or loosely bound nanostructures. Additionally, prolonged contact may lead to tip wear or sample deformation, limiting its applicability for delicate materials. In contrast, non-contact mode operates by oscillating the cantilever at a small distance above the sample surface without making direct contact. In this mode, the tip primarily experiences long-range attractive forces such as van der Waals interactions. The variations in these forces alter the oscillation amplitude or frequency of the cantilever, which is used to generate surface images. Non-contact mode is particularly advantageous for studying soft or sensitive materials, as it minimizes the risk of surface damage. However, due to weaker interaction forces, it may offer lower resolution and reduced signal strength compared to contact-based techniques. A more commonly employed and versatile mode is the tapping mode, also known as intermittent contact mode. In this mode, the cantilever oscillates at or near its resonance frequency, and the tip intermittently makes brief contact with the sample surface during each oscillation cycle. This significantly reduces lateral forces and minimizes friction between the tip and the sample, thereby preserving the integrity of both the tip and the specimen. Tapping mode provides a balance between high resolution and reduced sample damage, making it particularly suitable for imaging nanostructured materials, thin films, and biological samples. Furthermore, it allows simultaneous measurement of additional properties such as phase contrast, which can provide insights into material composition and mechanical properties.

Among these operational modes, tapping mode is most widely preferred for the characterization of nanomaterials due to its ability to deliver high-quality images while minimizing surface damage and deformation. Its adaptability and reliability make it an essential technique for accurate nanoscale surface analysis in advanced material systems.

2.7.2 Tip-Sample Interaction Forces and Image Formation

In AFM, the interaction between the probe tip and the sample surface is governed by various intermolecular forces. These include van der Waals forces, electrostatic forces, capillary forces, and short-range repulsive forces. The nature and magnitude of these forces depend on the distance between the tip and the sample surface.

At larger distances, attractive forces such as van der Waals interactions dominate, whereas at very small separations, repulsive forces arise due to overlap of electron clouds. The balance between these forces determines the operating mode of the AFM and influences the quality of the obtained images.

During scanning, the cantilever deflection caused by these interaction forces is continuously monitored by the laser–photodetector system. In contact mode, the deflection is directly related to the surface height, while in tapping and non-contact modes, the oscillation amplitude or frequency of the cantilever is used as the feedback parameter [33,34].

The collected signal is processed through a feedback mechanism that adjusts the vertical position (z-direction) of the scanner to maintain a constant interaction between the tip and the surface. The recorded height variations are then converted into a three-dimensional topographical image, providing detailed information about surface morphology, roughness, and nanoscale features.

2.7.3 AFM Analysis in the Present Work

In the present study, Atomic Force Microscopy was employed to investigate the surface morphology and nanoscale features of the synthesized thin films. AFM analysis provided valuable information regarding surface roughness, uniformity, and grain distribution of the prepared samples. NTMDTNTEGRA-prima instrument was used to perform atomic force microscopy (AFM) for the roughness measurements of thin film surface.

The measurements were carried out using a high-resolution AFM system under ambient conditions. The obtained topographical images enabled a detailed understanding of the surface characteristics, which play a crucial role in determining the gas sensing performance of the material. In particular, the surface roughness and distribution of nanostructures influence the adsorption of gas molecules and the overall sensing efficiency.

2.8 Raman Spectroscopy

Raman spectroscopy is a powerful, non-destructive optical characterization technique widely used to investigate the vibrational, rotational, and structural properties of materials. It is particularly effective for studying crystalline and nanostructured materials, including two-dimensional (2D) materials such as MoS_2. The technique provides detailed information about molecular bonding, crystal structure, phase identification, and lattice dynamics.

One of the key advantages of Raman spectroscopy is its ability to probe materials without extensive sample preparation, while offering high sensitivity to subtle structural changes. In the case of layered materials like MoS_2, Raman analysis plays a crucial role in determining the number of layers, crystallinity, and presence of defects [35,36].

2.8.1 Working Principle of Raman Spectroscopy

The working principle of Raman spectroscopy is based on the inelastic scattering of monochromatic light, typically generated from a laser source, when it interacts with the molecules or lattice vibrations (phonons) of a material. When a beam of incident photons strikes the sample, the majority of the light is scattered elastically without any change in energy or wavelength, a process known as Rayleigh scattering. However, a very small fraction of the incident photons—typically less than one in a million—undergoes inelastic scattering, resulting in a shift in energy due to interaction with the vibrational modes of the material. This phenomenon is referred to as Raman scattering and forms the basis of Raman spectroscopy. In Raman scattering, the energy difference between the incident and scattered photons corresponds to the vibrational energy levels of the molecules or the crystal lattice. This energy difference is known as the Raman shift and is commonly expressed in units of inverse centimeters (cm^{-1}). The Raman shift provides a unique spectral fingerprint of the material, as it reflects the specific vibrational modes associated with its molecular structure, bonding environment, and crystallographic arrangement. Based on the direction of energy transfer during the scattering process, Raman scattering is classified into two types: Stokes scattering and Anti-Stokes scattering. In Stokes scattering, the scattered photons possess lower energy (longer wavelength) than the incident photons because a portion of the photon energy is transferred to the material, exciting it to a higher vibrational state. In contrast, Anti-Stokes scattering occurs when the scattered photons gain energy (shorter wavelength) from the material, which is initially in an excited vibrational state. As a result, the photon emerges with higher energy than the incident radiation.

Among these two types, Stokes lines are generally more intense and are more commonly used for analytical purposes. This is because, at room temperature, most molecules exist in their ground vibrational state, making Stokes scattering more probable than Anti-Stokes scattering. Consequently, Raman spectroscopy primarily relies on the analysis of Stokes spectra to extract structural, chemical, and vibrational information about the material.

2.8.2 Basic Instrumentation

A typical Raman spectroscopy system consists of several key components that work together to generate, collect, and analyze the Raman signal, as illustrated in Fig. 2.10. The primary component is the laser source, which provides a monochromatic and coherent beam of light used to excite the sample. Commonly used lasers operate in the visible or near-infrared region and are selected based on the nature of the material and the desired depth of penetration. The laser beam is directed toward the sample through an optical system comprising lenses and mirrors, which focus the light onto a small spot on the sample surface and simultaneously collect the scattered radiation. The light scattered from the sample contains both Rayleigh (elastically scattered) and Raman (inelastically scattered) components. To isolate the weak Raman signal, optical filters are employed to effectively remove the intense Rayleigh scattered light, ensuring that only the inelastically scattered photons reach the detection system. The filtered light is then directed into a monochromator, typically equipped with a diffraction grating, which spatially separates the scattered light according to its wavelength. This separation is essential for resolving different Raman shifts corresponding to various vibrational modes of the material [8-11].

The dispersed light is subsequently detected using a highly sensitive charge-coupled device (CCD) detector, which converts the optical signal into an electrical signal for further processing. The CCD detector is capable of capturing weak Raman signals with high sensitivity and resolution, enabling accurate measurement of spectral features. The final output is a Raman spectrum, which represents the intensity of scattered light as a function of Raman shift (usually expressed in cm^{-1}). This spectrum serves as a unique fingerprint of the material, providing detailed information about its vibrational modes, molecular structure, bonding characteristics, and crystallinity. Thus, the integration of these components—laser source, optical system, filters, monochromator, and detector—enables precise and reliable Raman measurements, making the technique a powerful tool for structural and chemical characterization of materials [12,17].

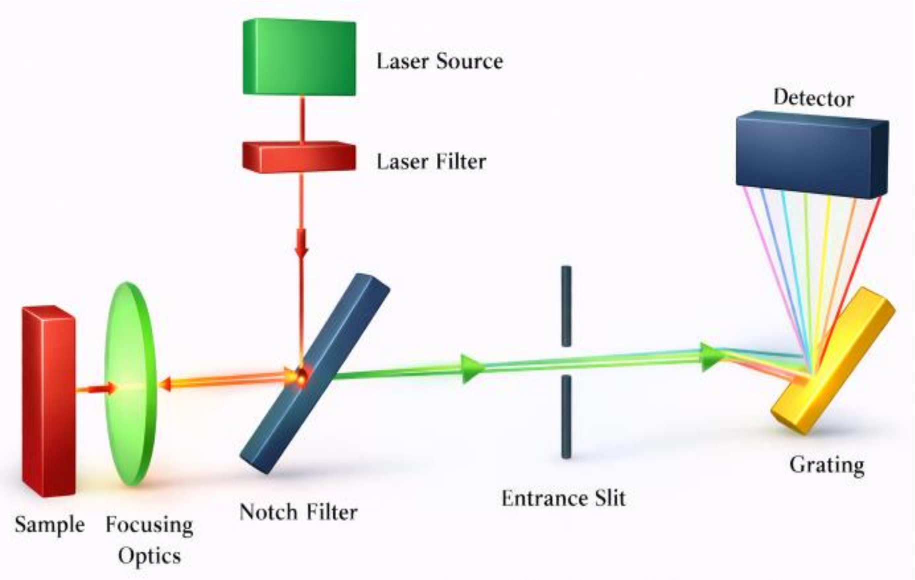

Figure 2.10: Instrumental set up of Raman Spectrometer.

2.8.3 Raman Modes of MoS_2 and Structural Analysis

Raman spectroscopy plays a crucial role in confirming the formation and evaluating the structural quality of MoS_2 thin films. It is a highly sensitive and non-destructive technique that provides valuable information about the vibrational properties of materials, making it particularly suitable for the characterization of layered transition metal dichalcogenides. The presence of characteristic Raman features in the recorded spectrum serves as clear evidence for the successful synthesis and crystallinity of MoS_2. In layered materials such as MoS_2, Raman spectroscopy reveals distinct vibrational modes associated with the movement of atoms within the crystal lattice. These vibrational modes arise from both in-plane and out-of-plane atomic motions, which are influenced by the bonding environment and interlayer interactions. The position, intensity, and shape of the observed Raman peaks are highly sensitive to structural parameters such as layer thickness, crystallinity, defects, and strain. Changes in peak positions or broadening of the Raman signals can indicate variations in lattice structure, presence of defects, or external influences such as stress and substrate interaction. Additionally, the relative intensity of different vibrational modes can provide insights into the uniformity and quality of the thin films. As the number of layers increases, subtle shifts in the Raman features are often observed, reflecting changes in interlayer coupling and vibrational dynamics.

Thus, Raman spectroscopy serves as an effective tool not only for confirming the formation of MoS_2 but also for assessing its structural integrity, layer-dependent characteristics, and overall material quality. Its ability to provide rapid, non-destructive, and detailed structural information makes it indispensable for the study of two-dimensional materials and their applications. Raman spectroscopy plays a crucial role in confirming the formation and structural quality of MoS_2 thin films. In layered transition metal dichalcogenides such as MoS_2, two prominent Raman-active vibrational modes are typically observed, namely the $\boldsymbol{E_{2g}^{1}}$ (in-plane mode) and the $\boldsymbol{A_{1g}}$ (out-of-plane mode).

- The $\boldsymbol{E_{2g}^{1}}$ mode corresponds to the in-plane vibration of molybdenum and sulfur atoms in opposite directions.
- The $\boldsymbol{A_{1g}}$ mode represents the out-of-plane vibration of sulfur atoms perpendicular to the basal plane.

The positions of these peaks are sensitive to the number of layers, strain, and defects present in the material. Typically, the separation between these two peaks increases with an increase in the number of layers. Therefore, Raman spectroscopy provides a convenient and reliable method to estimate layer thickness and assess the structural integrity of MoS_2 [37-39].

In addition, variations in the position and shape of Raman peaks provide important insights into the structural condition of the material. Any noticeable shift in peak position or broadening of the Raman features may indicate the presence of lattice strain, structural defects, or interactions between the film and the underlying substrate. Such changes can arise due to factors such as residual stress during film growth, defects like vacancies or dislocations, or external influences including temperature and surface interactions. Peak broadening is often associated with reduced crystallinity or increased disorder within the lattice, while peak shifts can reflect alterations in interatomic spacing. Therefore, careful analysis of these spectral features enables a deeper understanding of the structural quality and integrity of the material. As a result, Raman spectroscopy serves as a powerful and reliable tool for assessing material quality, identifying defects, and evaluating the overall performance potential of the synthesized films.

2.8.4 Raman Analysis in the Present Work

In the present study, Raman spectroscopy was employed to investigate the structural properties and confirm the formation of MoS_2 thin films. The Raman spectra were recorded using a suitable excitation laser under ambient conditions.

The observed Raman peaks corresponding to the $\boldsymbol{E^1_{2g}}$ and $\boldsymbol{A_{1g}}$ modes confirmed the successful synthesis of MoS_2. The peak positions, intensity, and separation between these modes were analyzed to evaluate the crystallinity, layer thickness, and structural quality of the films.

This analysis provided essential insights into the material properties, which are directly related to its gas sensing performance.

2.9 References

[1] L. G. De Arco, Y. Zhang, A. Kumar, and C. Zhou, "Synthesis, transfer, and devices of single-and few-layer graphene by chemical vapor deposition," IEEE Transactions on Nanotechnology, 8 (2009), 135-138.

[2] X. Liu, W. Yang, and Z. Liu, "Recent progress on synchrotron-based in-situ soft X-ray spectroscopy for energy materials," Advanced Materials, 26 (2014) 7710-7729.

[3] R. Kronberg, M. Hakala, N. Holmberg, and K. Laasonen, "Hydrogen adsorption on MoS_2 -surfaces: A DFT study on preferential sites and the effect of sulfur and hydrogen coverage," Physical Chemistry Chemical Physics,19 (2017) 16231-16241.

[4] X. Liu, W. Yang, and Z. Liu, "Recent progress on synchrotron-based in-situ soft X-ray spectroscopy for energy materials," Advanced Materials, 26 (2014) 7710-7729.

[5] N. Baig, I. Kammakakam, W. Falath, I. Kammakakam, Nanomaterials: A review of synthesis methods, properties, recent progress, and challenges, Mater. Adv. 2 (2021) 1821–1871.

[6] N. Rusman and M. Dahari, "A review on the current progress of metal hydrides material for solid-state hydrogen storage applications," International Journal of Hydrogen Energy, 41(2016) 12108-12126.

[7] V. Sharma, M.S. Mehata, Synthesis of photoactivated highly fluorescent Mn^{2+}-doped ZnSe quantum dots as effective lead sensor in drinking water, Mater. Res. Bull. 134 (2021) 111121.

[8] V.K. Singh, H. Mishra, R. Ali, S. Umrao, R. Srivastava, S. Abraham, A. Misra, V.N.

Singh, H. Mishra, R.S. Tiwari, A. Srivastava, In Situ Functionalized Fluorescent WS_2-QDs as Sensitive and Selective Probe for Fe^{3+} and a Detailed Study of Its Fluorescence Quenching, ACS Appl. Nano Mater. 2 (2019) 566–576.

[9] P. Sharma, M.S. Mehata, Colloidal MoS_2 quantum dots based optical sensor for detection of 2,4,6-TNP explosive in an aqueous medium, Opt. Mater. (Amst). 100 (2020) 109646.

[10] A.A. Adul-Rasool, D.M. Athair, H.K. Zaidan, A.M. Rheima, Z.T. Al-Sharify, S.H. Mohammed, E. kianfar, 0,1,2,3D nanostructures, types of bulk nanostructured materials, and drug nanocrystals: An overview, Cancer Treat. Res. Commun. 40 (2024) 100834.

[11] H.S. Neira, Ines S., Kolen'ko, Yury V., Lebedev, Oleg I., Tendeloo, Gustaaf Van, Gupta, F.& Y.M. Guitian, An Effective Morphology Control of Hydroxyapatite Crystals via Hydrothermal Synth., Cryst. Growth & Des. 9 (2009) 466-474.

[12] Y.X. Gan, A.H. Jayatissa, Z. Yu, X. Chen, M. Li, Hydrothermal Synthesis of Nanomaterials, J. Nanomater. 2020 (2020) 9182.

[13] L. Zhu, D. Shen, K. Hong Luo, Triple-emission nitrogen and boron co-doped carbon quantum dots from lignin: Highly fluorescent sensing platform for detection of hexavalent chromium ions, J. Colloid Interface Sci. 617 (2022) 557–567.

[14] Y. Wang, Y. Ni, Molybdenum disulfide quantum dots as a photoluminescence sensing platform for 2,4,6-trinitrophenol detection, Anal. Chem. 86 (2014) 7463–7470.

[15] J. Zhang, C. Jing, B. Wang, A Label-Free Fluorescent Sensor Based on Si,N-Codoped Carbon Quantum Dots with Enhanced Sensitivity for the Determination of Cr(VI), Materials. 15 (2022) 1733.

[16] B.D. Cullity, Elements of X-Ray Diffraction, Second edition., Addison-Wesley Publishing Company Inc., Reading MA 1978.

[17] L.H. Schwartz, J.B. Cohen, The Nature of Diffraction, in: Diffr. from Mater., Springer Berlin Heidelberg, (1987): pp. 46–76.

[18] C.N. Banwell, Fundamentals of molecular spectroscopy, 2nd Edition, McGraw-Hill, (1972).

[19] H.H. Willard, J.L.L. Merritt, J.A. Dean, J.F.A. Settle, Instrumental methods of analysis,

7th Edition, (1988).

[20] S.M. Bhagyaraj, O.S. Oluwafemi, N. Kalarikkal, S. Thomas, Characterization of nanomaterials: Advances and key technologies, Charact. Nanomater. Adv. Key Technol. , (2018) 1-390.

[21] G. Wypych, Handbook of UV Degradation and Stabilization: Second Edition, Handb. UV Degrad. Stab. Second Ed. (2015) 1- 419.

[22] J.R. Lakowicz, Introduction to Fluorescence, Princ. of Fluoresc Spectrosc. (1983) 1-18.

[23] C.R. Ronda, Luminescence: from theory to applications, Wiley-VCH Verlag GmbH & Co. KGaA, (2008) 260.

[24] K. Wakabayashi, Y. Yamaguchi, T. Sekiya, S. Kurita, Time-resolved luminescence spectra in colorless anatase TiO_2 single crystal, J. Lumin. 112 (2005) 50–53.

[25] R. Kumar, X. Liu, J. Zhang, and M. Kumar, "Room-temperature gas sensors under photoactivation: From metal oxides to 2D materials," Nano-Micro Letters, 12 (2020)1-37.

[26] J. Chen, N. Kuriyama, H. Yuan, H. T. Takeshita, and T. Sakai, "Electrochemical hydrogen storage in MoS_2 nanotubes," Journal of the American Chemical Society, vol. 123, pp. 11813-11814, 2001.

[27] N. Rusman and M. Dahari, "A review on the current progress of metal hydrides material for solid-state hydrogen storage applications," International Journal of Hydrogen Energy, 41(2016) 12108-12126.

[28] G. Eda, H. Yamaguchi, D. Voiry, T. Fujita, M. Chen, and M. Chhowalla, "Photoluminescence from chemically exfoliated MoS_2," Nano letters, 11 (2011) 5111-5116.

[29] A. V. Agrawal, R. Kumar, G. Yang, J. Bao, M. Kumar, and M. Kumar, "Enhanced adsorption sites in monolayer MoS_2 pyramid structures for highly sensitive and fast K.A. Altammar, A review on nanoparticles: characteristics, synthesis, applications, and challenges, Front. Microbiol. 14 (2023) 1155622.

[31] A. Lippitz, T. Hübert, XPS investigations of chromium nitride thin films, Surf. Coatings Technol. 200 (2005) 250–253.

[32] R. Lv, J.A. Robinson, R.E. Schaak, D. Sun, Y. Sun, T.E. Mallouk, M. Terrones,

Transition metal dichalcogenides and beyond: Synthesis, properties, and applications of single- and few-layer nanosheets, Acc. Chem. Res. 48 (2015) 56–64.

[33] A.M. Ealias, M.P. Saravanakumar, A review on the classification, characterisation, synthesis of nanoparticles and their application, IOP Conf. Ser. Mater. Sci. Eng. 263 (2017) 032019.

[34] K.A. Altammar, A review on nanoparticles: characteristics, synthesis, applications, and challenges, Front. Microbiol. 14 (2023) 1155622.

Chapter 3

Investigation of MoS_2-hydrogen interaction using *in-situ* X-ray diffraction studies

3.1 Introduction

In recent decades, the realm of nanomaterials has witnessed an extraordinary surge in interest, with researchers exploring the diverse and intriguing properties of two-dimensional (2D) materials. Among these materials, molybdenum disulfide (MoS_2), a transition metal dichalcogenide (TMD), has emerged as a standout candidate for applications spanning electronics, optoelectronics, energy storage, photodetectors and catalysis.[1-5] This versatile 2D material has attracted significant attention due to its unique structural and electronic characteristics, making it an exciting platform for cutting-edge research and technological advancement.[6,7] The interaction between 2D materials with various gases is an area of profound significance because it underpins their potential utilization in gas-sensing devices, catalytic reactions [8], and gas storage systems.[9,10] Understanding how gases interact with MoS_2 at the atomic and structural level is also crucial for optimizing its performance in these applications.

Globally, the matter of energy has become a cause for widespread apprehension, primarily driven by the depletion of fossil fuels. The escalation in energy demand is principally fueled by two paramount factors: the rapid expansion of the world's population and the concurrent elevation in the average standard of living.[11] In the contemporary context, the most urgent challenges faced by the society is navigating the endeavor to fulfill the growing energy requirements amid substantial limitations imposed by the diminishing reservoirs of traditional fuels such as coal, oil, and natural gas.[12] In addition, hydrogen gas (H_2), in particular, has garnered immense interest as a clean and sustainable energy carrier. The global interest in H_2 energy has grown substantially primarily attributed to its remarkably high heat combustion rate. Beyond its impressive combustion capabilities, H_2 energy offers a crucial advantage by fostering independence from finite fossil fuel resources. Unlike nonrenewable energy sources, H_2 combustion results in the generation of clean combustion products, contributing to a more environmentally sustainable energy landscape.[13,14,15]

Today, H_2 gas is widely employed in various sectors, including oil refining, chemical industry, space transportation, medicine and aerospace. However, due to its high explosiveness and flammability when its concentration exceeds 4% of the environment volume (attributed to its low ignition energy of 0.017 mJ), even a minor H_2 leakage poses serious risks.[14] To mitigate potential hazards and ensure safe H_2 operations, there is a need for a highly sensitive, selective, fast-recovery, and responsive H_2 gas sensor to detect leakages promptly. MoS_2, with its unique surface properties and catalytic potential, can be used in various technological applications such as LDH-based heterostructures as electrode materials for water splitting, energy storage devices and H_2-related technologies.[16,17] MoS2 can be prepared by various methods such as hierarchical NiCo-LDH@MoS_2/CuS heterostructure (HS) was prepared by facile two-step hydrothermal synthesis, A facile chemically exfoliated combined microwave-assisted method was used to synthesize $MoS_2{\cdot}ZnO$ nanocomposites. [17, 18] Among them, preparation of MoS_2 thin film by evaporation of Mo using e-beam technique followed by sulphuration in CVD techniques offers unique advantages such as this method provides high control over MoS_2 film thickness and crystallinity, especially compared to simpler, more scalable methods like thermal decomposition. However, it is more complex and expensive than other methods. Much like graphene, MoS_2 is composed of layers arranged in a vertical stack.[19] Each individual layer is created through covalent bonding between molybdenum (Mo) and sulfur (S) atoms. The cohesion between adjacent layers is facilitated by the presence of relatively weak van der Waals forces. This structural similarity highlights the layered nature of MoS_2, where the combination of covalent bonds within layers and van der Waals forces between layers contributes to its unique properties and versatile applications. [19] The presence of weak van der Waals interactions in MoS_2 enables gas molecules to easily infiltrate and diffuse between its layers.

Consequently, the resistance of MoS_2 can undergo significant changes as a result of the adsorption and diffusion of gas molecules within these layers. This property makes MoS_2 highly responsive to the presence of gases, offering potential applications in gas sensing and related fields where the material's electrical conductivity can be modulated by the interaction with different gas species. The interaction between MoS_2 and H_2 gas is governed by a multitude of factors, including temperature, pressure, and the structural integrity of MoS_2.[20,21] These factors intricately influence the adsorption, diffusion, and subsequent chemical reactions of H_2 on the MoS_2 surface.[22,37] To delve into the intricacies of this interaction and gain a comprehensive understanding, in-situ characterization techniques have become invaluable tools. Among these techniques, in-situ X-ray diffraction (XRD) stands out as a powerful technique for monitoring structural changes in materials during gas-solid interactions.[23] By allowing real-time observation of atomic rearrangements and phase transformations, *in-situ* XRD offers unique insights into the dynamics and thermodynamics of these interactions.[24] To the best of our knowledge, there is no report on the structural properties of MoS2 on the exposure to the hydrogen gas.

This chapter presents a systematic and detailed investigation into the MoS_2-H_2 gas interaction at different pressures using in-situ X-ray diffraction studies. In the case of nanostructured materials, there could be sample to sample variation during synthesis which leads to modification in the structural properties when they are exposed to hydrogen gas and later investigated using off-line XRD. Here, state-of-art *in-situ* XRD facility has been used in which all the studies has conducted in the same sample without changing experimental conditions. Our objective is to unravel the structural modifications that occur within MoS_2 under varying H_2 pressures and to elucidate the underlying mechanisms that govern this intricate interaction. This research is a crucial step towards realizing how MoS_2 behaves in the presence of H_2 gas, offering fundamental insights into the design, engineering, and optimization of MoS_2-based catalytic systems for H_2-related applications. Throughout this chapter, we will explore the current state of knowledge regarding the interaction between MoS_2 and H_2 gas, laying the foundation for our in-depth investigation. The unique properties of MoS_2, the significance of H_2 gas as an energy carrier, and the key challenges in harnessing MoS_2's potential for H_2-related applications is also discussed. In the subsequent sections, we will delve into the experimental methodology, data analysis, and results obtained from our in-situ X-ray diffraction studies on MoS_2- H_2 gas interactions at different pressures. The findings of this research not only enhance our fundamental knowledge of MoS_2's behavior but also provide valuable guidance for the design and development of advanced catalytic systems and H_2 storage materials, contributing to the ongoing efforts towards a sustainable energy future.

3.2 Experimental section

3.2.1 Preparation of Mo films:

The electron beam evaporation (e-beam) deposition method was employed for preparation of high-quality Mo thin films by using Mo target on Si/SiO_2 substrate. The key advantages of this technique lie in its ability to produce high-purity Mo films with excellent control over thickness and microstructure, making it indispensable in various industries ranging from electronics to thin-film coatings and beyond.[25,26] At first, the substrates were cleaned with trichloroethylene followed by acetone, and alcohol to remove contaminations and native oxide. The base vacuum of the order of 2 x10^{-6} mbar was maintained with the help of rotary vane and turbo-molecular pump. The deposition rate is kept at a slow rate of 0.7 – 0.8 nm/sec for the uniformed and to achieve desired thickness. Three different thicknesses (5 nm, 10 nm, 20 nm) of Mo film were obtained by keeping the same deposition rate. The film deposited at the RT having black color which may be due to oxygen deficiency and a large number of defects. Therefore, these films were further annealed in oxygen ambient at temperature of 400 °C for duration of 1 hour. After annealing, the color of films changed and they become totally transparent.

3.2.2 Sulfurization of Mo films:

Sulfurization of Mo films is a fundamental process to transform deposited molybdenum (Mo) thin films into two-dimensional molybdenum disulfide (MoS_2) layers. For this purpose, a double zone chemical vapor deposition (CVD) method was employed for the sulfurization. The sulfurization of thin film of 20 nm thickness were grown on Si/SiO_2 substrates via double zone sulfurization using an ambient-pressure CVD technique as shown in figure 3.1.

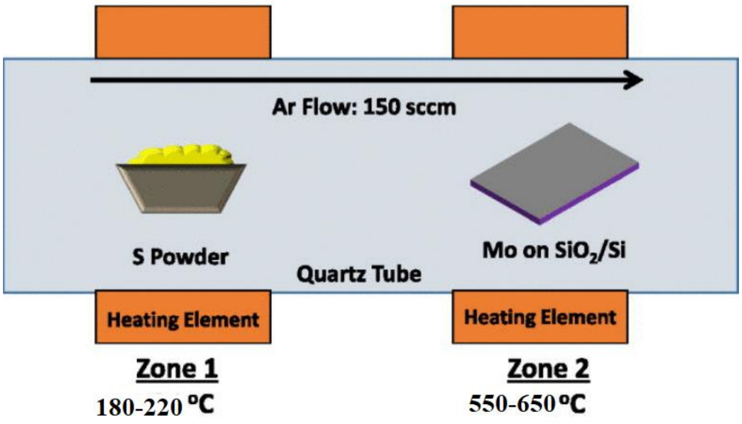

Figure 3.1: Sulfurization of Mo films using double zone CVD technique

Flushing of the quartz tube using Argon gas stream, followed by continuous Ar flow for 15 min, was performed. This reduces the oxygen content in the reactor prior to the sulfurization process. Before the experiment, a quartz boat containing 1.0 gm Sulphur powder (Sigma Aldrich, 99.999%) was placed upstream in the heating ring, and the Si/SiO_2 substrate covered with pre-exfoliated Mo film was placed face up on another quartz boat and located in the middle of the tubular furnace, as shown in Figure 3.1. The distance between the two quartz boats is about 150 mm. After that, the tubular furnace was heated to 600 °C at a rate of 20 °C/min. When the temperature of the tubular furnace rose to 470 °C, the Sulphur powder was heated to 200 °C through the heating ring at a rate of 20 °C/min. During this process, the Ar flow rate remained at 80 SCCM. After the growth time of 30 min, the furnace was cooled down naturally to room temperature with Ar flow of 100 SCCM.

3.2.3 Characterizations

XRD along with Raman spectroscopy was used to probe the structural properties of the as prepared and hydrogenated MoS_2 films. XRD patterns have been recorded using Bruker AXS D8 Advanced in-situ XRD facility equipped with Cu K_α source with wavelength 1.54 Å (40 kV and 40 mA power). The *in-situ* XRD setup has provision for creation of high vacuum using rotary vane pump and turbo-molecular pump.[24] A gas injection facility is also integrated to injection the H_2 gas in the controlled manner which allows us to record diffraction pattern in the controlled gas atmosphere. A schematic diagram of the *in-situ* XRD setup is shown in the figure 3.2. First, the MoS_2 films were mounted on sample holder and a high vacuum order of $1x10^{-5}$ mbar was created. After that, diffraction pattern of the MoS_2 films was recorded in the vacuum. Now, MoS_2 films was exposed to different concentrations of H_2 gas (3 %) mixed with noble gas Argon (Ar), one by one after different intervals of pressure ranging from 50 mbar to 900 mbar and diffraction pattern of the same sample is recorded after each pressure without changing position of sample. Since, all diffraction patterns are recorded on the same sample so effect of the sample-to-sample variation is ruled out. This process also allows us to compare of intensity of the diffraction peaks with change in the pressure of the H_2 gas. The data were recorded in locked coupled mode in the scan range of 2θ from 10^o to 60^o with step size of 0.02^o at a scan speed of 0.25^o/min.

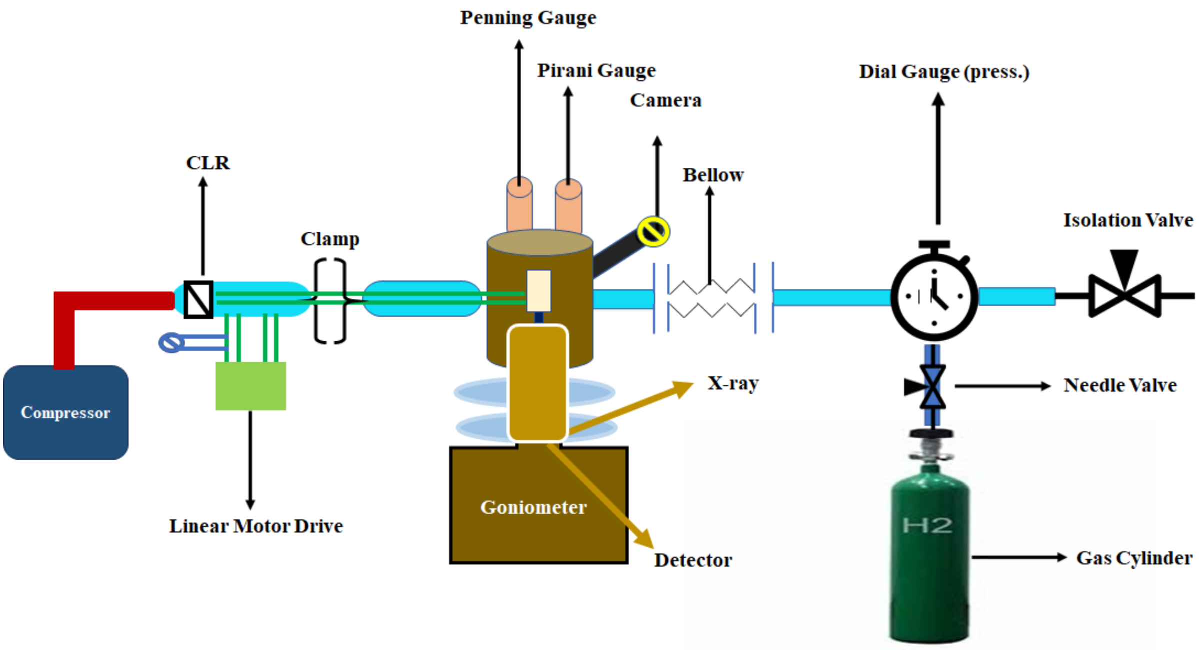

Figure 3.2: Schematic diagram of the in-situ XRD setup

Raman spectroscopy was performed on pure and MoS_2 samples exposed with different H_2 concentrations using Renishaw Invia Raman microscope with Argon laser as source (514.5 nm wavelength) for the scan range of 100 – 3200 cm^{-1}. The topography of the MoS_2 films including pristine were studied using Digital Instruments Nanoscope IIIa atomic force microscope (AFM) in the tapping mode.

3.3 Results and discussion

3.3.1 Structural Properties of the as-prepared MoS_2 thin film

Glancing angle X-ray diffraction (GIXRD) studies was carried out to understand the effect of film thickness, molybdenum temperature and sulfurization temperature on crystallinity and phase formation in the molybdenum thin film deposited on Si/SiO_2 substrate.

3.3.1.1 Effect of Mo film thickness:

Thin film of molybdenum having thickness of 5 nm and 10 nm films has been prepared using electron beam evaporation techniques. In order to understand the effect of film thickness on MoS_2 phase formation, these films were exposed to various synthesis conditions of varied molybdenum and sulfur temperatures (molybdenum at 550 °C, 600 °C, 650 °C and sulfur at 180 °C, 200 °C, 220 °C, 300 °C). Figure 3.3 shows the GIXRD pattern of MoS_2 thin films of the different thickness of (a) 5 nm, (b) 10 nm and (c) 20 nm, prepared by keeping molybdenum and sulfur at different temperature (molybdenum at 550 °C, 600 °C, 650 °C and sulfur at 180 °C, 200 °C, 220 °C, 300 °C), respectively. It is clear from the GIXRD plot of Figure 3.3 (a) that MoS_2 phase does not form in the case of 5 nm for all process temperatures except Mo 600 °C and Sulfur 200 °C. When film thickness is increased to 10 nm then sharp peaks are visible at 2θ value of 14.3°, 25.4°, 39.0° and 58.4° corresponding to (002), (004), (103) and (110) planes, respectively. The peaks well matched with JCPDS No. 37-1492, which confirms the successful synthesis of polycrystalline hexagonal-phase MoS_2 in the case of 10 nm films. This also shows that crystallinity is improved with increase in the film thickness. It may be noted that crystalline phase was not formed when the sulfurization was done at 300 °C by keeping Mo at 600 °C. This could be due to suppress of Mo/S interaction at the elected temperature. When thickness of the Mo film was subsequently increased to 20 nm then high quality MoS_2 phase was formed in all the experimental condition used in the present study. In addition, the GIXRD analysis clearly exhibits that the MoS_2 thin film (20 nm) corresponding to synthesis parameter (Mo temperature 650 °C and sulfurization temperature 220 °C) is the optimum condition to get high quality film due to presence of all peaks related to MoS_2 only. It may be noted that other synthesis condition of MoS_2 thin film (20 nm) film also contains polycrystalline MoS_2 phase but they have lesser intensity peaks as well as some impurity peaks.

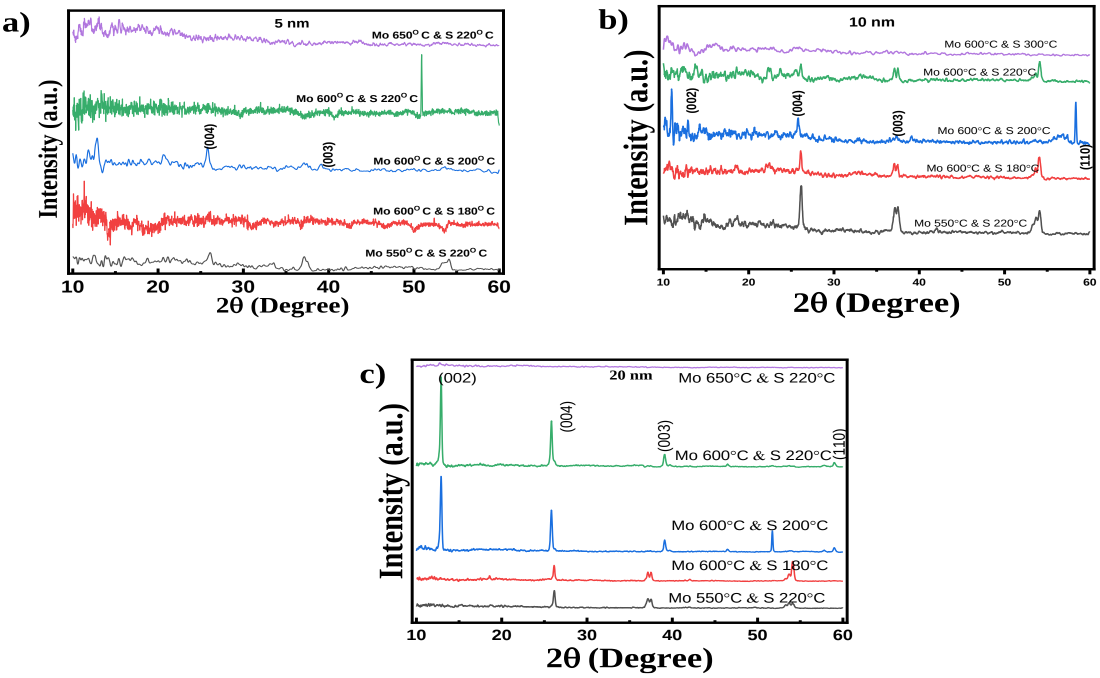

Figure 3.3: GIXRD analysis of MoS_2 thin films having **(a)** 5 nm, **(b)** 10 nm and **(c)** 20 nm thickness

3.3.1.2 Effect of process temperature

In order the understand the detailed investigation of process temperature on the structural properties and crystalline quality of the films, the XRD pattern of Mo (20 nm) synthesized at varying **(a)** Mo temperature and **(b)** sulfurization temperature are plotted in Figure 3.4. The process temperature effect can be studied by either varying the temperature of Mo film or the temperature of sulphur powder while keeping other at fixed temperature during synthesis of MoS_2 thin film. In the first case, the sulfurization temperature was kept at 220 °C and Mo thin film temperature was varied from 550 °C to 650 °C. When the annealing temperature of Mo film was 550 °C then few peaks of the MoS_2 can be clearly seen [Figure 3.4.a]. As the annealing temperature of Mo was subsequently increased to 600 °C then single phase MoS_2 film was synthesized. It contains all the peaks corresponding to hexagonal phase of the MoS_2. After that, the annealing temperature of the Mo was further increased to 650 °C then surprisingly all the peaks were disappeared and amorphous phase was formed. This indicates that the crystalline MoS_2 phase does not formed due to less interaction of sulphur at elevated temperature. Thus, highly crystalline single phase MoS_2 film can be synthesized by sulfurization at 220 °C by keeping Mo thin films at 600 °C. In order to understand the effect of sulfurization temperature on quality of the film, it was varied from 180 °C to 220 °C by keeping Mo thin films at the temperature of 600 °C. XRD pattern displayed in Figure 3.4(b) shows that intensity of the diffraction peaks are increasing with increase in the sulfurization temperature. Highly crystalline thin films of MoS2 can be synthesized at the sulfurization temperature of 220 °C by keeping Mo thin films at 600 °C.

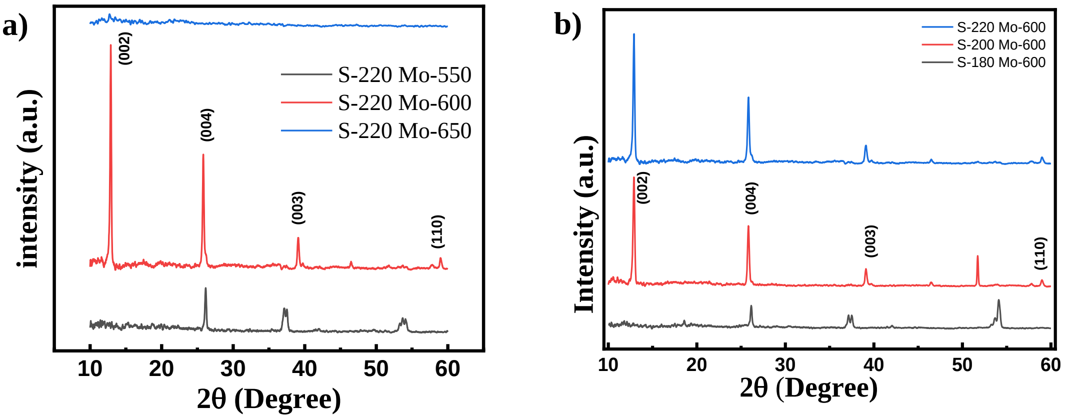

Figure 3.4: MoS_2 thin film synthesis with varying **(a)** sulfurization temperature **(b)** Mo film temperature

Thus, based on the results presented above, one can conclude that optimum process parameters such as film thickness (20 nm), Mo thin film temperaure (600 °C) and sulfurization temperature (220 °C) are required for getting good quality thin films of the MoS_2.

3.3.2 Surface Morphology

Scanning electron microscopy (SEM) was used for determining the surface morphology of as-prepared MoS_2 thin films (20 nm) grown under optimized conditions. A typical SEM image of the MoS_2 thin film is shown in Figure 3.5(a). As can be seen from the image, the MoS_2 nanosheets were uniformly grown on the substrate and it appears smooth, homogeneous and without topography contrast. The particle size from the SEM images is estimated using ImageJ software. The Figure 3.5(b) represents particle size distribution histogram which gives an estimation of average particle size. The calculated average particle size is 0.63± 0.20 μm. The compositions of MoS_2 thin film were investigated using energy dispersive spectroscopy (EDS) and tabulated in the Figure 3.5(c). The elemental distribution shows that sample primarily consists of Mo, O, S and Si. The extra Si element is also observed due to the Si/SiO_2 substrate.

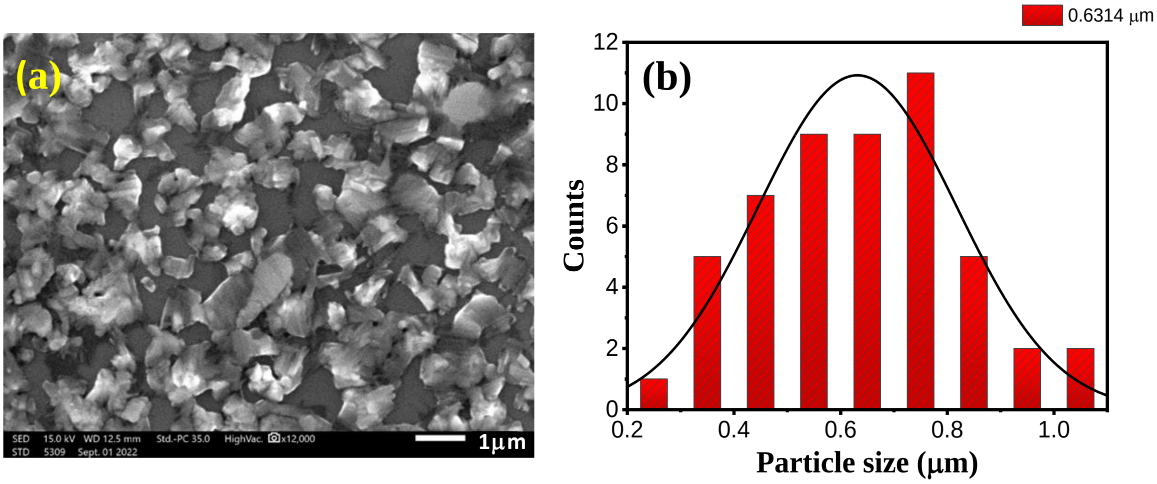

(c)

Display name	Standard data	Quantification method	Result type
Spc_001	**Standardless**	**ZAF**	**Metal**
Element	**Line**	**Mass%**	**Atom%**
O	**K**	**23.35±0.39**	**35.89±0.60**
Si	**K**	**71.32±0.56**	**62.45±0.49**
S	**K**	**0.56±0.16**	**0.43±0.12**
Mo	**L**	**4.78±0.50**	**1.22±0.13**
Total		**100.00**	**100.00**
Spc_001			**Fitting ratio 0.0593**

Figure 3.5 (a) SEM image of MoS_2 thin film prepared on Si/SiO_2 substrate **(b)** size distribution histogram (c) elemental distribution of MoS_2 thin film

Atomic force microscope (AFM) technique was also used to compare and analyze the surface characteristics of Mo and MoS_2 thin film with different thickness. Figure 3.6 shows the AFM images of Mo thin films of different thickness of (a) 5 nm, (b) 10 nm and (c) 20 nm. The surface roughness of these films was calculated using Nanoscope analysis 1.7 software and found to be 0.85 nm, 21 nm and 4.1 nm for 5 nm, 10 nm and 20 nm thick films, respectively. From the AFM image, one can conclude that the 20 nm thin film is of superior quality as compared to other films. In addition, all the MoS_2 thin film of different thickness have very low root-mean-squared (RMS) surface roughness as shown in Figure 3.6 d), e) and f). The low roughness minimizes surface defects, carrier scattering and ensuring a consistent and uniform interaction with analytes. The detailed of the film parameter has been shown in Table 3.1.

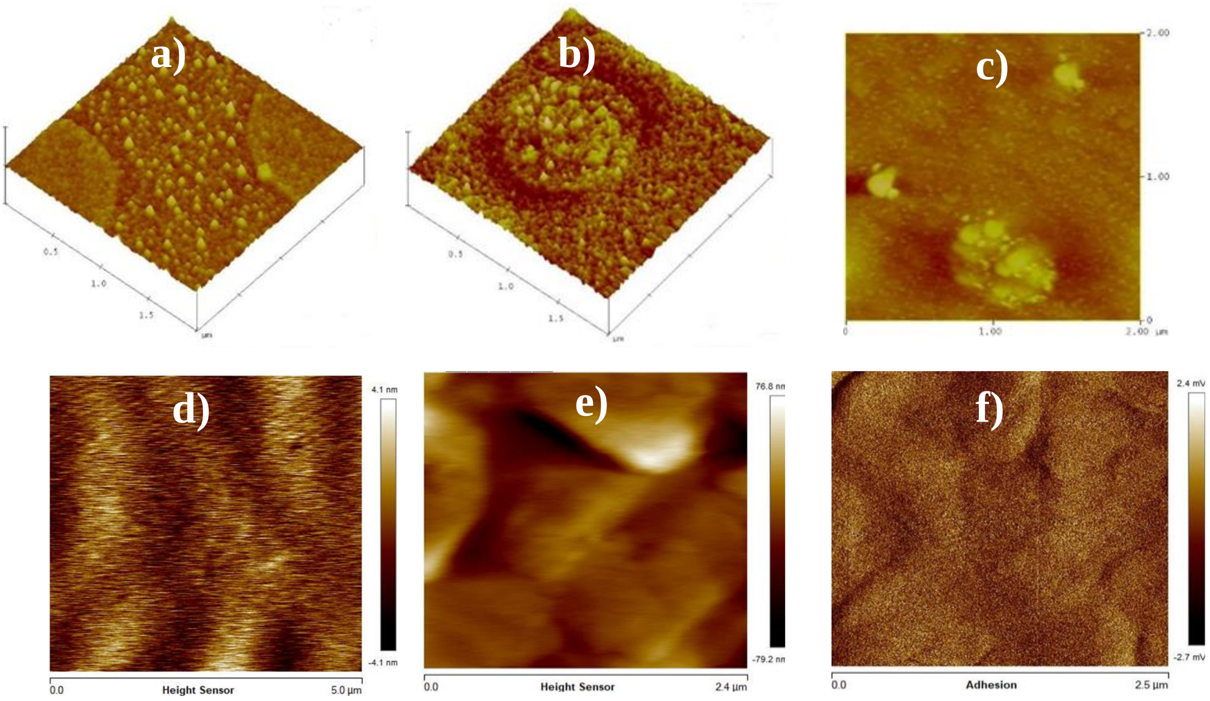

Figure 3.6: AFM image of Mo thin film with the thickness of, **(a)** 5 nm, **(b)** 10 nm, and **(c)** 20 nm and MoS_2 thin film with the thickness of **(d)** 5 nm, **(e)** 10 nm, **(f)** 20 nm

Table 3.1: The variation in the roughness of MoS_2 thin films with film thickness

S.No.	**Thickness of film (nm)**	**Roughness of film (nm)**
1	5	0.85
2	10	2.1
3	20	4.1

As one can be seen from the AFM image and Table 3.1, the roughness of the film having 5 nm thicknesses is lower than 20 nm thick film. Although, roughness of the 20 nm thick film is higher but it is used for further *in-situ* structural investigation because its crystallinity is very good and display all the characteristics peaks of MoS_2, which can be seen from GIXRD.

Formation of single phase MoS_2 and presence of the short rang order is further probed by the Raman spectroscopy technique. It is a powerful technique used to analyze the vibrational modes of materials, providing valuable information about their structure and composition. In the case of MoS_2 films, Raman spectroscopy not only offers insights into the quality and characteristics of the deposited material but also provides information about the phonon modes in MoS_2, which are related to the vibrational motion of atoms within the crystal lattice.

Raman spectrum of the MoS_2 thin films (t = 20 nm) is shown in the Figure 3.7. It exhibits the distinctive signal of 2H-MoS_2, with no apparent traces of polymer residue, carbon contamination or oxides.

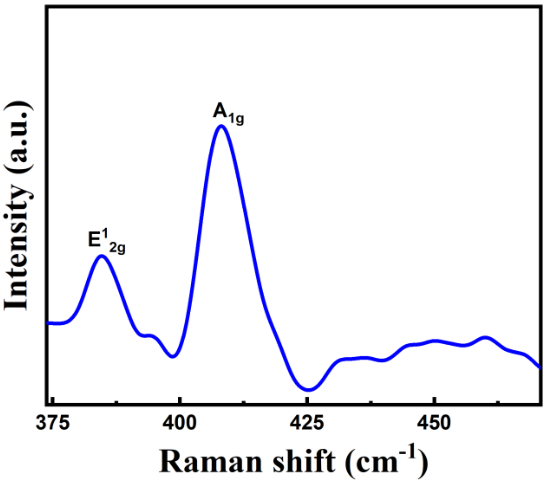

Figure 3.7: Raman spectra of the MoS_2 thin films of 20 nm thicknesses grown by vapor phase sulfurization of Mo thin films.

Raman spectrum comprises signature peaks E^1_{2g} at the wavenumber of 385 cm^{-1} corresponding to the in-plane vibrational modes of the MoS_2 lattice (in-plane vibration between Mo and S atom)· and A_{1g} at the wavenumber of 405 cm^{-1} represents the out-of-plane vibrations of the MoS_2 layers (out-of-plane expansion between S atom).[26,27,33] Generally, the A_{1g} mode gives the significant information about the van der Waals force among the adjacent MoS_2 layers, because of out-of-plane interaction with the adjacent atoms.[28,34] In this context, the presence of two distinct Raman peaks suggests that the MoS_2 film exhibits hexagonal coordination (2H) rather than the trigonal prismatic configuration (1T) as observed in mechanically exfoliated MoS_2.[29,32] Additionally, the frequency difference of these two peaks is found to be 20 cm^{-1}, which can be ascribed a few layers of MoS_2 thin film.[30,32] The well-matched characteristics peaks is a clear evidence of the formation of the impurity free single phase MoS_2.

3.3.3 Hydrogenation of MoS_2: Pressure Effect

To understand MoS_2-H_2 kinetic, an *in-situ* XRD studies was performed on MoS_2 thin film (20 nm) by exposing it to pure H_2 gas a pressure varying from vacuum to 1000 mbar. The diffraction was recorded in the vacuum and different hydrogen pressure at the measurement parameters of the diffractometer and without changing position of sample. Figure 3.8 (a) shows *in-situ* XRD patterns of as-prepared MoS_2 thin films in the vacuum and on exposure to H_2 environment by varying its pressure between vacuum to 1000 mbar. It shows that few new peaks were appeared even on film exposed to a very low pressure of H_2 (50 mbar). This clearly indicates very high sensitivity of MoS_2 towards H_2 gas at the room temperature. When the H_2 pressure is further increased from 50 mbar to 100 mbar, then intensity of the diffraction peaks are decreased. But, observation of new peaks and phase change was not observed event pressure of the H gas increased to 200 mbar. As H_2 gas pressure is subsequently increased up to 400 mbar then drastic reduction in the diffraction peaks is observed. This indicates that a large lattice strain and defects are produced by hydrogen if the pressure is P> 400 mbar. The production of the excessive defects generates structural distortion which leads to amorphization of the MoS_2. As the H_2 pressure is further increased to 1000 mbar, diffraction peak intensity corresponding to different planes tends to deteriorate and it vanishes completely at 1000 mbar pressure. On the basis of the diffraction data, one can infer that MoS_2 remains predominantly stable within the H_2 pressure range from vacuum to 400 mbar. However, beyond this pressure range, MoS_2 thin films undergo significant and abrupt transformations and it completely loses it phase at 1000 mbar pressure. To understand the H_2 pressure induced lattice micro-strain in the MoS_2 films, the inter-planer spacing of pure and hydrogenated MoS_2 was calculated. The variation in the inter-planer spacing (d) with H_2 pressure is shown in figure 3.8 (b). It exhibits that the inter-planer spacing increases with increase in the H_2 pressure which confirms the production of the lattice strain due to hydrogenation. Due to increase in hydrogen pressure from vacuum to 1000 mbar, the MoS_2 (002) inter planar spacing was observed. It was noticed that inter-planar spacing is a function of *in-situ* hydrogen pressure. Before exposure to hydrogen gas the inter-planar spacing of (002) plane was observed c= 12.25Å such as khan et al. XRD study shows hexagonal structure of few-layers of MoS_2 with observed (0 0 2) plane, with lattice parameter is ≈12.28 A° [29,37]. Subsequently, *in-situ* hydrogen pressure was increased to 50 mbar and corresponding inter-planar spacing was observed d=11.87Å, which was measured using XRD technique. The in-situ hydrogen pressure was increased up to 1000 mbar. The inter-planar spacing at 800 mbar and 100 mbar hydrogen pressure are d=11.89Å and 13.58 Å, respectively. This shows that the inter-planar spacing was almost constant up to 800 mbar hydrogen pressure. Further, there was a drastic increase in inter-planar spacing when pressure was increased from 800 to 1000 mbar which could leads to phase change in the MoS_2. This shows that there is a significant increase in inter-planar spacing due to hydrogen pressure. So, this threshold level of hydrogen pressure significantly affects the crystalline properties of MoS_2 structure. Thus, hydrogen pressure of 800 mbar can be considered as a transition pressure.

Apart from that relative change in the inter planer spacing $(d_p - d_0)/d_0$ was also calculated. Here, d_0 and d_P are inter planar spacing in vacuum and at a specific hydrogen pressure respective. The variation in the $(d_p - d_0)/d_0$ with pressure is shown in figure 3.8c). The results indicates that as pressure in increasing the inter planar spacing is also increasing.

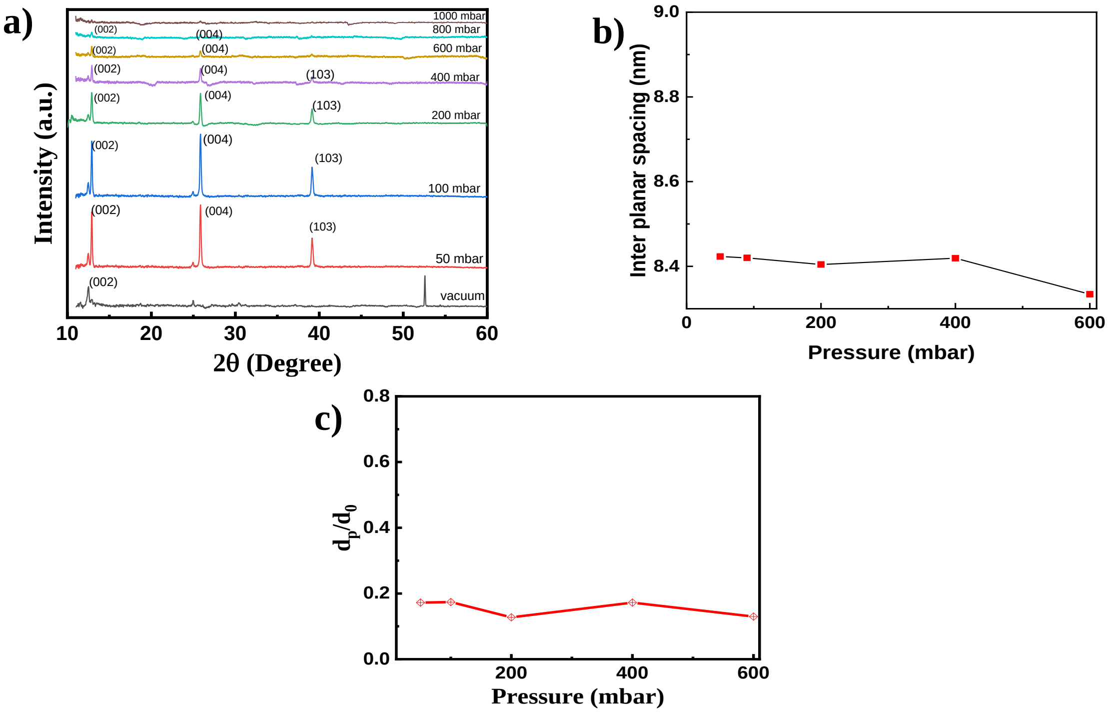

Figure 3.8 (**a**) *In-situ* XRD pattern of MoS_2 thin film (20 nm) recorded under vacuum and exposure to different H_2 gas pressure. The variation of (**b**) interplaner spacing and (**c**) relative change in the inter planar spacing $(d_p - d_0)/d_0$ at different H_2 gas pressure.

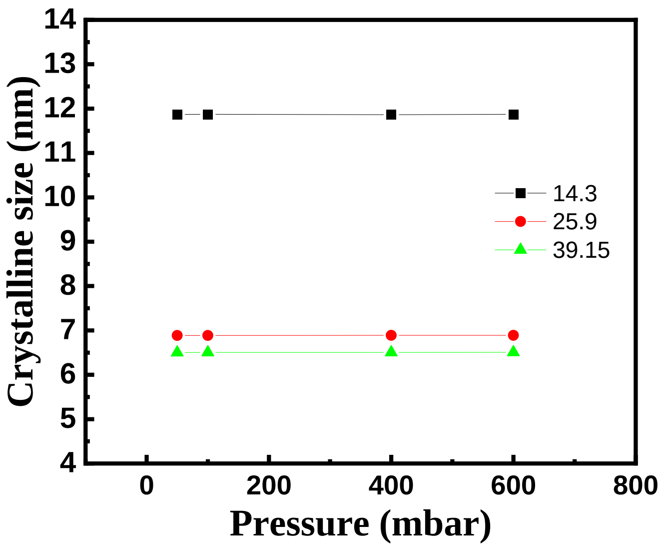

Figure 3.9: Change in the crystallite size vs partial pressure calculated for the diffraction peaks appeared at **(a)** 14.3°, **(b)** 25.4° and **(c)** 39.4°

The crystalline size of MoS_2 films exposed at various H_2 partial pressures was estimated from the XRD data presented in the Figure 3.8. It was calculated using Scherrer equation which is expressed as:

$$D = \frac{K\lambda}{\beta \cos(\theta)} \tag{3.1}$$

Where, D is the average crystallite size., K is the shape factor, typically around 0.9, λ is the wavelength of the X-ray radiation used for the diffraction, β is the full width at half maximum (FWHM) of the diffraction peak and θ is the Bragg angle. Figure 3.9 shows variation in the crystallite size with H_2 partial pressure for diffraction peaks appeared at the **(a)** 14.3°, **(b)** 25.4° and **(c)** 39.4°, corresponding to (002), (004) and (103) planes, respectively. It is evident that the crystallite size of MoS_2 thin films is increasing with H_2 gas pressure for all three crystalline planes which may be due to hydrogen-induced recrystallization. Hydrogen being a reducing agent can promote the removal of oxygen-containing functional groups and defects from the MoS_2 surface which leads to a more pristine and ordered atomic arrangement. Hydrogen induced reduction process may also facilitate the coalescence and growth of crystallites, promoting larger crystal sizes. Additionally, H_2 exposure can influence the energetics of grain boundaries, encouraging the migration and coarsening of grains.[29,30,31]

In order to understand the influence of hydrogenation on the crystallinity of the MoS_2 films, change of relative intensity (I/I_0) of all the characteristics peaks of MoS_2 with H_2 gas pressure is determined. Here, I_0 and I are the intensity of diffraction peak recorded in vacuum and at a particular pressure of H_2. Figure 3.10 (a) shows the variation in the relative intensity (I/I_0) with H_2 gas pressure. It shows that relative intensity of three characteristics peaks is reduced as the pressure of the H_2 gas is increased. This clearly shows that crystallinity of the MoS_2 is deteriorating on the exposure to H_2 gas. It may be noted that effect of hydrogenation on the peak appearing at the diffraction angle of 14.3° is negligible. The variation in relative intensity (I/I_0) for peaks appearing at the 25.4° and 39.15° are fitted using exponential function.

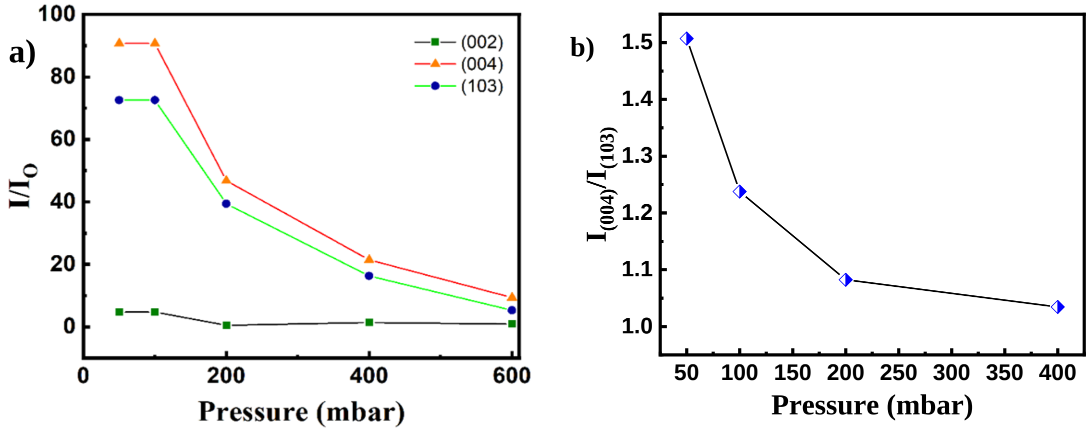

Figure 3.10 (a) XRD relative intensity vs pressure 14.3°, 25.4° and 39.0°**, (b)** Relative plane intensity $I_{(004)}/I_{(103}$ vs pressure (mbar)

Apart from this, to understand the H_2 induced preferred orientation, change in relative intensity corresponding to (004) plane and (103) plane with the variation of the pressure is also calculated. Figure 3.10 (b) displays a change in the relative plane intensity $I_{(004)}/I_{(103)}$ with partial pressure of H_2 It displays that the $I_{(004)}/I_{(103)}$ is decreased with increase in the pressure of H_2 gas. This suggest that there is preferred orientation along the (103) plan of the MoS_2. In order to validate H2 storage materials, a detail understanding comes from these studies [8,26,35]. This confirms that the H_2 makes a great impact through interaction on the crystal structure of MoS_2 thin film.

3.4 Conclusion

In synthesis process parameters optimization and hydrogenation properties of the molybdenum thin films of different thickness prepared using e-beam deposition technique followed by sulfurization using CVD system are reported. Optimization of *viz,* film thickness, sulfurization temperature by keeping Mo thin film at fixed temperature and Mo film temperature by keeping fixed sulfurization temperature has been carried out for getting highly crystalline MoS_2 film and confirmed its structural, micro-structural and compositional analysis using GIXRD, SEM, EDX, Raman spectroscopy techniques. The structural properties investigations confirms that crystalline MoS_2 thin films having optimum thickness of 20 nm can be prepared by sulfurization at 220 °C while keeping Mo thin film at 600 °C. The pressure dependent hydrogenation of the MoS_2 thin films investigated using *in-situ* XRD technique suggests that MoS_2 thin film remains predominantly stable within the pressure range from vacuum to 400 mbar. However, it undergoes significant and abrupt transformations when hydrogen gas pressure is subsequently increased. The MoS_2 thin films become completely amorphous at 800 mbar pressure. Thus, observation of order-disorder phase transformation has not only depended the understanding of MoS_2-H_2 interactions but also important for utilization of the MoS_2 thin films in the devices.

3.5 References

[1] Sharma, A., and G. Gupta, Recent Development and Prospects for Metal Selenide-Based Gas Sensors, *Materials Science and Engineering: B* 290 (2023): 116333.

[2] Dodda, A., D. Jayachandran, A. Pannone, N. Trainor, S. P. Stepanoff, M. A. Steves, et al., Active Pixel Sensor Matrix Based on Monolayer MoS_2 Phototransistor Array, *Nature Materials* 21 (2022): 1379–1387.

[3] Wang, T., S. Chen, H. Pang, H. Xue, and Y. Yu, MoS_2-Based Nanocomposites for Electrochemical Energy Storage, *Advanced Science* 4 (2017): 1600289.

[4] Huang, Y., Y. Sun, X. Zheng, T. Aoki, B. Pattengale, J. Huang, et al., Atomically Engineering Activation Sites onto Metallic 1T-MoS_2 Catalysts for Enhanced Electrochemical Hydrogen Evolution, *Nature Communications* 10 (2019): 982.

[5] Pataniya, Pratik M., Vikas Patel, and C. K. Sumesh, MoS_2/WSe_2 Nanohybrids for Flexible Paper-Based Photodetectors, *Nanotechnology* 32.31 (2021): 315709.

[6] Bao, X., Q. Ou, Z. Q. Xu, Y. Zhang, Q. Bao, and H. Zhang, Band Structure Engineering in 2D Materials for Optoelectronic Applications, *Advanced Materials Technologies* 3 (2018): 1800072.

[7] Xu, H., J. Zhu, Q. Ma, J. Ma, H. Bai, L. Chen, et al., Two-Dimensional MoS_2: Structural Properties, Synthesis Methods, and Regulation Strategies toward Oxygen Reduction, *Micromachines* 12 (2021): 240.

[8] Li, Guoqing, et al., All the Catalytic Active Sites of MoS_2 for Hydrogen Evolution, *Journal of the American Chemical Society* 138.51 (2016): 16632–16638.

[9] Kumar, R., X. Liu, J. Zhang, and M. Kumar, Room-Temperature Gas Sensors under Photoactivation: From Metal Oxides to 2D Materials, *Nano-Micro Letters* 12 (2020): 1–37.

[10] Chen, J., N. Kuriyama, H. Yuan, H. T. Takeshita, and T. Sakai, Electrochemical Hydrogen Storage in MoS_2 Nanotubes, *Journal of the American Chemical Society* 123 (2001): 11813–11814.

[11] Rusman, N., and M. Dahari, A Review on the Current Progress of Metal Hydrides Material for Solid-State Hydrogen Storage Applications, *International Journal of Hydrogen Energy* 41 (2016): 12108–12126.

[12] Jain, I., Hydrogen: The Fuel for 21st Century, *International Journal of Hydrogen Energy* 34 (2009): 7368–7378.

[13] Moon, S., K. Kim, and J. Kim, A Study on Public Acceptance of Hydrogen Portfolio Standard for Renewable Energy Expansion: Comparative Analysis of Hydrogen Production Mix Plans, *International Journal of Hydrogen Energy* 49 (2024): 538–552.

[14] Chen, W., L. Sui, X. Long, J. Liao, S. Wang, and X. Wei, Anatase TiO_2 Aerogel with High Specific Surface Areas and Porous Network Structures for Ultra-Fast Response Hydrogen Sensor, *International Journal of Hydrogen Energy* 50 (2024): 973–991.

[15] Pataniya, Pratik M., and C. K. Sumesh, MoS_2 Nanosheets on Cu-Foil for Rapid Electrocatalytic Hydrogen Evolution Reaction, *Journal of Electroanalytical Chemistry* 912 (2022): 116270.

[16] Kumar, S., A. Mirzaei, A. Kumar, M. H. Lee, Z. Ghahremani, T.-U. Kim, et al., Nanoparticles Anchored Strategy to Develop 2D MoS_2 and $MoSe_2$ Based Room Temperature Chemiresistive Gas Sensors, *Coordination Chemistry Reviews* 503 (2024): 215657.

[17] Yu, S., S. Song, R. Li, and B. Fang, The Lightest Solid Meets the Lightest Gas: An Overview of Carbon Aerogels and Their Composites for Hydrogen Related Applications, *Nanoscale* 12 (2020): 19536–19556.

[18] Chauhan, Payal, Dattatray J. Late, Vikas Patel, Parikshit Sahatiya, and C. K. Sumesh, Hierarchical NiCo-LDH@MoS_2/CuS Composite as Efficient Trifunctional Electrocatalyst for Overall Water Splitting and Asymmetric Supercapacitor, *Chemical Engineering Journal* 469 (2023): 143197.

[19] Patel, Meswa, Pratik Pataniya, Hitesh Vala, and C. K. Sumesh, One-Dimensional/Two-Dimensional/Three-Dimensional Dual Heterostructure Based on MoS_2 Modified ZnO-Heterojunction Diode with Silicon, *The Journal of Physical Chemistry C* 123.36 (2019): 21941–21949.

[20] Kapatel, Sanni, and C. K. Sumesh, One Pot Sono-Chemical Synthesis of 2D Layered MoS_2 Nanosheets, *AIP Conference Proceedings* 1728.1 (2016).

[21] Eda, G., H. Yamaguchi, D. Voiry, T. Fujita, M. Chen, and M. Chhowalla, Photoluminescence from Chemically Exfoliated MoS_2, *Nano Letters* 11.12 (2011): 5111–5116.

[22] Agrawal, A. V., R. Kumar, G. Yang, J. Bao, M. Kumar, and M. Kumar, Enhanced Adsorption Sites in Monolayer MoS_2 Pyramid Structures for Highly Sensitive and Fast Hydrogen Sensor, *International Journal of Hydrogen Energy* 45 (2020): 9268–9277.

[23] Cho, U. J., D. Jang, Y. Jeon, T. Kim, B. Jo, R. Kim, et al., A Palladium-Deposited Molybdenum Disulfide-Based Hydrogen Sensor at Room Temperature, *Applied Sciences* 13 (2023): 10594.

[24] Kronberg, R., M. Hakala, N. Holmberg, and K. Laasonen, Hydrogen Adsorption on MoS_2 Surfaces: A DFT Study on Preferential Sites and the Effect of Sulfur and Hydrogen Coverage, *Physical Chemistry Chemical Physics* 19 (2017): 16231–16241.

[25] Liu, X., W. Yang, and Z. Liu, Recent Progress on Synchrotron-Based In-Situ Soft X-Ray Spectroscopy for Energy Materials, *Advanced Materials* 26 (2014): 7710–7729.

[26] Kautz, E. J., D. K. Schreiber, A. Devaraj, and B. Gwalani, Mechanistic Insights into Selective Oxidation and Corrosion of Multi-Principal Element Alloys from High Resolution and In Situ Microscopy, *Materialia* 18 (2021): 101148.

[27] De Arco, L. G., Y. Zhang, A. Kumar, and C. Zhou, Synthesis, Transfer, and Devices of Single- and Few-Layer Graphene by Chemical Vapor Deposition, *IEEE Transactions on Nanotechnology* 8.2 (2009): 135–138.

[28] Patel, Meswa Harshadkumar, Pratik Pataniya, Hitesh Vala, and Challappally Kesav Sumesh, 1D/2D/3D Dual Heterostructure Based on MoS_2 Modified ZnO Heterojunction Diode with Silicon, *The Journal of Physical Chemistry C* 123.36 (2019): 21941–21949.

[29] Khan, M., S. Kumar, A. Mishra, I. Sulania, M. N. Tripathi, and A. Tripathi, Study of Structural and Electronic Properties of Few-Layer MoS_2 Film, *Materials Today: Proceedings* 57.1 (2022): 100–105.

[30] Kulriya, P. K., Mohit Kumar, Jitendra Singh, and D. K. Avasthi, Hydrogen Pressure Dependent In-Situ Electrical Studies on Pd/C Composite, *International Journal of Hydrogen Energy* 42.5 (2017): 3399–3406.

[31] Kulriya, P., F. Singh, A. Tripathi, R. Ahuja, A. Kothari, R. Dutt, et al., Setup for In Situ X-Ray Diffraction Study of Swift Heavy Ion Irradiated Materials, *Review of Scientific Instruments* 78 (2007).

[32] Yim, C., M. O'Brien, N. McEvoy, S. Riazimehr, H. Schäfer-Eberwein, A. Bablich, et al., Heterojunction Hybrid Devices from Vapor Phase Grown MoS_2, *Scientific Reports* 4 (2014): 5458.

[33] Li, H., Q. Zhang, C. C. R. Yap, B. K. Tay, T. H. T. Edwin, A. Olivier, et al., From Bulk to Monolayer MoS_2: Evolution of Raman Scattering, *Advanced Functional Materials* 22.7 (2012): 1385–1390.

[34] Zhou, K.-G., F. Withers, Y. Cao, S. Hu, G. Yu, and C. Casiraghi, Raman Modes of MoS_2 Used as Fingerprint of van der Waals Interactions in 2-D Crystal-Based Heterostructures, *ACS Nano* 8.10 (2014): 9914–9924.

[35] Lei, L., D. Huang, G. Zeng, M. Cheng, D. Jiang, C. Zhou, et al., A Fantastic Two-Dimensional MoS_2 Material Based on the Inert Basal Planes Activation: Electronic Structure, Synthesis Strategies, Catalytic Active Sites, Catalytic and Electronics Properties, *Coordination Chemistry Reviews* 399 (2019): 213020.

[36] Ma, L., D. N. Nath, E. W. Lee, C. H. Lee, M. Yu, A. Arehart, et al., Epitaxial Growth of Large Area Single-Crystalline Few-Layer MoS_2 with High Space Charge Mobility of 192 cm^2 V^{-1} s^{-1}, *Applied Physics Letters* 105 (2014).

[37] Marinov, D., J.-F. de Marneffe, Q. Smets, G. Arutchelvan, K. M. Bal, E. Voronina, et al., Reactive Plasma Cleaning and Restoration of Transition Metal Dichalcogenide Monolayers, *npj 2D Materials and Applications* 5 (2021): 17.

Chapter 4

Influence of Temperature and NO_2 Concentration on the Sensing Performance of Nanostructured MoS_2

4.1 Introduction

Detection of toxic gases such as nitrogen dioxide (NO_2) is essential for safeguarding human health, ensuring workplace safety, and monitoring environmental pollution. NO_2, a by-product of combustion in vehicles and industrial processes, is harmful even at low concentrations (as low as 10–20 parts per million (ppm)) and can cause severe respiratory, neurological, and cardiovascular issues at higher exposures. Conventional gas sensors based on metal oxide semiconductors (e.g., SnO_2, ZnO, WO_3) offer low cost and robustness but often require high operating temperatures (>200 °C), suffer from poor selectivity, and show slow recovery times, particularly in humid or complex gas environments [1–3]. Two-dimensional (2D) transition metal dichalcogenides (TMDs), and in particular molybdenum disulfide (MoS_2), have emerged as promising alternatives for next-generation gas sensors. MoS_2 offers a high specific surface area, tunable bandgap (1.2–1.8 eV), rich surface chemistry, and strong adsorption affinity for oxidizing gases such as NO2 [4,5]. Its layered structure provides abundant active sites (including edge defects and sulfur vacancies) that facilitate charge transfer upon gas adsorption, enabling detection at lower temperatures and with higher selectivity than many metal oxides [6].

Furthermore, MoS_2 demonstrates better chemical stability in oxidizing environments compared to other 2D materials such as black phosphorus or MXenes, which are prone to degradation in air [7]. Recent studies have explored MoS_2 in both pristine and hybrid forms. For example, Park et al. (2022) demonstrated room-temperature NO_2 detection using few-layer MoS_2 with UV activation, achieving a detection limit of 50 ppb [8]. Zhang et al. (2023) reported MoS_2–ZnO heterostructures with enhanced sensitivity and recovery speed due to synergistic band alignment effects [9]. Similarly, MoS_2/graphene hybrids have been shown to combine high carrier mobility with strong adsorption, yielding ultrafast responses under ambient conditions [10]. The graphene/MoS_2 hybrids also displayed an enhanced performance in several applications, such as lithium-ion batteries [10], supercapacitors [11], field-effect transistors (FETs) [12], and photodetectors [13]. Enhancement in the sensing efficiency in MoS_2/graphene hybrid materials is observed due to electric charge transport via heterojunction's structure and its unique electronic structure, which is mediated by band energy synchronisation [14]. The ultra-thin MoS_2 sensor demonstrated an impressive reaction/recovery against NO_2 gas with excellent stability and repeatability as compared to other target gases such as H_2, NH_3, SO_2, CO_2 [15].

Compared to these binary and ternary systems, pure MoS_2 offers the advantage of simpler synthesis, well-controlled film quality, and fewer interfacial complications, while still achieving competitive performance when growth parameters and electrode design are optimized. In addition, it also requires an inert environment for gas detection due to MoS_2's low stability and selectivity. Despite these advances, the influence of operating temperature and gas concentration on the intrinsic NO_2 sensing properties of well-defined nanostructured MoS_2 films remains insufficiently explored. Most prior works focus on room-temperature performance or hybrid material systems, leaving a gap in understanding the temperature-dependent kinetics and stability of pure MoS_2 in NO_2-rich and potentially harsh environments.

In this chapter, we systematically investigate the effect of both temperature (50–150 °C) and NO_2 concentration (1–100 ppm) on the sensing performance of CVD-grown MoS_2 thin films with optimized interdigitated electrodes. The sensor exhibited high selectivity, fast response (102 sec) and recovery (94 sec) time at 20 ppm concentration of NO_2 at 150 °C. In addition, significantly improvement in response at high temperature and structural defects at higher concentrations is also observed. The results provide insights into the trade-offs between response magnitude, speed, and long-term stability, offering guidance for designing MoS_2-based sensors for industrial and environmental monitoring.

4.2 Experimental Sections

4.2.1 Designing and Fabrication of Gas Sensor Platform

The 0.5 mm thick alumina substrate was used to create the gas sensor platform. The electrode pattern was made of metallic Molybdenum (Mo) with a layer thickness of 200 nm. Sputter deposition was used to deposit a thin layer of molybdenum (Mo). The electrode pattern was defined using a physical mask. The spacing was kept at 300 µm, and the electrode line width was 300 µm. The heating element (resistor) and gas sensor electrode were combined into a single device platform. The dimensions of the sensor die were 3.0 mm by 3.0 mm. For gas sensing, the sensor was installed on the header of the customised transistor outline (TO) packages. After process parameters optimization, gas sensing layer (MoS_2) was coated on the interdigital transducer electrodes (IDT). Humidity strongly influences Chemiresistive gas sensing by competing with target gas molecules for surface adsorption sites. In this study, sensing measurements were conducted under controlled dry air conditions to suppress humidity-related interference and to isolate the intrinsic interaction between NO_2 molecules and the MoS_2 sensing layer, thereby enabling clear evaluation of temperature-dependent sensing behaviour. The schematic and optical image of the MoS_2 gas sensor device shown in Figure 4.1.

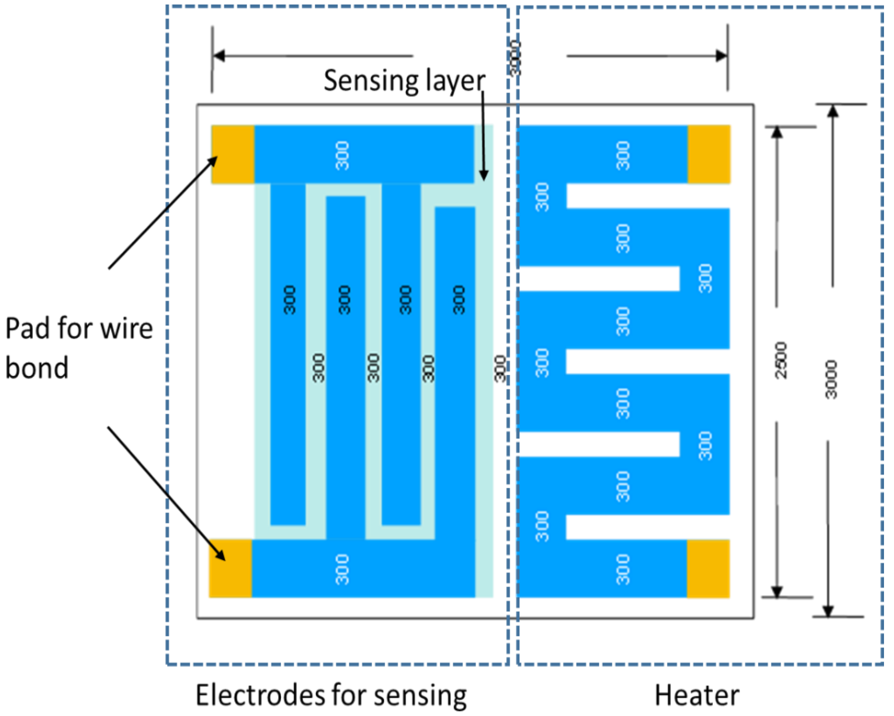

Figure 4. 1: Schematic and optical image of the MoS_2 gas sensor device showing the interdigitated electrodes used for resistance measurements and the integrated micro-heater for temperature control.

4.2.2 Preparation of MoS_2 films:

Based on observations from double-zone CVD-grown MoS_2 films, a three-zone CVD approach was adopted to achieve greater control over precursor evaporation and film growth kinetics. The additional temperature zone enables independent regulation of sulfur, molybdenum precursor and substrate temperatures, thereby allowing precise control over nucleation density, crystallinity, grain size and defect concentration. Such control is expected to improve film uniformity and charge transport while maintaining an optimum number of active sites for gas adsorption. Figure 4.2 shows the schematic of three-zone tubular CVD furnace used to deposit the MoS_2 thin film on the alumina substrate having dimensions of 3.0 mm by 3.0 mm. The thickness of MoS_2 film was kept ~20 nm to ensure continuous film coverage, high crystallinity, and stable electrical contact with the interdigitated electrodes, while maintaining reliable controllability of the CVD growth process. We have also deposited thinner films (5 nm and 10 nm) which displayed discontinuity and increased contact resistance that were not found suitable for sensing applications. Similarly, thicker films can reduce surface sensitivity due to dominant bulk conduction pathways. Before deposition, the alumina substrate was first ultrasonically cleaned with acetone and isopropyl alcohol (IPA), and then gaseous nitrogen was used to dry it. An extra cleaning procedure was performed prior to the alumina substrate being put into the CVD furnace's middle zone. The quartz boat was filled with high purity (99.999 %) of molybdenum trioxide (MoO_3) and the alumina boat was filled with high purity (99.995 %) sulfur procured from the Sigma Aldrich. The three zones for alumina are kept at 800 °C for the substrate, 650 °C for MoO_3, and 200 °C for sulfur. High-purity Ar gas flowed with a mass flow controller (MFC) at 200 sccm during the growth process [16].

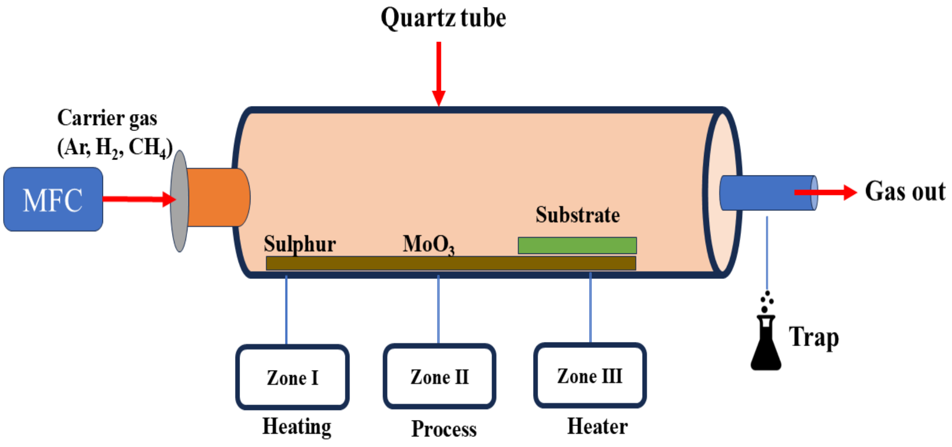

Figure 4.2: Synthesis of MoS_2 films using three zone chemical vapour deposition (CVD) technique.

4.2.3 Characterizations of MoS_2 films:

The Bruker AXS D8-advanced X-ray diffractometer (XRD equipment) equipped with a Cu K_α source with a wavelength of 1.54 Å (40 kV and 40 mA power), was used to record the XRD patterns. With a laser wavelength of 532.5 nm, the short-range ordering and molecular structure of pure MoS_2 were examined using a Raman spectrometer (WITec alpha 300 RA). MoS_2's surface shape and elemental analysis were assessed using ZEISS EVO 40 energy dispersive spectroscopy (EDS) and scanning electron microscopy (SEM). NTMDTNTEGRA-prima instrument was used to perform atomic force microscopy (AFM) for the roughness measurements of thin film surface.

4.3 Results and discussion

4.3.1 Structural Analysis:

X-ray diffraction (XRD) technique was used to determine the degree of crystallinity of the MoS_2 thin film deposited on the alumina substrate. Figure 4.3(a) shows the XRD pattern of the MoS_2 thin-film. The XRD peaks were appeared at the 2-theta values of 14.3°, 25.4°, 39.0°, and 58.4°, which correspond to values of at (002), (004), (103) and (110) planes as confirmed from the JCPDS No: 75-1539. This clearly confirms the synthesis of impurity free polycrystalline MoS_2 phase.

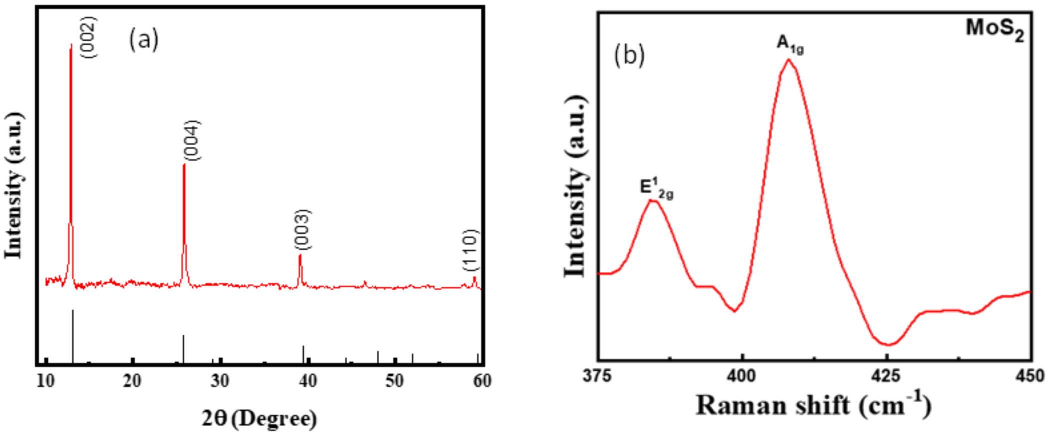

Figure 4.3: (a) XRD pattern and (b) Raman spectrum of MoS_2 thin films having of 20 nm thickness grown by CVD.

To probe the short-range ordering in the MoS_2 thin films, the Raman spectroscopy technique is considered as most suitable tool. Figure 4.3(b) displays Raman spectrum of the MoS_2 thin films. It exhibits the distinctive signal of 2H-MoS_2, with no observable evidence of carbon or oxides contamination. The characteristic peak appeared at the wavenumber of 385 cm^{-1}, corresponding to E^1_{2g} due to in-plane vibrational modes of the MoS_2 lattice, where another peak appeared at the wavenumber of 405 cm^{-1}, represents the out-of-plane vibrations of the MoS_2 layers. The well-matched unique peaks clearly show the formation of impurity free single phase MoS_2.

4.3.2 Micro-structural Analysis:

The surface morphology of the MoS_2 thin film (20 nm) was assessed using scanning electron microscopy (SEM). Figure 4.4 (a) displays a typical SEM picture of the MoS_2 thin film deposited using the CVD technique on alumina substrate. It shows that the MoS_2 nanosheets were evenly distributed throughout the substrate, giving the impression that there is no topographical contrast and that the surface is uniform. Initially, MoS_2 thin film grew as nanoparticles until it reached a threshold thickness. The nucleation sites merged, forming MoS_2 thin films. The nucleation sites in the favoured curved direction progressively changed into vertically developed structures, resulting in a MoS_2 flower-like structure as shown in Figure 4.4(a). It may be noted that the film-like surface morphology of chemical vapour deposited MoS_2 films differs significantly from films made using exfoliation or sputtering processes, which could improve gas sensing capability. Energy dispersive spectroscopy (EDS) was used to examine the composition of MoS_2 thin films, as shown in below Table 4.1. This shows that Mo, O, S, and Al elements make up the majority of the MoS_2 thin film, according to the element distribution. The alumina substrate also contributes to the presence of the additional aluminium and oxygen element. The particle size distribution histogram, shown in Figure 4 (b), provides an estimate of the average particle size was 0.71 μm.

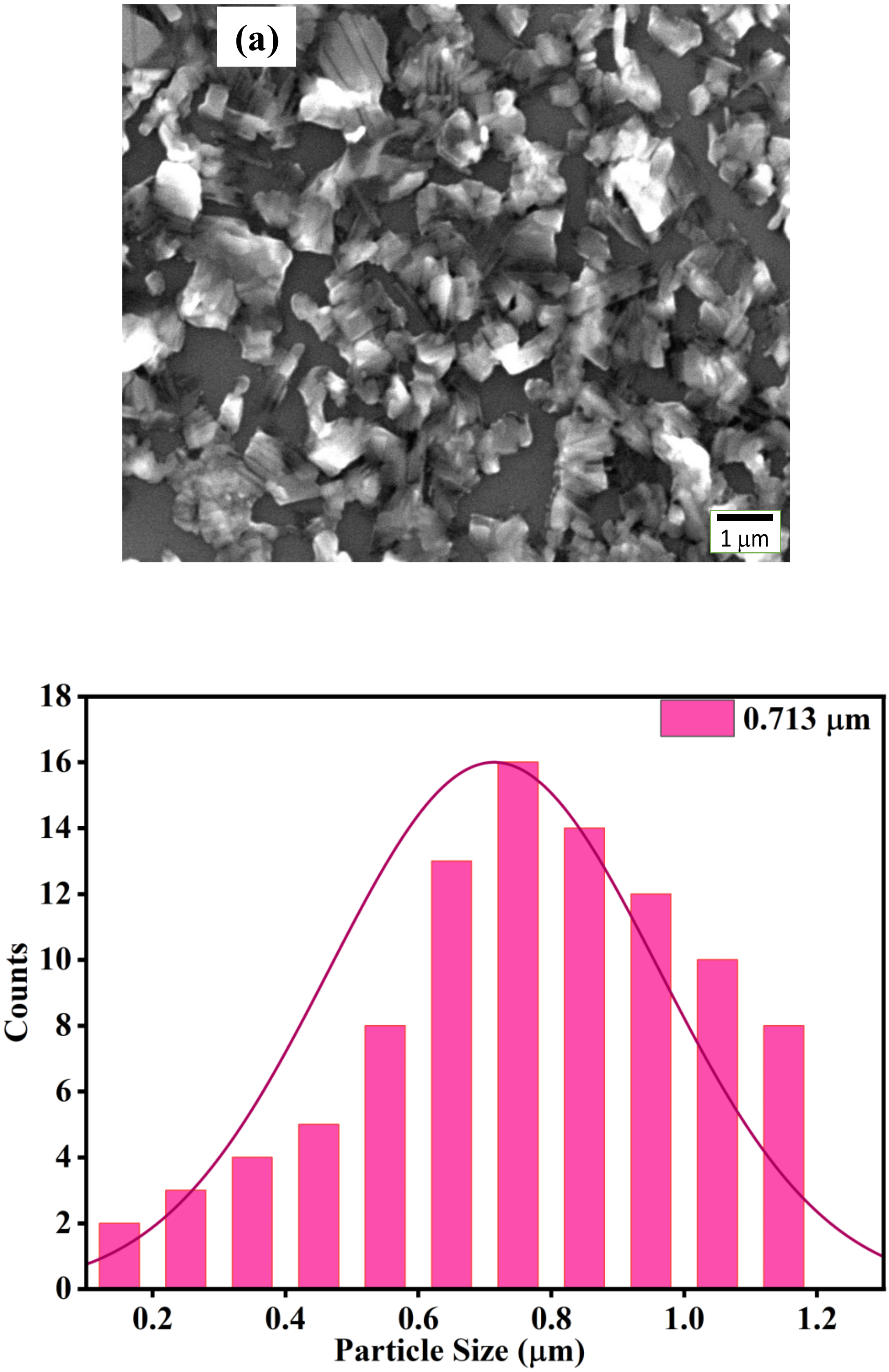

Figure 4.4: (a) SEM micrograph and (b) size distribution plot of as-synthesized MoS_2 thin films.

Table 4.1: Elemental composition obtained through EDS analysis of MoS_2 deposited on alumina substrate

Element	Line	Mass (%)	Atom (%)
O	K	25.18±0.43	39.52±0.67
Al	K	63.89±0.54	57.12±0.49
S	K	0.95±0.19	0.74±0.15
Mo	L	9.98±0.60	2.61±0.16

Figure 4.5 shows AFM images of MoS_2 thin films synthesized using chemical vapour deposition (CVD) method. The surface roughness of film was calculated using Nasoscope analysis 1.5 software. It shows that thickness of film is 20 nm and roughness was found 4.2 nm.

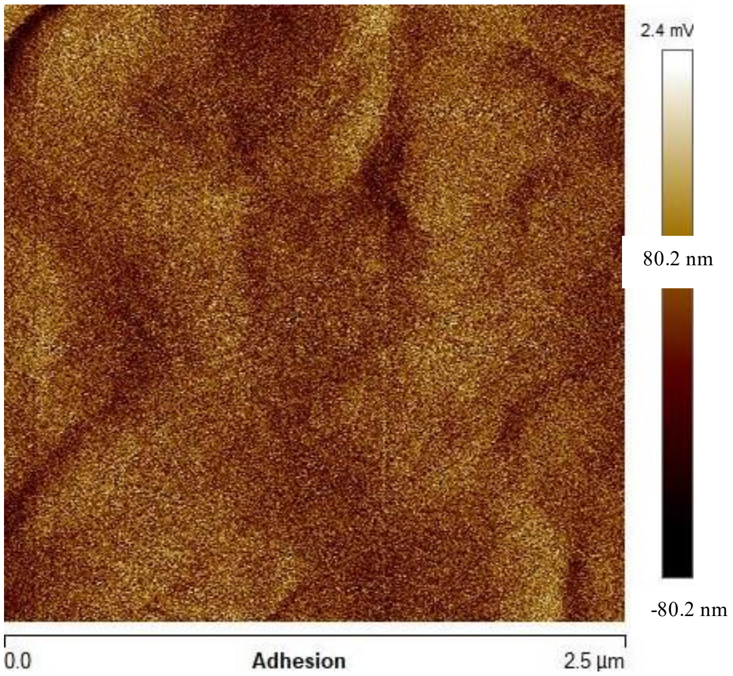

Figure 4.5: AFM image of as-grown MoS_2 thin films.

4.3.3 Sensing Characteristics of MoS_2 Thin Films:

The sensing performance of MoS_2 thin film was determined by electrical transport properties studies and measuring the response time, recovery time and sensitivity on the exposure to sensing gas. The predominant carrier in the sensing material and the kind of gas in the environment determine the change in the electrical resistance on the exposure to the NO_2 gas. Although, NO_2 is hazardous even at trace concentrations, the concentration range investigated in this work was intentionally selected to clearly resolve temperature-dependent sensing trends, response magnitude, and response–recovery kinetics under controlled laboratory conditions. The emphasis of this study is on understanding how operating temperature governs sensing behavior and performance trade-offs in pristine MoS_2 sensors, rather than on demonstrating trace-level detection limits. It has been reported that oxidizing gases act as acceptors, increasing resistance in n-type materials, whereas reducing gases act as donors, decreasing resistance in n-type materials [17]. In the case of p-type materials, the opposite pattern is observed. In the present study, the n-type MoS_2 sensor displays an increase in the electrical resistance of the MoS_2 thin film due to an oxidizing gas (NO_2). For the MoS_2-Al_2O_3 sample, electrical measurements were performed in two probe geometries to validate the MoS_2 film's behaviour. Using a planar contact arrangement, I-V characteristics were measured. The two contacts were taken from interdigital electrodes. MoS_2's n-type semiconducting behaviour is confirmed by the rectifying behaviour displayed by the I-V characteristic. The response of the sensor is defined as

$$Response\ (\%) = \frac{Rg-Ra}{Ra} \times 100 \tag{4.1}$$

Where, R_a and R_g are the electrical resistance of sensors in dry air and oxidizing gas atmosphere, respectively. Figure 4.6 (a) shows the relative response of MoS_2 films towards NO_2 gas taken at different temperatures ranging from 50 °C, 75 °C, 100 °C, 125 °C and 150 °C at 20 ppm. This plot indicates that the relative response of MoS_2 films increases with an increase in the temperature. The highest response of 14.2 % was observed for 20 ppm concentration at 150 °C temperature. When sensing gas is removed then the value of relative response was decreased. The value of the relative response after removal of the sensing gas highest at 50 °C. This is reduced when the temperature is increased from 50 °C to 100 °C. However, the minimum value of the relative response remained identical for 100 °C, 125 °C and 150 °C temperatures. This indicates that some permanent structural defects were created in the film which were not removed even the temperature was increased above 100 °C. In addition to temperature, concentration of the sensing gas also plays an important role in the determination of the sensing properties of gas. Figure 4.6 (b) exhibits the electrical resistance versus time plot for NO_2 gas sensing performed at 150 °C by exposing to the sensing gas at various concentrations starting from 1 to 100 ppm at concentrations of 1 ppm, 10 ppm, 20 ppm, 50 ppm, and 100 ppm. The maximum value of the electrical resistance is the same for all the values of the concentration but the time required to attain the maximum value depends upon the concentration. The minimum value of resistance after unloading the sensing gas is continuously decreasing as the concentration increases. The lowest value is achieved for the sample exposed to the highest concentration (100 ppm) of the sensing gas. Figure 4.6 (c) displays the relative response of NO_2 gas at various concentrations starting from 1 ppm to 100 ppm at concentrations of 1 ppm, 10 ppm, 20 ppm, 50 ppm, and 100 ppm performed at 150 °C. The relative response of NO_2 gas is increased as the concentration is increased from 1 ppm to 100 ppm. The variation in the relative response for 20 ppm concentration at 150 °C is shown in Figure 4.6 (d). Figure 4.6 (e) shows the repeatability of 20 ppm concentration sensing at the same temperature and further, the response and recovery time of the as-prepared gas sensor were calculated for the sensing peak of 20 ppm and 150 °C. The calculated values of the response time and recovery time are 102 sec and 94 sec, respectively as shown in Figure 4.6(f). The response time is defined as the duration required to reach 90% of the total resistance change upon NO_2 exposure, whereas the recovery time corresponds to 90% restoration of the baseline resistance after gas removal. The comparatively faster recovery arises from temperature-assisted desorption processes, which enhance the release of adsorbed NO_2 molecules from the MoS_2 surface. This kind of response is better than the early reported MoS_2 gas sensor for NO_2 gas sensing as depicted in Table 4.2 as well. In addition, baseline drift si also observed during repeated sensing cycles, particularly at elevated operating temperatures. This arises from slow desorption kinetics and partial irreversible adsorption of NO_2 molecules at defect-rich or edge sites of MoS_2. This behavior is characteristic of 2D material-based chemiresistive sensors exposed to oxidizing gases and primarily affects the absolute baseline rather than the relative sensing response.

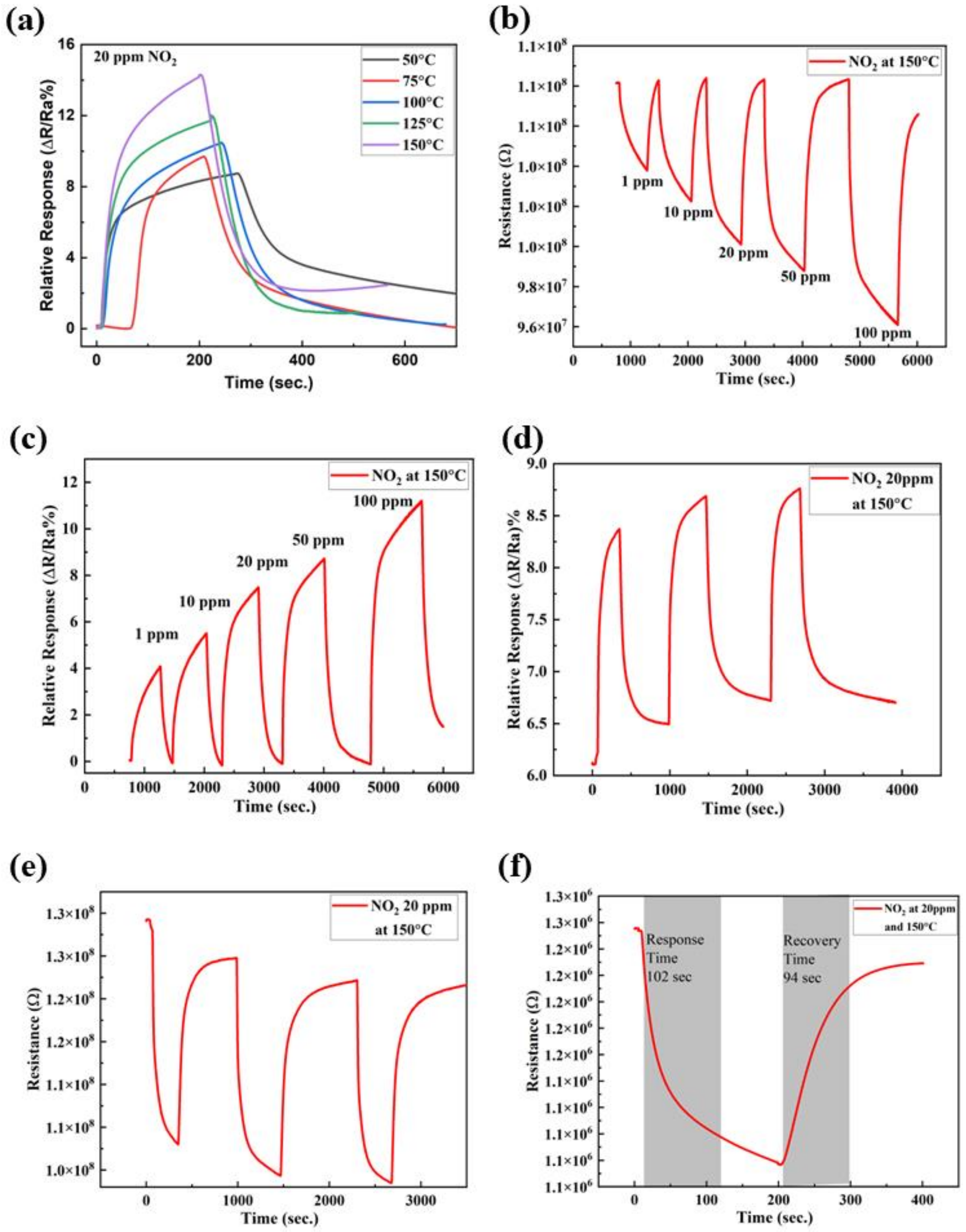

Figure 4.6 : Represent sensing response of NO_2 as (a) the relative response at different temperatures at 20 ppm concentration (b) the resistance versus time plot at 150 °C with varying concentrations (c) the relative response at 150 °C with varying concentrations, (d) the

repeatability of response at 20 ppm (e) its corresponding resistance plot and (f) the calculations of response and recovery time.

Response and recovery periods for a 20 nm thick MoS_2 sensor at 150 °C were measured for different NO_2 concentrations. These data reveal that when NO_2 gas concentrations increase, so do response and recovery times. As the quantity of exposed gas increases then the number of gas molecules that can interact with the detecting surface. Increased gas molecule adsorption increases response time while also increasing the electron concentration for exchange between sensing material and gas molecules. Many molecules must be desorbed from the surface during recovery, which increases the time required for the surface to restore its original resistance. As a result, the interaction kinetics of gas molecules at varied concentrations on the sensor surface generate varying response and recovery durations. Response and recovery time plot for NO_2 concentration is shown in Figure 4.7. This clearly shows that response and recovery time are increasing with an increase in the concentration of the NO_2 gas. It is worth to mention here that the sensor temperature was controlled using a variable voltage controller, while a constant 3V bias was applied to the contact pad. The sensing performance was evaluated by monitoring resistance variations upon exposure to target gases NO_2 at a concentration of 1 %. During sensing measurements, the temperature and relative humidity (RH) witin the sensing chamber were continually monitored and adjusted using a digital hygrometer (HTC instrument HT-306) [18]. Relative response of MoS_2 for NO_2 gas at different concentration with error bars shown in Figure 4.8.

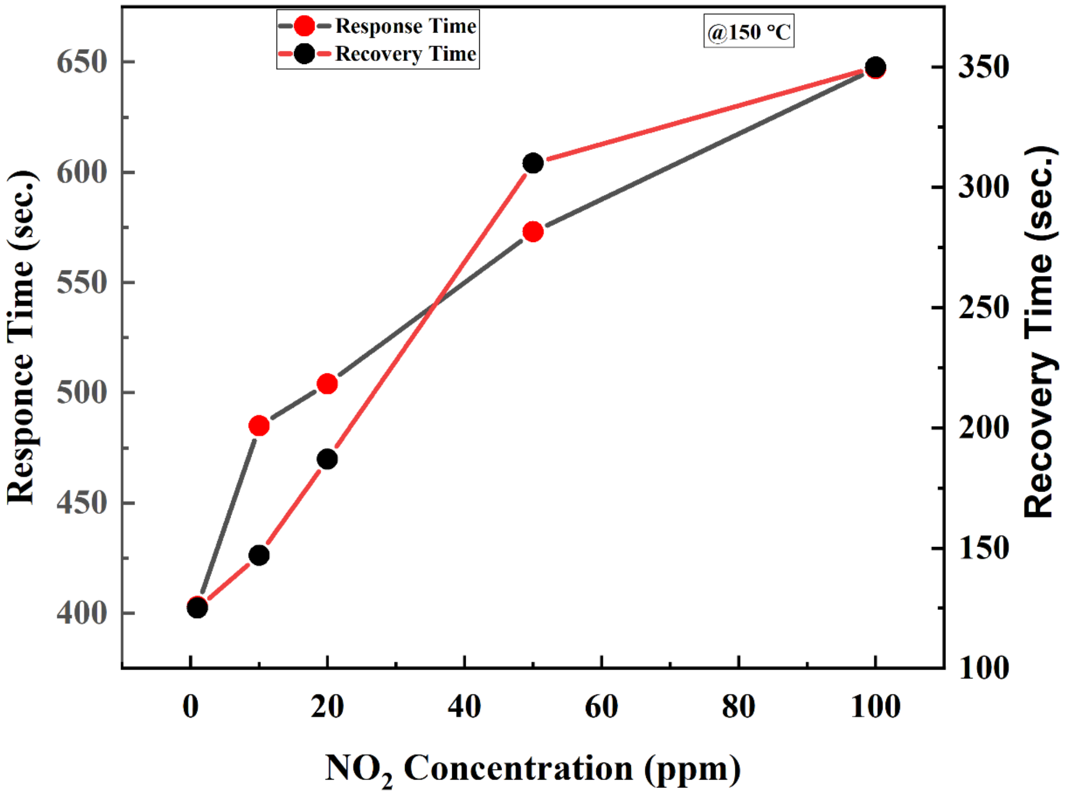

Figure 4.7 : Response and recovery time plot with respect to different gas concentration (NO_2) at 150 °C temperature.

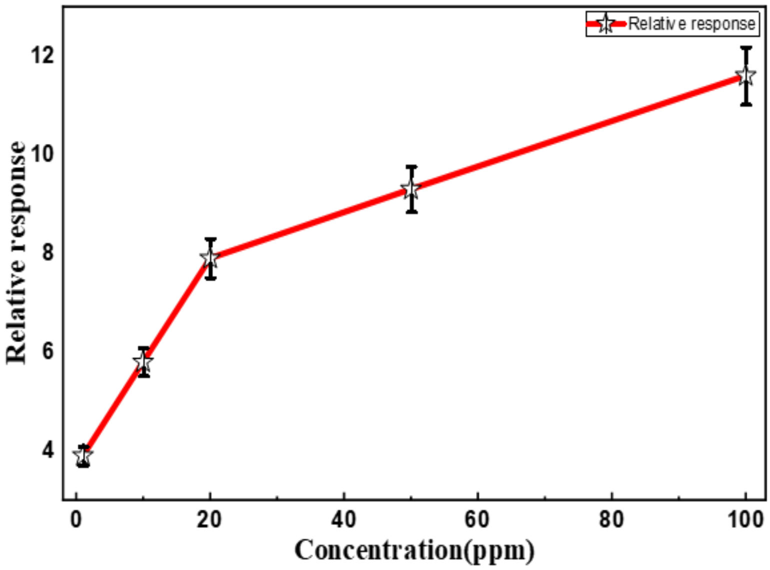

Figure 4.8 : Relative response of MoS_2 for NO_2 gas at different concentration.

The limit of detection (LOD) may be estimated using the standard relation LOD = 3 σ/S, where σ represents the standard deviation of the baseline resistance noise and S denotes the slope of the calibration curve in the low-concentration regime. This approach provides an estimate of the sensor's capability for detecting lower NO_2 concentrations. The caclauted value of the limit of detection is 0.067 ppm.

In MoS_2 films, the sulfur vacancies and other flaws in the MoS_2 film serve as the gas molecules active sites. Initially, partial oxidation of the MoS_2 top layer is caused by oxygen gas molecules in the environment through the chemisorbing at the surface of the sensing film and forming oxygen species. Conduction band electrons are extracted from the MoS_2 film by these ions acting as electron trap centres. Thus, initially electrical resistant of the sensor increases as the concentration of free electrons in the conduction band begins to drop. A significant factor in altering the sensing material's initial electrical resistant was the chemisorption of oxygen gas molecules.

$O_2(gas) \rightarrow O_2(ads)$

$O_2(ads) + e^{-}_{MoS2} \rightarrow O_2(ads)$

When MoS_2 film is exposed to NO_2 gas then the electrons from the MoS_2 conduction band are transferred to the NO_2 molecules and get adsorbed on the film surface [18]. Conversely, NO_2 gas creates NO_2 ions by reaction with oxygen ions (O_2). This procedure raises the gas sensor's overall electrical resistant while lowering the concentration of electrons in the detecting material. Figure 4.9 shows the mechanism for the sensing of NO_2 gas with MoS_2.

$NO_2(gas) + e_{MoS2} \rightarrow NO_2(ads)$

$NO_2(ads) + O_2(ads) \rightarrow NO_2(gas) + 2O(ads)$

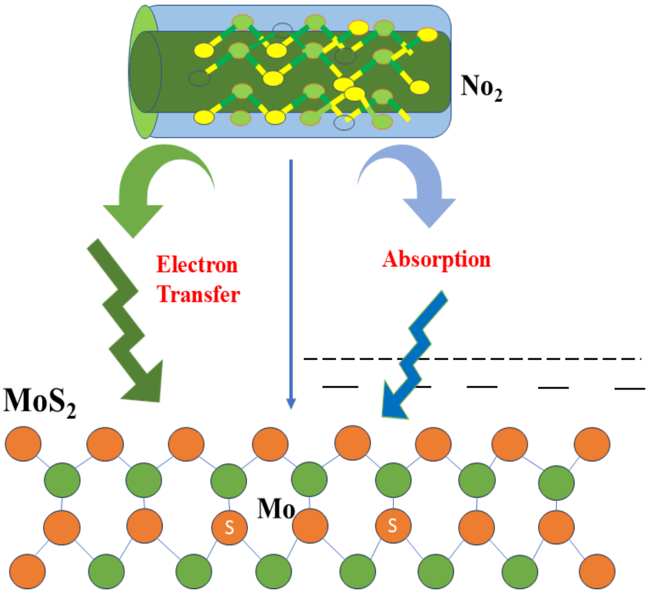

Figure 4.9: Mechanism for the sensing of NO_2 gas with MoS_2

During the recovery process, NO_2 ions react to O_2 ions in sensing chamber to release NO_2 gas into the environment when the flow of NO_2 gas stops. Oxygen ions once more approach the active surface to create native oxide. The sensor resistant returns to its starting value when the electrons that NO_2 had trapped are released back into MoS_2 conduction band.

The adsorption and desorption of oxygen is also affected by the operating temperature. At relatively low operating temperatures, molecularly adsorbed oxygen species dominate the surface, whereas increasing temperature promotes the formation of more reactive oxygen species with enhanced electron withdrawal capability. This temperature-dependent evolution of surface oxygen species contributes to the observed enhancement in charge transfer and sensing response. Recent NO_2 sensing studies based on MoS_2 have employed diverse performance-enhancement strategies. UV-assisted heterostructure sensing in the $MoS_2/PtSe_2$ system has been demonstrated high sensitivity towards NO_2 gas at room temperature under UV illumination [22]. Edge-engineered heterostructures, such as the $Mo2TiC_2Tx/MoS_2$ platform reported by Zhao et al. [23], exploit enriched edge sites and interfacial coupling to improve sensing performance. Electrocatalytic and radical-assisted approaches have been explored by Li et al. [24] through CoP/MoS_2 systems, where surface radical generation enhances the NO_2 response at room temperature. In addition, Bharathi et al. [25] reported edge-activated, solution-processed Ni–MoS_2 nanosheets, highlighting the role of edge activation in achieving high sensitivity. In contrast to these approaches, the present work focuses on pristine CVD-grown MoS_2 and systematically examines temperature-driven sensing behavior using an integrated micro-heater, providing complementary insight into performance tuning without additional material modification or external activation. The comparison of performance metrics for the MoS_2-based gas sensors from several investigations, including the present one, is shown in Table 4.2.

Table 4.2: Literature review MoS_2 nanostructures for NO_2 gas response.

Material	**Method**	**Morphology**	**NO_2 conc.**	**T (°C)**	**Gas Response (%)**	**Response/recovery time**	**Ref.**
MoS_2	CVD	Flakes	100 ppm	100	21.56	71/310 sec	[7]
MoS_2	One step hydrothermal	Hollow sphere	20 ppb	150	40.3	79/225 sec	[18]
n-MoS_2 p-MoS_2	Chemical exfoliation	Flakes	100 ppm	200	5.8 1.15	2460/2340 sec 660/720 sec	[19]
MoS_2	Mechanical exfoliation	Five layer	100 ppm	RT	–	180/600 sec	[20]
MoS_2	CVD	Bilayer film	1 ppm	RT	2.6	678/318 sec	[21]
MoS_2	CVD	Vertically aligned layers	800 ppb	RT	13	344/581 sec	[22]
MoS_2	CVD	Flakes	50 ppm	RT	19.25	33.5/140.1 sec	[23]
MoS_2	CVD	Nanosheet	100 ppm	RT	20	15/180 sec	[24]
Ni-MoS_2	CVD	Flakes	200 ppm	RT	45.2	28/250 sec	[25]
MoS_2	CVD	Film	100 ppm	150	14	102/94 sec	This work

The performance metrics for MoS_2-based gas sensors from several investigations show that sensing response critically depends upon various factors such as the surface morphology, methods for the preparation of film, concentration of sensing gas and operating temperature. If one compares the temperature dependent sensing response of CVD grown MoS_2 films, it is observed that the response decreases with increasing temperature. Tthe response time improves significantly, decreasing from 678 sec at room temperature to 102 sec at 150 °C, confirming enhanced response speed at elevated temperatures. This clearly suggest that the operating temperature plays a decisive role in controlling adsorption–desorption kinetics and charge transfer processes at the MoS_2 surface. Increasing operating temperature enhances the interaction between adsorbed NO_2 molecules and the sensing layer, resulting in improved response magnitude and faster recovery, while simultaneously introducing a trade-off with baseline stability. These observations highlight the importance of temperature optimization for achieving balanced sensor performance. Inspite all excellent sensing performance of MoS_2 thin films at high temperature, it consumes higher power which can increase the cost of the device. Therefore, further research on the optimizing the operating temperature of MoS_2 based sensor without compromising sensor performance is required. Although the present study demonstrates a significant response of the MoS_2 thin-film sensor toward NO_2, its selectivity against common interfering gases such as NH_3, CO, H_2, volatile organic compounds, and humidity has not been systematically investigated. Therefore, the sensor's selectivity under complex environmental conditions cannot be conclusively established at this stage. Since humidity and interfering gases may compete for adsorption sites and alter charge transfer processes, they can potentially influence the sensor response and recovery characteristics.

4.4. Conclusion

The effect of gas concentrations and temperatures on the sensing response of the CVD grown MoS_2 thin films measured on exposure to NO_2 gas display excellent response for MoS_2 film thickness of 20 nm. The interdigitated contacts having improved shape also used to increase the gas sensing response of the sensor. The as-prepared MoS_2 thin films were characterized using XRD, FESEM, EDS, AFM and Raman spectroscopy techniques. XRD analysis showed the formation of polycrystalline phases of MoS_2. Structural and elemental analysis showed purity and uniformity of MoS_2. The MoS_2 sensor with a thickness of 20 nm results to reasonable responsivity (~14.2%), prompt response (~102 sec.), and recovered (~94 sec.) to 20 ppm NO_2 in dry air at 150 °C. The sensing response is dominated by surface adsorption-induced charge transfer between NO_2 molecules and MoS_2, consistent with a surface-controlled chemiresistive mechanism. The three-zone CVD-grown MoS_2 films exhibited improved structural uniformity and crystallinity compared with the double-zone-grown films. Better control over defect density and film morphology resulted in enhanced charge transport, improved reproducibility, and superior sensing performance. The comparative investigation of double-zone and three-zone CVD methods establishes a direct correlation between synthesis conditions, structural properties and gas sensing behaviour, demonstrating that optimisation of growth kinetics is essential for achieving high-performance MoS_2-based gas sensors. The sensor exhibited stable and repeatable responses over multiple consecutive sensing cycles, indicating reliable short-term operational stability under the tested conditions. The sensing response of MoS_2-based gas critically depends upon various factors such as the surface morphology, methods for the preparation of the film, concentration of sensing gas and operating temperature.

4.5 References

[1] S.J. McDonnell, R.M. Wallace, Atomically-thin layered films for device applications based upon 2D TMDC materials, Thin Solid Films 616 (2016) 482–501.

[2] S. Varghese, S. Varghese, S. Swaminathan, K. Singh, V. Mittal, Two-Dimensional materials for sensing: graphene and beyond, Electronics 4 (2015) 651–687.

[3] A. Shokri, N. Salami, Gas sensor based on MoS_2 monolayer, Sens. Actuators, B Chem. 236 (2016) 378–385.

[4] A.A. Mane, A.V Moholkar, Effect of solution concentration on physicochemical and NO_2 gas sensing properties of sprayed MoO_3 nanobelts, Thin Solid Films 648 (2018) 50–61.

[5] J. Guo, R. Wen, J. Zhai, Z.L. Wang, Enhanced NO_2 gas sensing of a single-layer MoS_2 by photogating and piezo-phototronic effects, Sci. Bull. 64 (2019) 128–135.

[6] W. Li, Y. Zhang, X. Long, J. Cao, X. Xin, X. Guan, J. Peng, X. Zheng, Gas sensors based on mechanically exfoliated MoS_2 nanosheets for room-temperature NO_2 detection, Sensors (Basel) 19 (2019) 1–12.

[7] R. Kumar, N. Goel, M. Kumar, UV-activated MoS_2 based fast and reversible NO_2 sensor at room temperature, ACS Sens. 2 (2017) 1744–1752.

[8] A. Kuc, T. Heine, A. Kis, Electronic properties of transition-metal dichalcogenides, MRS Bull. 40 (2015) 577–584.

[9] Sha, Rinky, and Tarun Kanti Bhattacharyya, MoS_2-based nanosensors in biomedical and environmental monitoring applications, Electrochimica Acta 349 (2020): 136370.

[10] Wang, Juan, et al, Synthesis of MoS_2 and Graphene Composites as the Anode Materials for Li–Ion Batteries, Energy Technology 6.10 (2018): 1913-1920.

[11] Palsaniya, Shatrudhan, Harshal B. Nemade, and Ashok Kumar Dasmahapatra, Synthesis of polyaniline/graphene/MoS_2 nanocomposite for high performance supercapacitor electrode, Polymer 150 (2018): 150-158.

[12] Yu, Lili, et al, Graphene/MoS_2 hybrid technology for large-scale two-dimensional electronics, *Nano letters* 14.6 (2014): 3055-3063.

[13] Roy, Kallol,et al, Graphene–MoS_2 hybrid structures for multifunctional photoresponsive memory devices, Nature nanotechnology 8.11 (2013): 826-830.

[14] Dutta, Priyanka, and Govind Gupta, Environmental gas sensors based on electroactive hybrid organic–inorganic nanocomposites using nanostructured materials, Physical Chemistry Chemical Physics 24.47 (2022): 28680-28699.

[15] Davila,M.E.; Xian,L.; Cahangirov,S.; Rubio,A.; LeLay,G.Germanene: Anoveltwo-dimensionalgermanium allotrope akin to graphene and silicene. New J. Phys. 2014, 16, 095002.

[16] Kumar, Sunil, et al., A systematic review on 2D MoS_2 for nitrogen dioxide (NO_2) sensing at room temperature, Materials Today Communications 34 (2023): 105045.

[17] M. Donarelli, S. Prezioso, F. Perrozzi, F. Bisti, M. Nardone, L. Giancaterini, C. Cantalini, L. Ottaviano, Response to NO_2 exfoliated MoS_2 and other gases of resistive chemically -based gas sensors, Sens. Actuators, B Chem (2015) 602–613.

[18] B. Liu, L. Chen, G. Liu, A.N. Abbas, M. Fathi, C. Zhou, High-performance chemical sensing using schottky-contacted chemical vapor deposition grown monolayer MoS_2 transistors, ACS Nano 8 (2014) 5304.

[19] D.J. Late, Y.-K. Huang, B. Liu, J. Acharya, S.N. Shirodkar, J. Luo, A. Yan, D. Charles, U.V Waghmare, V.P. Dravid, C.N.R. Rao, Sensing behavior of atomically thin-layered MoS_2 transistors, ACS Nano 7 (2013) 4879–4891.

[20] S.-Y. Cho, S.J. Kim, Y. Lee, J.-S. Kim, W.-B. Jung, H.-W. Yoo, J. Kim, H. Jung, Highly enhanced gas adsorption properties in vertically aligned MoS_2 Nano 9 (2015) 9314.

[21] T. Xu, Y. Pei, Y. Liu, D. Wu, Z. Shi, J. Xu, Y. Tian, X. Li, High-response NO gas sensor based on bilayer MoS_2 resistive grown by a new two-step chemical vapor deposition method, “J. Alloys Compd. 725 (2017) 253–259.

[22] Rizu MI, Fadil D, Llobet E. UV-enhanced exfoliated MoS2/PtSe2 heterostructure for ultra-sensitive NO2 detection at room temperature. npj 2D Materials and Applications. 2025 Apr 7;9(1):28.

[23]Zhao, Qiuni, Wenzhe Zhou, Mingxiang Zhang, Yang Wang, Zaihua Duan, Chaoliang Tan, Bohao Liu et al. "Edge-enriched Mo2TiC2Tx/MoS2 heterostructure with coupling interface for selective NO2 monitoring." Advanced Functional Materials 32, no. 39 (2022): 2203528.

[24] Li, Xixi, Xiao Wang, Zhaokun Sun, Feifei Li, Yao Fu, Keyang Zhao, Gang Zhao, Cunguang Zhu, and Xijin Xu. "Surface free radicals activated CoP/MoS2 sensors through electrocatalytic water splitting for enhanced NO2 sensing at room temperatures." Chemical Engineering Journal 495 (2024): 153381.

[25] Bharathi, P., S. Harish, G. Mathankumar, M. Krishna Mohan, J. Archana, S. Kamalakannan, M. Prakash, M. Shimomura, and M. Navaneethan. "Solution processed edge activated Ni-MoS2 nanosheets for highly sensitive room temperature NO2 gas sensor applications." Applied Surface Science 600 (2022): 154086.

Chapter 5

Conclusion, Future Scope, and Social Impact

5.1 Conclusion

The present work provides a systematic investigation into the synthesis, characterization, and gas sensing performance of nanostructured MoS_2 thin films. The key conclusions drawn from this research are elaborated below:

5.1.1 Key Findings

This study highlights the increasing demand for reliable gas sensing technologies due to environmental pollution and industrial safety concerns. It establishes that two-dimensional materials like MoS_2 possess unique properties such as high surface area and enhanced adsorption capability, making them highly suitable for gas sensing applications. The limitations of conventional sensing technologies further justify the need for such advanced materials.

5.1.2 Structural and Morphological Analysis

The structural analysis confirmed the successful formation of polycrystalline MoS_2 with a hexagonal phase. Morphological studies revealed a uniform distribution of nanosheets and flower-like structures, which significantly increase the active surface area. These structural features play a crucial role in enhancing gas adsorption and improving sensing performance.

5.1.3 Hydrogen Interaction Studies (In-situ XRD)

The in-situ XRD investigation provided valuable insights into the interaction between MoS_2 and hydrogen gas. It was observed that hydrogen exposure leads to measurable changes in diffraction patterns, indicating structural modifications within the material. This real-time analysis helped in understanding the dynamic behavior of MoS_2 under gas exposure conditions.

5.1.4 NO_2 Gas Sensing Performance

The gas sensing studies demonstrated that MoS_2 behaves as an n-type semiconductor, showing an increase in resistance upon exposure to NO_2 gas. The sensor exhibited improved performance with increasing temperature and gas concentration. Optimal sensing behavior was observed at elevated temperatures, with reasonably fast response and recovery times, indicating its potential for practical applications.

5.1.5 Performance Limitations

Despite the promising results, certain limitations were identified. At higher gas concentrations, structural defects were observed, which affected the recovery characteristics of the sensor. Additionally, the selectivity of the sensor toward specific gases remains a challenge, and the influence of environmental factors such as humidity requires further investigation.

5.1.6 Overall Conclusion

Overall, the study establishes a clear relationship between synthesis conditions, material properties, and sensing performance. The results confirm that nanostructured MoS_2 is a promising material for developing efficient gas sensors. The use of advanced characterization techniques has significantly contributed to understanding the sensing mechanism at a deeper level.
MoS_2 thin films were successfully synthesized using e-beam deposition followed by sulfurization via CVD. Structural and morphological characterizations confirmed the formation of highly crystalline, uniform, and continuous MoS_2 thin films with optimized thickness (~20 nm). Raman spectroscopy, XRD, SEM, EDEX, AFM, and analysis verified phase purity and nanosheet morphology suitable for gas sensing applications.

In-situ XRD studies under hydrogen exposure revealed important insights into the structural stability of MoS_2. The films remained stable up to 400 mbar hydrogen pressure but exhibited crystalline-to-amorphous transformation at higher pressures (800 mbar), indicating pressure-dependent structural evolution. These findings contribute to the understanding of gas-material interaction mechanisms and device reliability under reactive environments.

Gas sensing investigations demonstrated that nanostructured MoS_2 exhibits strong sensitivity toward NO_2 gas. The sensor resistance increased upon exposure to NO_2, confirming n-type semiconducting behaviour. The optimal sensing response (~14.2%) was achieved at 20 ppm NO_2 concentration at 150 °C, with fast response and recovery times. The study further confirmed improved selectivity toward NO_2 compared to other interfering gases.

Overall, this work establishes MoS_2 thin films as promising candidates for selective and efficient NO_2 gas detection. The results highlight that careful optimization of synthesis parameters, thickness control, and operating temperature significantly enhances sensor performance.

5.2 Future Scope of Work

Although this research provides important insights, several areas can be explored further to enhance the performance and applicability of MoS_2-based gas sensors.

5.2.1 Improvement in Selectivity

Future research should focus on improving the selectivity of MoS_2 sensors toward specific gases. This can be achieved through doping, surface modification, or functionalization techniques, which can tailor the interaction between the sensing material and target gas molecules.

5.2.2 Development of Heterostructures

The formation of heterostructures by combining MoS_2 with other materials can significantly enhance sensing performance. Such hybrid systems can improve charge transfer mechanisms and provide better sensitivity and faster response times due to synergistic effects.

5.2.3 Room Temperature Gas Sensing

Achieving efficient gas sensing at room temperature remains a key objective. Future work can explore methods such as UV activation or catalytic enhancement to reduce the operating temperature, thereby making the sensors more energy-efficient and suitable for portable devices.

5.2.4 Environmental Stability Studies

Further studies are required to evaluate the performance of sensors under real-world environmental conditions. The effects of humidity, pressure, and mixed gas environments need to be investigated to ensure long-term stability and reliability.

5.2.5 Device Miniaturization and Integration

The development of compact and integrated sensing devices is essential for practical applications. Future work can focus on integrating MoS_2 sensors into microelectronic systems, wearable devices, and IoT platforms for continuous monitoring.

5.2.6 Advanced Characterization Techniques

Advanced in-situ characterization methods can provide deeper insights into gas–material interactions at the atomic level. Techniques such as in-situ Raman spectroscopy and electron microscopy can help in understanding structural changes during sensing.

5.2.7 Expansion to Other Gases

The sensing capability of MoS_2 can be extended to other hazardous gases. This will broaden the application of these sensors in environmental monitoring, industrial safety, and healthcare sectors.

5.3 Social Impact

The development of advanced gas sensing technologies has wide-ranging benefits for society.

5.3.1 Environmental Monitoring

The sensors developed in this work can contribute significantly to monitoring air pollution by detecting harmful gases such as NO_2. This can help in controlling pollution levels and maintaining environmental sustainability.

5.3.2 Public Health Benefits

Early detection of toxic gases can prevent serious health issues. Continuous monitoring systems can reduce exposure to harmful pollutants and improve public health outcomes.

5.3.3 Industrial Safety

Hydrogen detection is critical in industrial environments due to its flammable nature. The sensors can help in detecting leaks at an early stage, thereby preventing accidents and ensuring safety.

5.3.4 Clean Energy Applications

Hydrogen is considered a clean energy source, and safe handling of hydrogen is essential for its widespread use. This research supports the development of reliable sensing systems for hydrogen-based energy technologies.

5.3.5 Smart Cities and IoT Integration

Integration of gas sensors into smart systems can enable real-time monitoring of environmental conditions. This supports the development of smart cities with improved air quality management.

5.3.6 Economic and Technological Impact

The use of cost-effective materials and scalable techniques makes these sensors economically viable. This can promote industrial growth and technological advancements in sensor development.

5.3.7 Scientific Contribution

This research contributes to the scientific understanding of gas sensing mechanisms in 2D materials. It provides a strong foundation for future research in nanotechnology and advanced sensing applications.

In conclusion, this thesis demonstrates the potential of MoS_2 as an efficient gas sensing material. The findings of this work not only enhance the understanding of gas sensing mechanisms but also pave the way for future advancements in sensor technology. The research holds significant promise for addressing real-world challenges related to environmental monitoring, industrial safety, and sustainable energy.

ANNEXURE-IV

DELHI TECHNOLOGICAL UNIVERSITY
(Formerly Delhi College of Engineering)
Shahbad Daulatpur, Main Bawana Road, Delhi-42

PLAGIARISM VERIFICATION

Title of the Thesis: **Development of 2D Molybdenum Disulfide Based NO_2 Gas Sensor**
Total Pages: **150**
Name of the Scholar: **Mr. Ramesh Kumar**

Supervisor (s): (1) **Prof. Vinod Singh**

(2) **Prof. Mahesh Kumar**

Department: **Applied Physics**

This is to report that the above thesis was scanned for similarity detection. Process and outcome is given below:

Software used: **TURNITIN** Similarity Index: **9%**, Total Word Count: **30,489**

Date: **03-05-2026**

Candidate's Signature **Signature of Supervisor(s)**

Applied Physics A (2025) 131:14
https://doi.org/10.1007/s00339-024-08143-w

Applied Physics A
Materials Science & Processing

Investigation of MoS_2-hydrogen interaction using in-situ X-ray diffraction studies

Ramesh Kumar[1] · Nitesh K. Chourasia[2,4] · Pawan K. Kulriya[2] · Mahesh Kumar[3] · Vinod Singh[1]

Received: 3 August 2024 / Accepted: 25 November 2024 / Published online: 10 December 2024

Abstract
The present manuscript examines the significant effects of hydrogen (H_2) exposure on the structural properties of molybdenum disulfide (MoS_2) thin films through in-situ X-ray diffraction (XRD) analysis. Molybdenum (Mo) thin films were initially deposited using the electron beam (e-beam) deposition method and subsequently sulfurized via chemical vapor deposition (CVD) to obtain MoS_2 thin films. The quality of the MoS_2 films was optimized by varying the thickness of the Mo layer, sulfurization temperature, and the temperature of the Mo film. It was determined that crystalline MoS_2 thin films with an optimal thickness of 20 nm can be achieved through sulfurization at 220 °C, while maintaining the Mo thin film at 600 °C. Pressure-dependent hydrogenation of the MoS_2 thin films, as investigated by in-situ XRD, reveals an increase in crystallite size accompanied by a decrease in the relative intensity of the diffraction peaks with rising hydrogen pressure. Furthermore, a microstrain of approximately 6.3% is induced in the MoS_2 films upon exposure to 1% and 10% hydrogen. Notably, the MoS_2 thin films remain predominantly stable up to a hydrogen pressure of 400 mbar; however, they undergo abrupt transformations and become entirely amorphous when the hydrogen gas pressure is subsequently elevated to 800 mbar. These observations of hydrogen-induced crystalline-amorphous phase transformation in MoS_2 not only enhance the understanding of the interactions between MoS_2 and hydrogen but also have critical implications for the application of MoS_2 thin films in various devices.

Keywords Hydrogenation · MoS_2 · In-situ XRD · Phase transformation

1 Introduction

In recent decades, the realm of nanomaterials has witnessed an extraordinary surge in interest, with researchers exploring the diverse and intriguing properties of two-dimensional (2D) materials. Among these materials, molybdenum disulfide (MoS_2), a transition metal dichalcogenide (TMD), has emerged as a standout candidate for applications spanning electronics, optoelectronics, energy storage, photodetectors and catalysis [1–5]. This versatile 2D material has attracted significant attention due to its unique structural and electronic characteristics, making it an exciting platform for cutting-edge research and technological advancement [6, 7]. The interaction between 2D materials with various gases is an area of profound significance because it underpins their potential utilization in gas-sensing devices, catalytic reactions [8], and gas storage systems [9, 10]. Understanding how gases interact with MoS_2 at the atomic and structural level is also crucial for optimizing its performance in these applications. Globally, the matter of energy has become a cause for widespread apprehension, primarily driven by the depletion of fossil fuels. The escalation in energy demand is principally fueled by two paramount factors: the rapid expansion of the world's population and the concurrent elevation in the average standard of living [11]. In the contemporary context, the most urgent challenges faced by the society is navigating the endeavor to fulfill the growing energy requirements amid substantial limitations imposed by the diminishing reservoirs of traditional fuels such as coal, oil, and natural gas [12]. In addition, hydrogen gas (H_2), in particular, has garnered immense interest as a clean

---

✉ Vinod Singh
vinodsingh@dtu.ac.in

[1] Present Address: Department of Applied Physics, Delhi Technological University, New Delhi 110042, India

[2] School of Physical Sciences, Jawaharlal Nehru University, New Delhi 110067, India

[3] Department of Electrical Engineering, Indian Institute of Technology Jodhpur, Jodhpur, India

[4] Department of Physics, Faculty of Science, Shree Guru Gobind Singh Tricentenary University, Gurugram, Haryana 122505, India

and sustainable energy carrier. The global interest in H_2 energy has grown substantially primarily attributed to its remarkably high heat combustion rate. Beyond its impressive combustion capabilities, H_2 energy offers a crucial advantage by fostering independence from finite fossil fuel resources. Unlike non-renewable energy sources, H_2 combustion results in the generation of clean combustion products, contributing to a more environmentally sustainable energy landscape [13–15]. Today, H_2 gas is widely employed in various sectors, including oil refining, chemical industry, space transportation, medicine and aerospace. However, due to its high explosiveness and flammability when its concentration exceeds 4% of the environment volume (attributed to its low ignition energy of 0.017 mJ), even a minor H_2 leakage poses serious risks [14]. To mitigate potential hazards and ensure safe H_2 operations, there is a need for a highly sensitive, selective, fast-recovery, and responsive H_2 gas sensor to detect leakages promptly. MoS_2, with its unique surface properties and catalytic potential, can be used in various technological applications such as LDH-based heterostructures as electrode materials for water splitting, energy storage devices and H_2-related technologies [16, 17]. MoS2 can be prepared by various methods such as hierarchical NiCo-LDH@MoS_2/CuS heterostructure (HS) was prepared by facile two-step hydrothermal synthesis, A facile chemically exfoliated combined microwave-assisted method was used to synthesize MoS2·ZnO nanocomposites [17, 18]. Among them, preparation of MoS2 thin film by evaporation of Mo using e-beam technique followed by sulphuration in CVD techniques offers unique advantages such as this method provides high control over MoS2 film thickness and crystallinity, especially compared to simpler, more scalable methods like thermal decomposition. However, it is more complex and expensive than other methods. Much like graphene, MoS_2 is composed of layers arranged in a vertical stack [19]. Each individual layer is created through covalent bonding between molybdenum (Mo) and sulfur (S) atoms. The cohesion between adjacent layers is facilitated by the presence of relatively weak van der Waals forces. This structural similarity highlights the layered nature of MoS_2, where the combination of covalent bonds within layers and van der Waals forces between layers contributes to its unique properties and versatile applications [19]. The presence of weak van der Waals interactions in MoS_2 enables gas molecules to easily infiltrate and diffuse between its layers. Consequently, the resistance of MoS_2 can undergo significant changes as a result of the adsorption and diffusion of gas molecules within these layers. This property makes MoS_2 highly responsive to the presence of gases, offering potential applications in gas sensing and related fields where the material's electrical conductivity can be modulated by the interaction with different gas species. The interaction between MoS_2 and H_2 gas is governed by a multitude of factors, including temperature, pressure, and the structural integrity of MoS_2 [20, 21]. These factors intricately influence the adsorption, diffusion, and subsequent chemical reactions of H_2 on the MoS_2 surface [22, 37]. To delve into the intricacies of this interaction and gain a comprehensive understanding, in-situ characterization techniques have become invaluable tools. Among these techniques, in-situ X-ray diffraction (XRD) stands out as a powerful technique for monitoring structural changes in materials during gas–solid interactions [23]. By allowing real-time observation of atomic rearrangements and phase transformations, *in-situ* XRD offers unique insights into the dynamics and thermodynamics of these interactions [24]. To the best of our knowledge, there is no report on the structural properties of MoS2 on the exposure to the hydrogen gas. This article presents a systematic and detailed investigation into the MoS_2-H_2 gas interaction at different pressures using in-situ X-ray diffraction studies. In the case of nanostructured materials, there could be sample to sample variation during synthesis which leads to modification in the structural properties when they are exposed to hydrogen gas and later investigated using off-line XRD. Here, state-of-art *in-situ* XRD facility has been used in which all the studies has conducted in the same sample without changing experimental conditions. Our objective is to unravel the structural modifications that occur within MoS_2 under varying H_2 pressures and to elucidate the underlying mechanisms that govern this intricate interaction. This research is a crucial step towards realizing how MoS_2 behaves in the presence of H_2 gas, offering fundamental insights into the design, engineering, and optimization of MoS_2-based catalytic systems for H_2-related applications. Throughout this article, we will explore the current state of knowledge regarding the interaction between MoS_2 and H_2 gas, laying the foundation for our in-depth investigation. The unique properties of MoS_2, the significance of H_2 gas as an energy carrier, and the key challenges in harnessing MoS_2's potential for H_2-related applications is also discussed. In the subsequent sections, we will delve into the experimental methodology, data analysis, and results obtained from our in-situ X-ray diffraction studies on MoS_2- H_2 gas interactions at different pressures. The findings of this research not only enhance our fundamental knowledge of MoS_2's behavior but also provide valuable guidance for the design and development of advanced catalytic systems and H_2 storage materials, contributing to the ongoing efforts towards a sustainable energy future.

2 Experimental details

2.1 Preparation of Mo films

The electron beam evaporation (e-beam) deposition method was employed for preparation of high quality Mo thin films by using Mo target on Si/SiO_2 substrate. The key advantages of this technique lie in its ability to produce high-purity Mo films with excellent control over thickness and microstructure, making it indispensable in various industries ranging from electronics to thin-film coatings and beyond [25, 26]. At first, the substrates were cleaned with trichloroethylene followed by acetone, and alcohol to remove contaminations and native oxide. The base vacuum of the order of 2×10^{-6} mbar was maintained with the help of rotary vane and turbo-molecular pump. The deposition rate is kept at a slow rate of 0.7 – 0.8 nm/sec for the uniformed and to achieve desired thickness. Three different thicknesses (5 nm, 10 nm, 20 nm) of Mo film were obtained by keeping the same deposition rate. The film deposited at the RT having black color which may be due to oxygen deficiency and a large number of defects. Therefore, these films were further annealed in oxygen ambient at temperature of 400 °C for duration of 1 h. After annealing, the color of films changed and they become totally transparent.

2.2 Sulfurization of Mo films

Sulfurization of Mo films is a fundamental process to transform deposited molybdenum (Mo) thin films into two-dimensional molybdenum disulfide (MoS_2) layers. For this purpose, a double zone chemical vapor deposition (CVD) method was employed for the sulfurization. The sulfurization of thin film of 20 nm thickness were grown on Si/SiO_2 substrates via double zone sulfurization using an ambient-pressure CVD technique as shown in Fig. 1.

Flushing of the quartz tube using Argon gas stream, followed by continuous Ar flow for 15 min, was performed. This reduces the oxygen content in the reactor prior to the sulfurization process. Before the experiment, a quartz boat containing 1.0 gm Sulphur powder (Sigma Aldrich, 99.999%) was placed upstream in the heating ring, and the Si/SiO_2 substrate covered with pre-exfoliated Mo film was placed face up on another quartz boat and located in the middle of the tubular furnace, as shown in Fig. 1. The distance between the two quartz boats is about 150 mm. After that, the tubular furnace was heated to 600 °C at a rate of 20 °C/min. When the temperature of the tubular furnace rose to 470 °C, the Sulphur powder was heated to 200 °C through the heating ring at a rate of 20 °C/min. During this process, the Ar flow rate remained at 80 SCCM. After the growth time of 30 min, the furnace was cooled down naturally to room temperature with Ar flow of 100 SCCM.

2.3 Characterizations

XRD along with Raman spectroscopy was used to probe the structural properties of the as prepared and hydrogenated MoS_2 films. XRD patterns have been recorded using Bruker AXS D8 Advanced in-situ XRD facility equipped with Cu K_α source with wavelength 1.54 Å (40 kV and 40 mA power). The *in-situ* XRD setup has provision for creation of high vacuum using rotary vane pump and turbo-molecular pump [24]. A gas injection facility is also integrated to injection the H_2 gas in the controlled manner which allows us to record diffraction pattern in the controlled gas atmosphere. A schematic diagram of the *in-situ* XRD setup is shown in the Fig. 2. First, the MoS_2 films were mounted on sample holder and a high vacuum order of 1×10^{-5} mbar was created. After that, diffraction pattern of the MoS_2 films was recorded in the vacuum. Now, MoS_2 films was exposed to different concentrations of H_2 gas (3%) mixed with noble gas Argon (Ar), one by one after different intervals of pressure ranging from 50 to 900 mbar and diffraction pattern of the same sample is recorded after each pressure without changing position of sample. Since, all diffraction patterns are recorded on the same sample so effect of the sample to sample variation is ruled out. This process also allows us to compare of intensity of the diffraction peaks with change in the pressure of the H_2 gas. The data were recorded in locked coupled mode in the scan range of 2θ from 10° to 60° with step size of 0.02° at a scan speed of 0.25°/min.

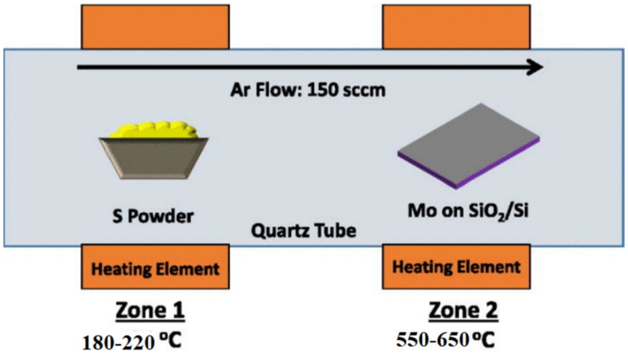

Fig. 1 Sulfurization of Mo films using double zone CVD technique

Raman spectroscopy was performed on pure and MoS_2 samples exposed with different H_2 concentrations using Renishaw Invia Raman microscope with Argon laser as source (514.5 nm wavelength) for the scan range of 100–3200 cm^{-1}. The topography of the MoS_2 films including pristine were studied using Digital Instruments Nanoscope IIIa atomic force microscope (AFM) in the tapping mode.

3 Results and discussions

3.1 Structural properties of the as-prepared MoS_2 thin film

Glancing angle X-ray diffraction (GIXRD) studies was carried out to understand the effect of film thickness, molybdenum temperature and sulfurization temperature on

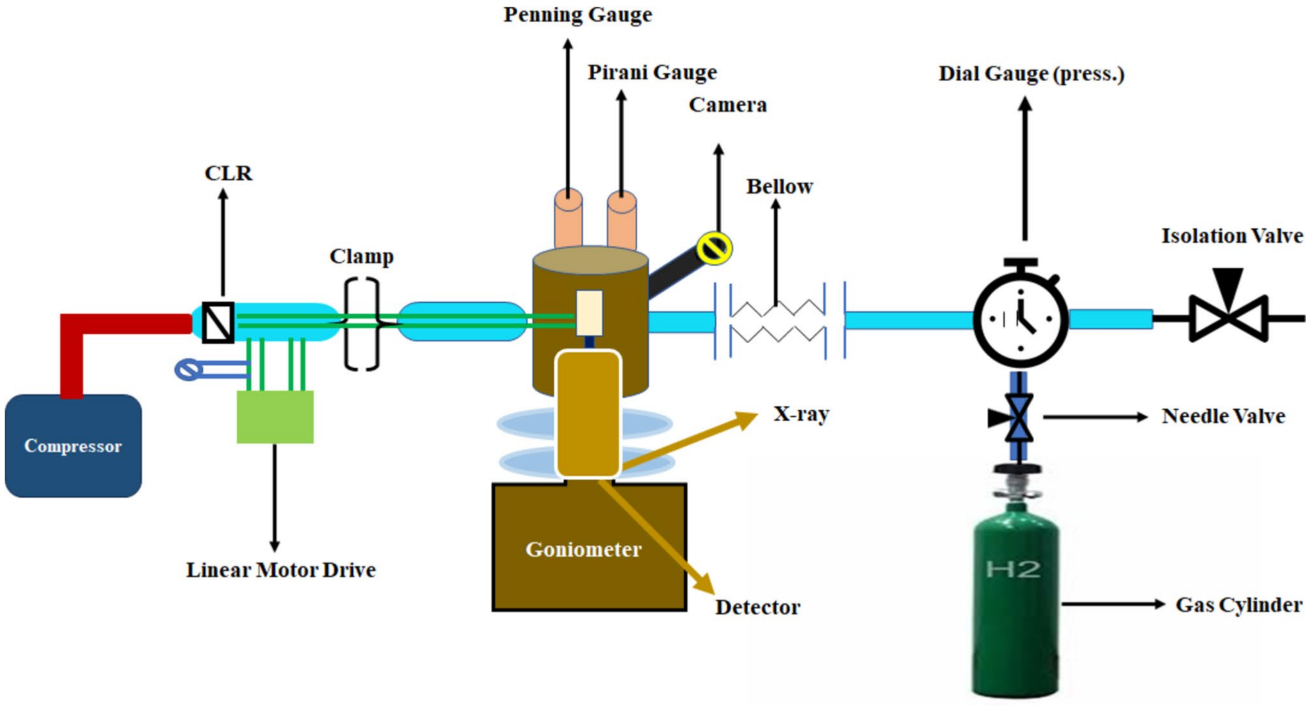

Fig. 2 Schematic diagram of the in-situ XRD setup

crystallinity and phase formation in the molybdenum thin film deposited on Si/SiO$_2$ substrate.

3.1.1 Effect of Mo film thickness

Thin film of molybdenum having thickness of 5 nm and 10 nm films has been prepared using electron beam evaporation techniques. In order to understand the effect of film thickness on MoS$_2$ phase formation, these films were exposed to various synthesis conditions of varied molybdenum and sulfur temperatures (molybdenum at 550 °C, 600 °C, 650 °C and sulfur at 180 °C, 200 °C, 220 °C, 300 °C). Figure 3 shows the GIXRD pattern of MoS$_2$ thin films of the different thickness of (a) 5 nm, (b) 10 nm and (c) 20 nm, prepared by keeping molybdenum and sulfur at different temperature (molybdenum at 550 °C, 600 °C, 650 °C and sulfur at 180 °C, 200 °C, 220 °C, 300 °C), respectively. It is clear from the GIXRD plot of Fig. 3a that MoS$_2$ phase does not form in the case of 5 nm for all process temperatures except Mo 600 °C and Sulfur 200 °C. When film thickness is increased to 10 nm then sharp peaks are visible at 2θ value of 14.3°, 25.4°, 39.0° and 58.4° corresponding to (002), (004), (103) and (110) planes, respectively. The peaks well matched with JCPDS No. 37–1492, which confirms the successful synthesis of polycrystalline hexagonal-phase MoS$_2$ in the case of 10 nm films. This also shows that crystallinity is improved with increase in the film thickness. It may be noted that crystalline phase was not formed when the sulfurization was done at 300 °C by keeping Mo at 600 °C. This could be due to suppress of Mo/S interaction at the elected temperature. When thickness of the Mo film was subsequently increased to 20 nm then high quality MoS$_2$ phase was formed in all the experimental condition used in the present study. In addition, the GIXRD analysis clearly exhibits that the MoS$_2$ thin film (20 nm) corresponding to synthesis parameter (Mo temperature 650 °C and sulfurization temperature 220 °C) is the optimum condition to get high quality film due to presence of all peaks related to MoS$_2$ only. It may be noted that other synthesis condition of MoS$_2$ thin film (20 nm) film also contains polycrystalline MoS$_2$ phase but they have lesser intensity peaks as well as some impurity peaks.

3.1.2 Effect of process temperature

In order the understand the detailed investigation of process temperature on the structural properties and crystalline quality of the films, the XRD pattern of Mo (20 nm) synthesized at varying (a) Mo temperature and (b) sulfurization temperature are plotted in Fig. 4. The process temperature effect can be studied by either varying the temperature of Mo film or the temperature of sulphur powder while keeping other at fixed temperature during synthesis of MoS$_2$ thin film. In the first case, the sulfurization temperature was kept at 220 °C and Mo thin film temperature was varied from 550 to 650 °C. When the annealing temperature of Mo film

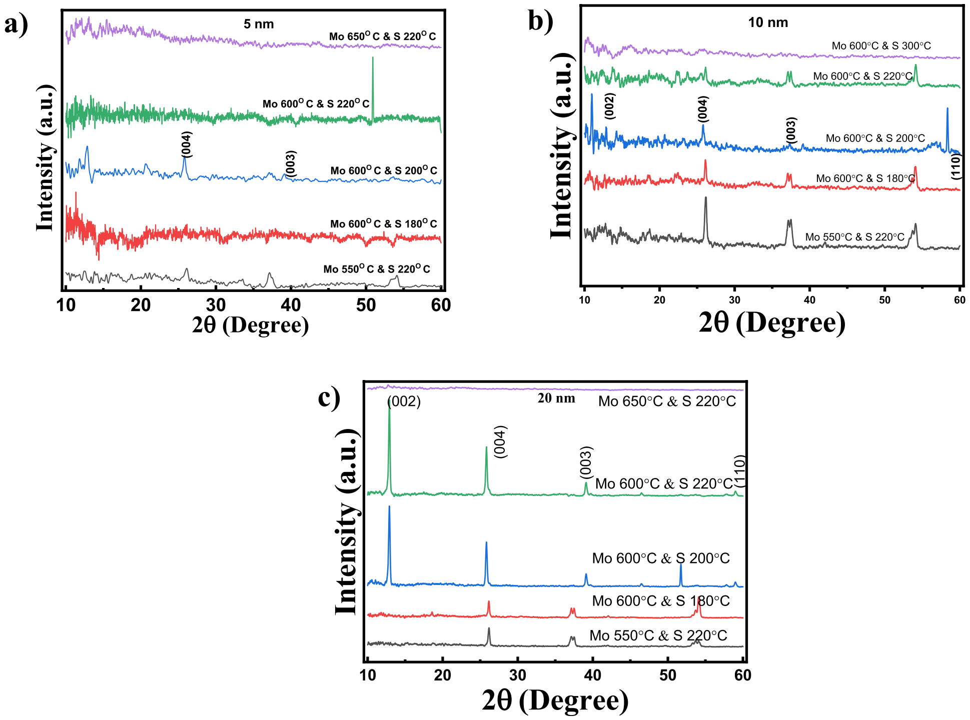

Fig. 3 GIXRD analysis of MoS_2 thin films having **a** 5 nm, **b** 10 nm and **c** 20 nm thickness

was 550 °C then few peaks of the MoS_2 can be clearly seen [Fig. 4a]. As the annealing temperature of Mo was subsequently increased to 600 °C then single phase MoS_2 film was synthesized. It contains all the peaks corresponding to hexagonal phase of the MoS_2. After that, the annealing temperature of the Mo was further increased to 650 °C then surprisingly all the peaks were disappeared and amorphous phase was formed. This indicates that the crystalline MoS_2 phase does not formed due to less interaction of sulphur at elevated temperature. Thus, highly crystalline single phase MoS_2 film can be synthesized by sulfurization at 220 °C by keeping Mo thin films at 600 °C. In order to understand the effect of sulfurization temperature on quality of the film, it was varied from 180 to 220 °C by keeping Mo thin films at the temperature of 600 °C. XRD pattern displayed in Fig. 4b shows that intensity of the diffraction peaks are increasing with increase in the sulfurization temperature. Highly crystalline thin films of MoS2 can be synthesized at the sulfurization temperature of 220 °C by keeping Mo thin films at 600 °C.

Thus, based on the results presented above, one can conclude that optimum process parameters such as film thickness (20 nm), Mo thin film temperaure (600 °C) and sulfurization temperature (220 °C) are required for getting good quality thin films of the MoS_2.

3.2 Surface morphology

Scanning electron microscopy (SEM) was used for determining the surface morphology of as-prepared MoS_2 thin films (20 nm) grown under optimized conditions. A typical SEM image of the MoS_2 thin film is shown in Fig. 5a.

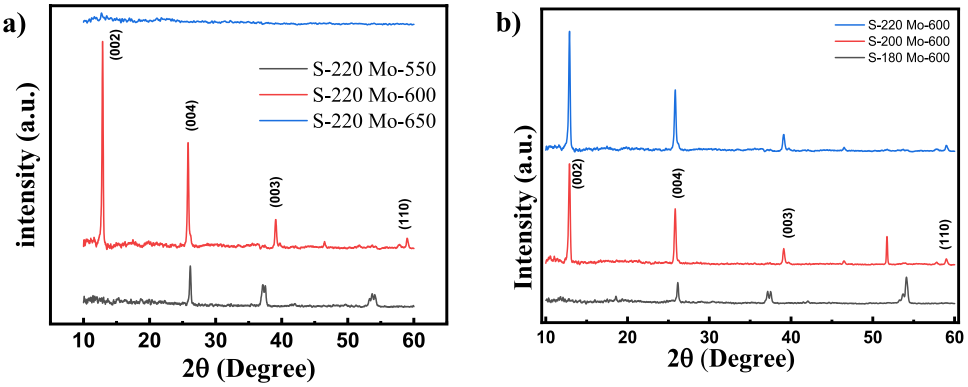

Fig. 4 MoS_2 thin film synthesis with varying **a** sulfurization temperature **b** Mo film temperature

As can be seen from the image, the MoS_2 nanosheets were uniformly grown on the substrate and it appears smooth, homogeneous and without topography contrast. The particle size from the SEM images is estimated using imageJ software. The Fig. 5b represents particle size distribution histogram which gives an estimation of average particle size. The calculated average particle size is 0.63 ± 0.20 µm. The compositions of MoS_2 thin film were investigated using energy dispersive spectroscopy (EDS) and tabulated in the Fig. 5c. The elemental distribution shows that sample primarily consists of Mo, O, S and Si. The extra Si element is also observed due to the Si/SiO_2 substrate.

Atomic force microscope (AFM) technique was also used to compare and analyze the surface characteristics of Mo and MoS_2 thin film with different thickness. Figure 6 shows the AFM images of Mo thin films of different thickness of (a) 5 nm, (b) 10 nm and (c) 20 nm. The surface roughness of these films was calculated using Nasoscope analysis 1.7 software and found to be 0.85 nm, 21 nm and 4.1 nm for 5 nm, 10 nm and 20 nm thick films, respectively. From the AFM image, one can conclude that the 20 nm thin film is of superior quality as compared to other films. In addition, all the MoS_2 thin film of different thickness have very low root-mean-squared (RMS) surface roughness as shown in Fig. 6d–f. The low roughness minimizes surface defects, carrier scattering and ensuring a consistent and uniform interaction with analytes. The detailed of the film parameter has been shown in Table 1.

As one can be seen from the AFM image and Table 1, the roughness of the film having 5 nm thicknesses is lower than 20 nm thick film. Although, roughness of the 20 nm thick film is higher but it is used for further *in-situ* structural investigation because its crystallinity is very good and display all the characteristics peaks of MoS_2, which can be seen from GIXRD.

Formation of single phase MoS_2 and presence of the short rang order is further probed by the Raman spectroscopy technique. It is a powerful technique used to analyze the vibrational modes of materials, providing valuable information about their structure and composition. In the case of MoS_2 films, Raman spectroscopy not only offers insights into the quality and characteristics of the deposited material but also provides information about the

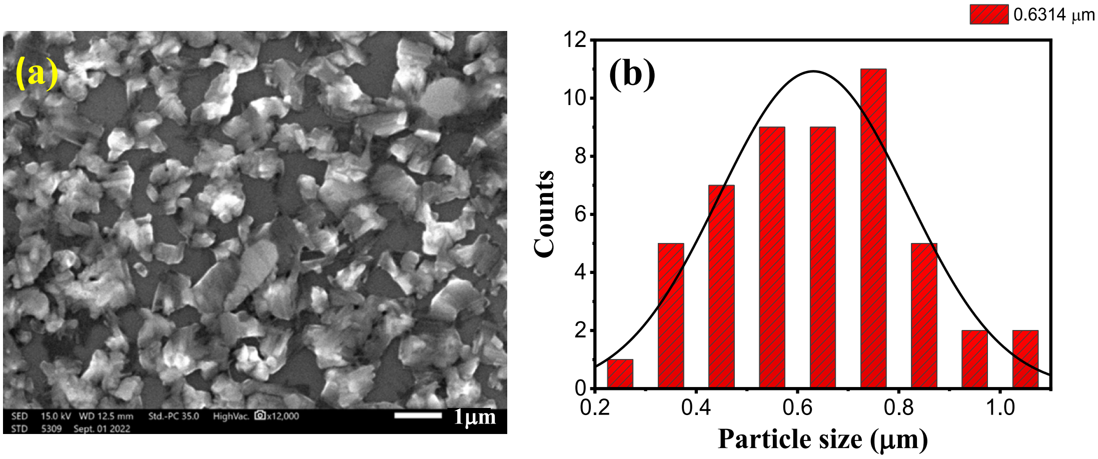

(c)

Display name	Standard data	Quantification method	Result type
Spc_001	Standardless	ZAF	Metal
Element	Line	Mass%	Atom%
O	K	23.35±0.39	35.89±0.60
Si	K	71.32±0.56	62.45±0.49
S	K	0.56±0.16	0.43±0.12
Mo	L	4.78±0.50	1.22±0.13
Total		100.00	100.00
Spc_001			Fitting ratio 0.0593

Fig. 5 **a** SEM image of MoS_2 thin film prepared on Si/SiO_2 substrate **b** size distribution histogram **c** elemental distribution of MoS_2 thin film

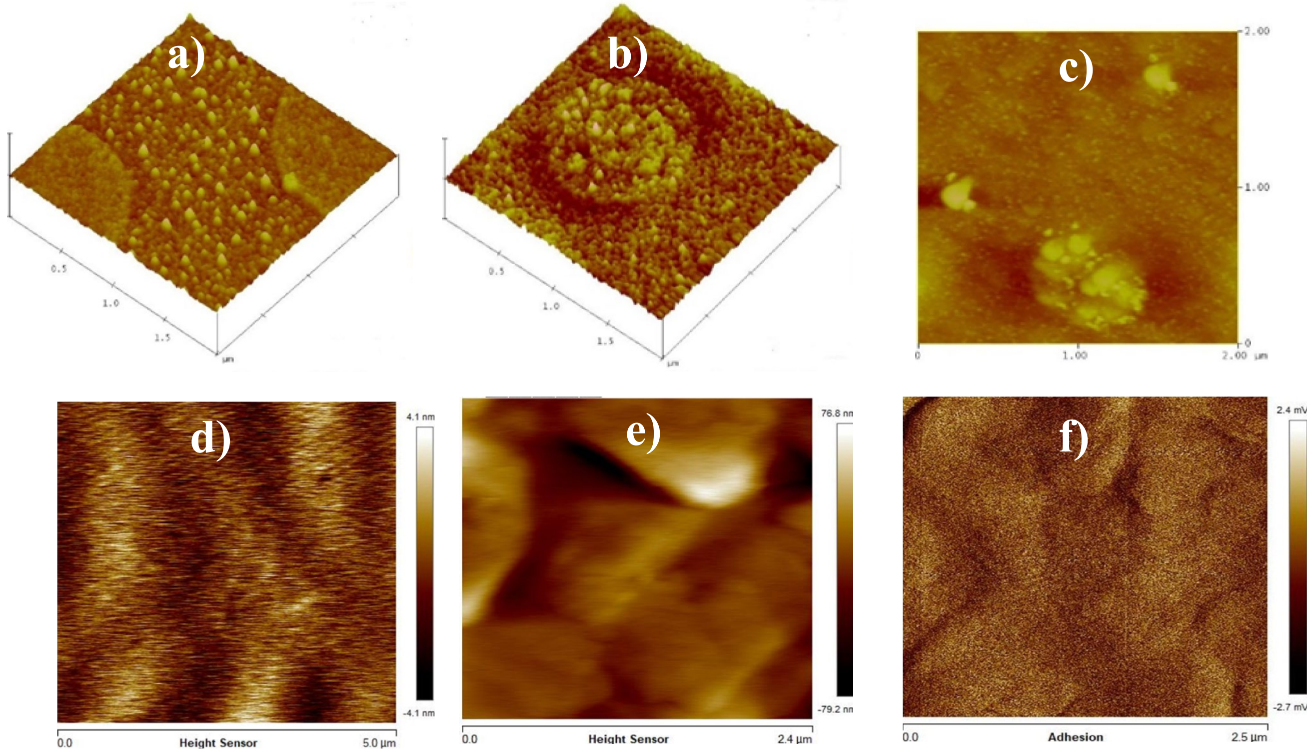

Fig. 6 AFM image of Mo thin film with the thickness of, **a** 5 nm, **b** 10 nm, and **c** 20 nm and MoS_2 thin film with the thickness of **d** 5 nm, **e** 10 nm, **f** 20 nm

Table 1 The variation in the roughness of MoS_2 thin films with film thickness

S.N	Thickness of film (nm)	Roughness of film (nm)
1	5	0.85
2	10	2.1
3	20	4.1

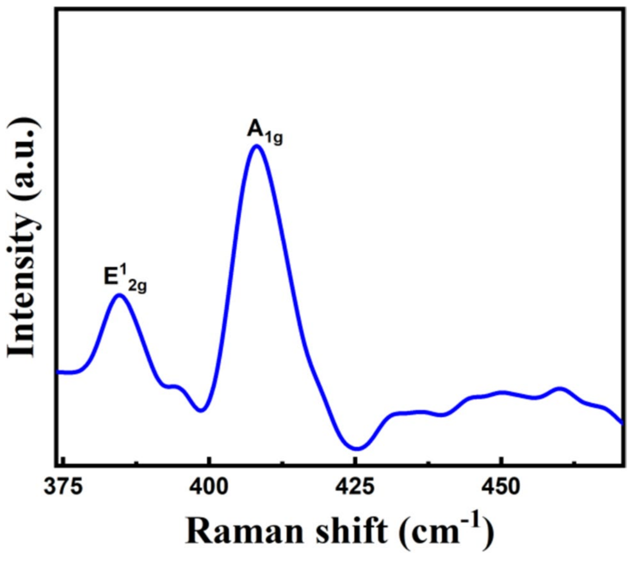

Fig. 7 Raman spectra of the MoS_2 thin films of 20 nm thicknesses grown by vapor phase sulfurization of Mo thin films

phonon modes in MoS_2, which are related to the vibrational motion of atoms within the crystal lattice.

Raman spectrum of the MoS_2 thin films (t = 20 nm) is shown in the Fig. 7. It exhibits the distinctive signal of 2H-MoS_2, with no apparent traces of polymer residue, carbon contamination or oxides.

Raman spectrum comprises signature peaks E^1_{2g} at the wavenumber of 385 cm^{-1} corresponding to the in-plane vibrational modes of the MoS_2 lattice (in-plane vibration between Mo and S atom)˙ and A_{1g} at the wavenumber of 405 cm^{-1} represents the out-of-plane vibrations of the MoS_2 layers (out-of-plane expansion between S atom) [26, 27, 33]. Generally, the A_{1g} mode gives the significant information about the van der Waals force among the adjacent MoS_2 layers, because of out-of-plane interaction with the adjacent atoms [28, 34]. In this context, the presence of two distinct Raman peaks suggests that the MoS_2 film exhibits hexagonal coordination (2H) rather than the trigonal prismatic configuration (1 T) as observed in mechanically exfoliated MoS_2 [29, 32]. Additionally, the frequency difference of these two peaks is found to be 20 cm^{-1}, which can be ascribed a few layers of MoS_2 thin film [30, 32]. The well-matched characteristics peaks is a clear evidence of the formation of the impurity free single phase MoS_2.

3.3 Hydrogenation of MoS_2: pressure effect

To understand MoS_2-H_2 kinetic, an *in-situ* XRD studies was performed on MoS_2 thin film (20 nm) by exposing it to pure H_2 gas a pressure varying from vacuum to 1000 mbar. The diffraction was recorded in the vacuum and different hydrogen pressure at the measurement parameters of the diffractometer and without changing position of sample. Figure 8a shows *in-situ* XRD patterns of as-prepared MoS_2 thin films in the vacuum and on exposure to H_2 environment by varying its pressure between vacuum to 1000 mbar. It shows that few new peaks were appeared even on film exposed to a very low pressure of H_2 (50 mbar). This clearly indicates very high sensitivity of MoS_2 towards H_2 gas at the room temperature. When the H_2 pressure is further increased from 50 to 100 mbar, then intensity of the diffraction peaks are decreased. But, observation of new peaks and phase change was not observed event pressure of the H gas increased to 200 mbar. As H_2 gas pressure is subsequently increased up to 400 mbar then drastic reduction in the diffraction peaks is observed. This indicates that a large lattice strain and defects are produced by hydrogen if the pressure is $P > 400$ mbar. The production of the excessive defects generates structural distortion which leads to amorphization of the MoS_2. As the H_2 pressure is further increased to 1000 mbar, diffraction peak intensity corresponding to different planes tends to deteriorate and it vanishes completely at 1000 mbar pressure. On the basis of the diffraction data, one can infer that MoS_2 remains predominantly stable within the H_2 pressure range from vacuum to 400 mbar. However, beyond this pressure range, MoS_2 thin films undergo significant and abrupt transformations and it completely loses it phase at 1000 mbar pressure. To understand the H_2 pressure induced lattice micro-strain in the MoS_2 films, the inter-planer spacing of pure and hydrogenated MoS_2 was calculated. The variation in the inter-planer spacing (d) with H_2 pressure is shown in Fig. 8b. It exhibits that the inter-planer spacing increases with increase in the H_2 pressure which confirms the production of the lattice strain due to hydrogenation. Due to increase in hydrogen pressure from vacuum to 1000 mbar, the MoS_2 (002) inter planar spacing was observed. It was noticed that inter-planar spacing is a function of *in-situ* hydrogen pressure. Before exposure to hydrogen gas the inter-planar spacing of (002) plane was observed $c = 12.25$ Å such as khan et al. XRD study shows hexagonal structure of few-layers of MoS_2 with observed (0 0 2) plane, with lattice parameter is ≈12.28 A° [29, 37]. Subsequently, *in-situ* hydrogen pressure was increased to 50 mbar and corresponding inter-planar spacing was observed $d = 11.87$ Å, which was measured using XRD

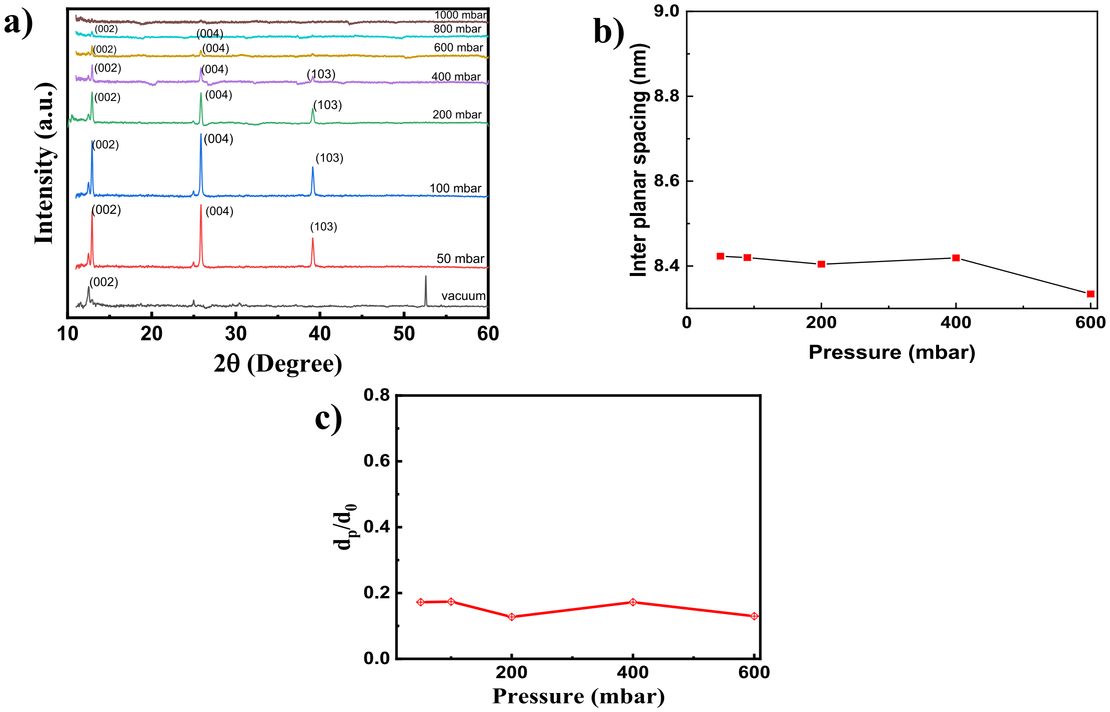

Fig. 8 **a** *In-situ* XRD pattern of MoS_2 thin film (20 nm) recorded under vacuum and exposure to different H_2 gas pressure. The variation of **b** interplaner spacing **d** and **c** relative change in the inter planar spacing $(d_p - d_0)/d_0$ at different H_2 gas pressure

technique. The in-situ hydrogen pressure was increased up to 1000 mbar. The inter-planar spacing at 800 mbar and 100 mbar hydrogen pressure are d = 11.89 Å and 13.58 Å, respectively. This shows that the inter-planar spacing was almost constant up to 800 mbar hydrogen pressure. Further, there was a drastic increase in inter-planar spacing when pressure was increased from 800 to 1000 mbar which could leads to phase change in the MoS2. This shows that there is a significant increase in inter-planar spacing due to hydrogen pressure. So, this threshold level of hydrogen pressure significantly affects the crystalline properties of MoS_2 structure. Thus, hydrogen pressure of 800 mbar can be considered as a transition pressure.

Apart from that relative change in the inter planer spacing $(d_p- d_0)/d_0$ was also calculated. Here, d_0 and d_P are inter planar spacing in vacuum and at a specific hydrogen pressure respective. The variation in the $(d_p- d_0)/d_0$ with pressure is shown in Fig. 8c. The results indicates that as pressure in increasing the inter planar spacing is also increasing.

The crystalline size of MoS_2 films exposed at various H_2 partial pressures was estimated from the XRD data presented in the Fig. 8. It was calculated using Scherrer equation which is expressed as:

$$D = \frac{K\lambda}{\beta\cos(\theta)}$$

where, D is the average crystallite size., K is the shape factor, typically around 0.9, λ is the wavelength of the X-ray radiation used for the diffraction, β is the full width at half maximum (FWHM) of the diffraction peak and θ is the Bragg angle. Figure 9 shows variation in the crystallite size with H_2 partial pressure for diffraction peaks appeared at the (a) 14.3°, (b) 25.4° and (c) 39.4°, corresponding to (002), (004) and (103) planes, respectively. It is evident that the crystallite size of MoS_2 thin films is increasing with H_2 gas pressure for all three crystalline planes which may be due to hydrogen-induced recrystallization. Hydrogen being a reducing agent can promote the removal of oxygen-containing functional groups and defects from the MoS_2 surface which leads to a more pristine and ordered atomic arrangement. Hydrogen induced reduction process may also facilitate the coalescence and growth of crystallites, promoting larger crystal sizes. Additionally, H_2 exposure can influence the energetics of grain boundaries, encouraging the migration and coarsening of grains [29–31].

In order to understand the influence of hydrogenation on the crystallinity of the MoS_2 films, change of relative intensity (I/I_0) of all the characteristics peaks of MoS_2 with H_2 gas pressure is determined. Here, I_0 and I are the intensity of diffraction peak recorded in vacuum and at a particular pressure of H_2. Figure 10a shows the variation in the relative intensity (I/I_0) with H_2 gas pressure. It shows that relative intensity of three characteristics peaks is reduced as the pressure of the H_2 gas is increased. This clearly shows that crystallinity of the MoS_2 is deteriorating on the exposure to H_2 gas. It may be noted that effect of hydrogenation on the peak appearing at the diffraction angle of 14.3° is negligible. The variation in relative intensity (I/I_0) for peaks appearing at the 25.4° and 39.15° are fitted using exponential function.

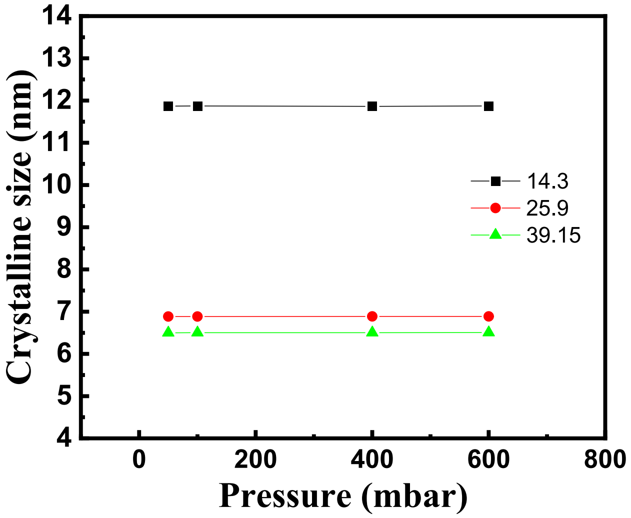

Fig. 9 Change in the crystallite size vs partial pressure calculated for the diffraction peaks appeared at **a** 14.3°, **b** 25.4° and **c** 39.4°

Apart from this, to understand the H_2 induced preferred orientation, change in relative intensity corresponding to (004) plane and (103) plane with the variation of the pressure is also calculated. Figure 10b displays a change in the relative plane intensity $I_{(004)}/I_{(103)}$ with partial pressure of H_2 It displays that the $I_{(004)}/I_{(103)}$ is decreased with increase in the pressure of H_2 gas. This suggest that there is preferred orientation along the (103) plan of the MoS_2. In order to validate H2 storage materials, a detail understanding comes from these studies [8, 26, 35]. This confirms that the H_2 makes a great impact through interaction on the crystal structure of MoS_2 thin film.

3.4 Conclusion

In summary, synthesis process parameters optimization and hydrogenation properties of the molybdenum thin films of different thickness prepared using e-beam deposition technique followed by sulfurization using CVD system are reported. Optimization of viz, film thickness, sulfurization temperature by keeping Mo thin film at fixed temperature and Mo film temperature by keeping fixed sulfurization temperature has been carried out for getting

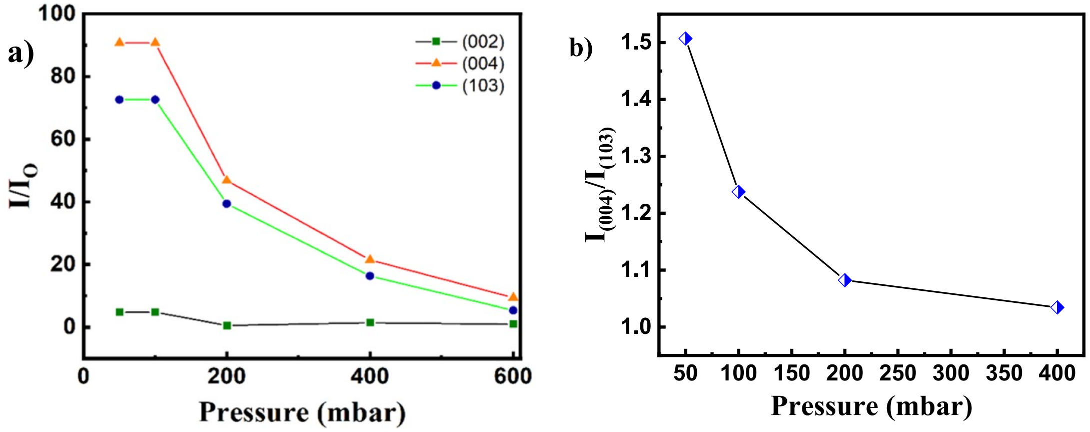

Fig. 10 **a** XRD relative intensity vs pressure 14.3°, 25.4° and 39.0°, **b** Relative plane intensity $I_{(004)}/I_{(103)}$ vs pressure (mbar)

highly crystalline MoS_2 film and confirmed its structural, micro-structural and compositional analysis using GIXRD, SEM, EDX, Raman spectroscopy techniques. The structural properties investigations confirms that crystalline MoS_2 thin films having optimum thickness of 20 nm can be prepared by sulfurization at 220 °C while keeping Mo thin film at 600 °C. The pressure dependent hydrogenation of the MoS_2 thin films investigated using *in-situ* XRD technique suggests that MoS_2 thin film remains predominantly stable within the pressure range from vacuum to 400 mbar. However, it undergoes significant and abrupt transformations when hydrogen gas pressure is subsequently increased. The MoS_2 thin films become completely amorphous at 800 mbar pressure. Thus, observation of order–disorder phase transformation has not only deepens the understanding of MoS_2-H_2 interactions but also important for utilization of the MoS_2 thin films in the devices.

Acknowledgements This work was supported by "Science and Engineering Research Board," India. Nitesh K. Chourasia acknowledges the "Science and Engineering Research Board" for National Post-Doctoral Fellowship (PDF/2021/001490). One of the authors, Ramesh Kumar is thankful to Delhi Technological University for providing Institute Research Fellowship.

Author contributions Ramesh Kumar- Original manuscript writing, investigation, characterization, and synthesis. Nitesh K. Chourasia- Editing and drafting. Pawan K. Kulriya- Formal analysis and visualization. Mahesh Kumar- Conceptualization, supervision, and validation. Vinod Singh- Resources, supervision, and validation.

Funding Science and Engineering Research Board, PDF/2021/001490, Nitesh K. Chourasia.

Data availability Data will be available on request.

Declarations

Conflict of interest All co-authors have seen and agree with the contents of the manuscript and there is no financial interest to report.

References

1. A. Sharma, G. Gupta, Recent development and prospects for metal Selenide-based gas sensors. Mater. Sci. Eng. B **290**, 116333 (2023)
2. A. Dodda, D. Jayachandran, A. Pannone, N. Trainor, S.P. Stepanoff, M.A. Steves et al., Active pixel sensor matrix based on monolayer MoS2 phototransistor array. Nat. Mater. **21**, 1379–1387 (2022)
3. T. Wang, S. Chen, H. Pang, H. Xue, Y. Yu, MoS2-based nanocomposites for electrochemical energy storage. Adv. Sci. **4**, 1600289 (2017)
4. Y. Huang, Y. Sun, X. Zheng, T. Aoki, B. Pattengale, J. Huang et al., Atomically engineering activation sites onto metallic 1T-MoS2 catalysts for enhanced electrochemical hydrogen evolution. Nat. Commun. **10**, 982 (2019)
5. P.M. Pratik, V. Patel, C.K. Sumesh, MoS2/WSe2 nanohybrids for flexible paper-based photodetectors. Nanotechnology **32**(31), 315709 (2021)
6. X. Bao, Q. Ou, Z.Q. Xu, Y. Zhang, Q. Bao, H. Zhang, Band structure engineering in 2D materials for optoelectronic applications. Adv. Mater. Technol. **3**, 1800072 (2018)
7. H. Xu, J. Zhu, Q. Ma, J. Ma, H. Bai, L. Chen et al., Two-dimensional MoS2: Structural properties, synthesis methods, and regulation strategies toward oxygen reduction. Micromachines **12**, 240 (2021)
8. G. Li et al., All the catalytic active sites of MoS2 for hydrogen evolution. J. Am. Chem. Soc. **138**(51), 16632–16638 (2016)
9. R. Kumar, X. Liu, J. Zhang, M. Kumar, Room-temperature gas sensors under photoactivation: From metal oxides to 2D materials. Nano Micro Lett. **12**, 1–37 (2020)

10. J. Chen, N. Kuriyama, H. Yuan, H.T. Takeshita, T. Sakai, Electrochemical hydrogen storage in MoS2 nanotubes. J. Am. Chem. Soc. **123**, 11813–11814 (2001)
11. N. Rusman, M. Dahari, A review on the current progress of metal hydrides material for solid-state hydrogen storage applications. Int. J. Hydrog. Energy **41**, 12108–12126 (2016)
12. I. Jain, Hydrogen the fuel for 21st century. Int. J. Hydrog. Energy **34**, 7368–7378 (2009)
13. S. Moon, K. Kim, J. Kim, A study on public acceptance of hydrogen portfolio standard for renewable energy expansion: Comparative analysis of hydrogen production mix plans. Int. J. Hydrog. Energy **49**, 538–552 (2024)
14. W. Chen, L. Sui, X. Long, J. Liao, S. Wang, X. Wei, Anatase TiO2 aerogel with high specific surface areas and porous network structures for ultra-fast response hydrogen sensor. Int. J. Hydrog. Energy **50**, 973–991 (2024)
15. P.M. Pratik, C.K. Sumesh, MoS2 nanosheets on Cu-foil for rapid electrocatalytic hydrogen evolution reaction. J. Electroanal. Chem. **912**, 116270 (2022)
16. S. Kumar, A. Mirzaei, A. Kumar, M.H. Lee, Z. Ghahremani, T.-U. Kim et al., Nanoparticles anchored strategy to develop 2D MoS2 and MoSe2 based room temperature chemiresistive gas sensors. Coord. Chem. Rev. **503**, 215657 (2024)
17. S. Yu, S. Song, R. Li, B. Fang, The lightest solid meets the lightest gas: An overview of carbon aerogels and their composites for hydrogen related applications. Nanoscale **12**, 19536–19556 (2020)
18. P. Chauhan, J.L. Dattatray, V. Patel, P. Sahatiya, C.K. Sumesh, Hierarchical NiCo-LDH@MoS2/CuS composite as efficient trifunctional electrocatalyst for overall water splitting and asymmetric supercapacitor. Electrochimica Acta **469**, 143197 (2023)
19. M. Patel, P. Pataniya, H. Vala, C.K. Sumesh, One-dimensional/two-dimensional/three-dimensional dual heterostructure based on MoS2-modified ZnO-heterojunction diode with silicon. J. Phys. Chem. C **123**(36), 21941–21949 (2019)
20. Kapatel, Sanni, C. K. Sumesh (2016) One pot sono-chemical synthesis of 2D layered MoS2 nanosheets. AIP Conference Proceedings. Vol. 1728. No. 1. AIP Publishing
21. G. Eda, H. Yamaguchi, D. Voiry, T. Fujita, M. Chen, M. Chhowalla, Photoluminescence from chemically exfoliated MoS2. Nano Lett. **11**, 5111–5116 (2011)
22. A.V. Agrawal, R. Kumar, G. Yang, J. Bao, M. Kumar, M. Kumar, Enhanced adsorption sites in monolayer MoS2 pyramid structures for highly sensitive and fast hydrogen sensor. Int. J. Hydrog. Energy **45**, 9268–9277 (2020)
23. U.J. Cho, D. Jang, Y. Jeon, T. Kim, B. Jo, R. Kim et al., A palladium-deposited molybdenum disulfide-based hydrogen sensor at room temperature. Appl. Sci. **13**, 10594 (2023)
24. R. Kronberg, M. Hakala, N. Holmberg, K. Laasonen, Hydrogen adsorption on MoS 2-surfaces: A DFT study on preferential sites and the effect of sulfur and hydrogen coverage. Phys. Chem. Chem. Phys. **19**, 16231–16241 (2017)
25. X. Liu, W. Yang, Z. Liu, Recent progress on synchrotron-based in-situ soft X-ray spectroscopy for energy materials. Adv. Mater. **26**, 7710–7729 (2014)
26. E.J. Kautz, D.K. Schreiber, A. Devaraj, B. Gwalani, Mechanistic insights into selective oxidation and corrosion of multi-principal element alloys from high resolution and in situ microscopy. Materialia **18**, 101148 (2021)
27. L.G. De Arco, Y. Zhang, A. Kumar, C. Zhou, Synthesis, transfer, and devices of single-and few-layer graphene by chemical vapor deposition. IEEE Trans. Nanotechnol. **8**, 135–138 (2009)
28. M. Patel, P. Pataniya, H. Vala, C.K. Sumesh, One-dimensional/two-dimensional/three-dimensional dual heterostructure based on MoS 2-modified ZnO-heterojunction diode with silicon. J. Phys. Chem. C (2019). https://doi.org/10.1021/acs.jpcc.9b05134
29. M. Khan, S. Kumar, A. Mishra, I. Sulania, M.N. Tripathi, A. Tripathi, Study of structural and electronic properties of few-layer MoS2 film. Mater. Today Proc. **57**, 100–105 (2022)
30. P.K. Kulriya, M. Kumar, J. Singh, D.K. Avasthi, Hydrogen pressure dependent in-situ electrical studies on Pd/C composite. Int. J. Hydrog. Energy **42**, 3399–3406 (2017)
31. P. Kulriya, F. Singh, A. Tripathi, R. Ahuja, A. Kothari, R. Dutt et al., Setup for in situ X-ray diffraction study of swift heavy ion irradiated materials. Rev. Sci. Instrum. (2007). https://doi.org/10.1063/1.2804171
32. C. Yim, M. O'Brien, N. McEvoy, S. Riazimehr, H. Schäfer-Eberwein, A. Bablich et al., Heterojunction hybrid devices from vapor phase grown MoS2. Sci. Rep. **4**, 5458 (2014)
33. H. Li, Q. Zhang, C.C.R. Yap, B.K. Tay, T.H.T. Edwin, A. Olivier et al., From bulk to monolayer MoS2: Evolution of Raman scattering. Adv. Func. Mater. **22**, 1385–1390 (2012)
34. K.-G. Zhou, F. Withers, Y. Cao, S. Hu, G. Yu, C. Casiraghi, Raman modes of MoS2 used as fingerprint of van der Waals interactions in 2-D crystal-based heterostructures. ACS Nano **8**, 9914–9924 (2014)
35. L. Lei, D. Huang, G. Zeng, M. Cheng, D. Jiang, C. Zhou et al., A fantastic two-dimensional MoS2 material based on the inert basal planes activation: Electronic structure, synthesis strategies, catalytic active sites, catalytic and electronics properties. Coord. Chem. Rev. **399**, 213020 (2019)
36. L. Ma, D.N. Nath, E.W. Lee, C.H. Lee, M. Yu, A. Arehart et al., Epitaxial growth of large area single-crystalline few-layer MoS2 with high space charge mobility of 192 cm2 V− 1 s− 1. Appl. Phys. Lett. (2014). https://doi.org/10.1063/1.4893143
37. D. Marinov, J.F. de Marneffe, Q. Smets, G. Arutchelvan, K.M. Bal, E. Voronina et al., Reactive plasma cleaning and restoration of transition metal dichalcogenide monolayers. npj 2D Mater. Appl. **5**, 17 (2021)

J Mater Sci: Mater Electron **(2026) 37:383**

Influence of temperature and NO_2 concentration on the sensing performance of nanostructured MoS_2

Ramesh Kumar[1], Jitendra Singh[2], Pawan K. Kulriya[3], Mahesh Kumar[4], and Vinod Singh[1,*]

[1] *Department of Applied Physics, Delhi Technological University, New Delhi 110042, India*
[2] *CSIR-Central Electronics Engineering Research Institute, Pilani, Rajasthan 333031, India*
[3] *School of Physical Sciences, Jawaharlal Nehru University, New Delhi 110067, India*
[4] *Department of Electrical Engineering, Indian Institute of Technology Jodhpur, Jodhpur 342030, India*

Received: 19 November 2025
Accepted: 8 February 2026

ABSTRACT

Gas sensors play a critical role in monitoring hazardous industrial emissions and improving indoor air quality. Among two-dimensional (2D) transition metal dichalcogenides (TMDs), molybdenum disulfide (MoS_2) has emerged as a promising sensing material due to its high surface area, tunable bandgap, and strong surface reactivity. This work systematically investigates the influence of operating temperature and nitrogen dioxide (NO_2) concentration on the performance of nanostructured MoS_2 thin-film sensors fabricated via chemical vapor deposition (CVD). Highly crystalline, continuous MoS_2 films (20 nm thick) were deposited on alumina substrates with optimized interdigitated electrode geometry to enhance gas–surface interaction. Structural and morphological characterization using X-ray diffraction (XRD), field-emission scanning electron microscopy (FESEM), atomic force microscopy (AFM), and Raman spectroscopy confirmed the phase purity, uniform nanosheet morphology, and low surface roughness. Electrical transport measurements revealed that sensor resistance increased upon NO_2 exposure, consistent with n-type semiconducting behavior. The sensor exhibited high selectivity toward NO_2 over other common gases, with the optimal response (~ 14.2%) observed at 20 ppm and 150 °C, along with fast response (102 s) and recovery (94 s) times. Elevated temperature not only significantly improved response but also induced irreversible structural defects at higher concentrations. These findings demonstrate that precisely engineered MoS_2 films offer a pathway toward compact, selective, and thermally tunable NO_2 sensors for environmental and industrial monitoring applications.

Address correspondence to E-mail: vinodsingh@dtu.ac.in

https://doi.org/10.1007/s10854-026-16798-9

1 Introduction

Detection of toxic gases such as nitrogen dioxide (NO_2) is essential for safeguarding human health, ensuring workplace safety, and monitoring environmental pollution. NO_2, a by-product of combustion in vehicles and industrial processes, is harmful even at low concentrations (as low as 10–20 parts per million (ppm)) and can cause severe respiratory, neurological, and cardiovascular issues at higher exposures. Conventional gas sensors based on metal oxide semiconductors (e.g., SnO_2, ZnO, WO_3) offer low cost and robustness but often require high operating temperatures (> 200 °C), suffer from poor selectivity, and show slow recovery times, particularly in humid or complex gas environments [1–3]. Two-dimensional (2D) transition metal dichalcogenides (TMDs), and in particular molybdenum disulfide (MoS_2), have emerged as promising alternatives for next-generation gas sensors. MoS_2 offers a high specific surface area, tunable bandgap (1.2–1.8 eV), rich surface chemistry, and strong adsorption affinity for oxidizing gases such as NO2 [4, 5]. Its layered structure provides abundant active sites (including edge defects and sulfur vacancies) that facilitate charge transfer upon gas adsorption, enabling detection at lower temperatures and with higher selectivity than many metal oxides [6]. Furthermore, MoS_2 demonstrates better chemical stability in oxidizing environments compared to other 2D materials such as black phosphorus or MXenes, which are prone to degradation in air [7]. Recent studies have explored MoS_2 in both pristine and hybrid forms. For example, Park et al. (2022) demonstrated room-temperature NO_2 detection using few-layer MoS_2 with UV activation, achieving a detection limit of 50 ppb [8]. Zhang et al. (2023) reported MoS_2–ZnO heterostructures with enhanced sensitivity and recovery speed due to synergistic band alignment effects [9]. Similarly, MoS_2/graphene hybrids have been shown to combine high carrier mobility with strong adsorption, yielding ultrafast responses under ambient conditions [10]. The graphene/MoS_2 hybrids also displayed an enhanced performance in several applications, such as lithium-ion batteries [10], supercapacitors [11], field-effect transistors (FETs) [12], and photodetectors [13]. Enhancement in the sensing efficiency in MoS_2/graphene hybrid materials is observed due to electric charge transport via heterojunction's structure and its unique electronic structure, which is mediated by band energy synchronization [14]. The ultra-thin MoS_2 sensor demonstrated an impressive reaction/recovery against NO_2 gas with excellent stability and repeatability as compared to other target gases such as H_2, NH_3, SO_2, and CO_2 [15]. Compared to these binary and ternary systems, pure MoS_2 offers the advantage of simpler synthesis, well-controlled film quality, and fewer interfacial complications, while still achieving competitive performance when growth parameters and electrode design are optimized. In addition, it also requires an inert environment for gas detection due to MoS_2's low stability and selectivity. Despite these advances, the influence of operating temperature and gas concentration on the intrinsic NO_2 sensing properties of well-defined nanostructured MoS_2 films remains insufficiently explored. Most prior works focus on room-temperature performance or hybrid material systems, leaving a gap in understanding the temperature-dependent kinetics and stability of pure MoS_2 in NO_2-rich and potentially harsh environments.

In this work, we systematically investigate the effect of both temperature (50–150 °C) and NO_2 concentration (1–100 ppm) on the sensing performance of CVD-grown MoS_2 thin films with optimized interdigitated electrodes. The sensor exhibited high selectivity, fast response (102 s), and recovery (94 s) time at 20 ppm concentration of NO_2 at 150 °C. In addition, significant improvement in response at high temperature and structural defects at higher concentrations is also observed. The results provide insights into the trade-offs between response magnitude, speed, and long-term stability, offering guidance for designing MoS_2-based sensors for industrial and environmental monitoring.

2 Experimental details

2.1 Designing and fabrication of gas sensor platform

The 0.5-mm-thick alumina substrate was used to create the gas sensor platform. The electrode pattern was made of metallic Molybdenum (Mo) with a layer thickness of 200 nm. Sputter deposition was used to deposit a thin layer of molybdenum (Mo). The electrode pattern was defined using a physical mask. The spacing was kept at 300 μm, and the electrode line width was 300 μm. The heating element (resistor) and gas sensor electrode were combined into a single device platform. The dimensions of the sensor die were 3.0 mm by 3.0 mm. For gas sensing, the sensor was installed on the header of the customized transistor outline (TO) packages. After process parameters optimization, gas sensing layer (MoS_2) was coated on the interdigital transducer electrodes (IDT). Humidity strongly influences Chemiresistive gas sensing by competing with target gas molecules for surface adsorption sites. In this study, sensing measurements were conducted under controlled dry air conditions to suppress humidity-related interference and to isolate the intrinsic interaction between NO_2 molecules and the MoS_2 sensing layer, thereby enabling clear evaluation of temperature-dependent sensing behavior. The schematic and optical image of the MoS_2 gas sensor device is shown in Fig. 1.

2.2 Preparation of MoS_2 films

Figure 2 shows the schematic of three-zone tubular CVD furnace used to deposit the MoS_2 thin film on the alumina substrate having dimensions of 3.0 mm by 3.0 mm. The thickness of MoS_2 film was kept ~ 20 nm to ensure continuous film coverage, high crystallinity, and stable electrical contact with the interdigitated electrodes while maintaining reliable controllability of the CVD growth process. We have also deposited thinner films (5 nm and 10 nm) which displayed discontinuity and increased contact resistance that were not found suitable for sensing applications. Similarly, thicker films can reduce surface sensitivity due to dominant bulk conduction pathways. Before deposition, the alumina substrate was first ultrasonically cleaned with acetone and isopropyl alcohol (IPA), and then gaseous nitrogen was used to dry it. An extra cleaning procedure was performed prior to the alumina substrate being put into the CVD furnace's middle zone. The quartz boat was filled with high purity (99.999%) of molybdenum trioxide (MoO_3), and the alumina boat was filled with high purity (99.995%) sulfur procured from the Sigma Aldrich. The three zones for alumina are kept at 800 °C for the substrate, 650 °C for MoO_3, and 200 °C for sulfur. High-purity Ar gas flowed with a mass flow controller (MFC) at 200 sccm during the growth process [16].

2.3 Characterizations of MoS_2 films

The Bruker AXS D8-advanced X-ray diffractometer (XRD equipment) equipped with a Cu K_α source with a wavelength of 1.54 Å (40 kV and 40 mA power) was used to record the XRD patterns. With a laser wavelength of 532.5 nm, the short-range ordering and molecular structure of pure MoS_2 were examined using a Raman spectrometer (WITec alpha 300 RA).

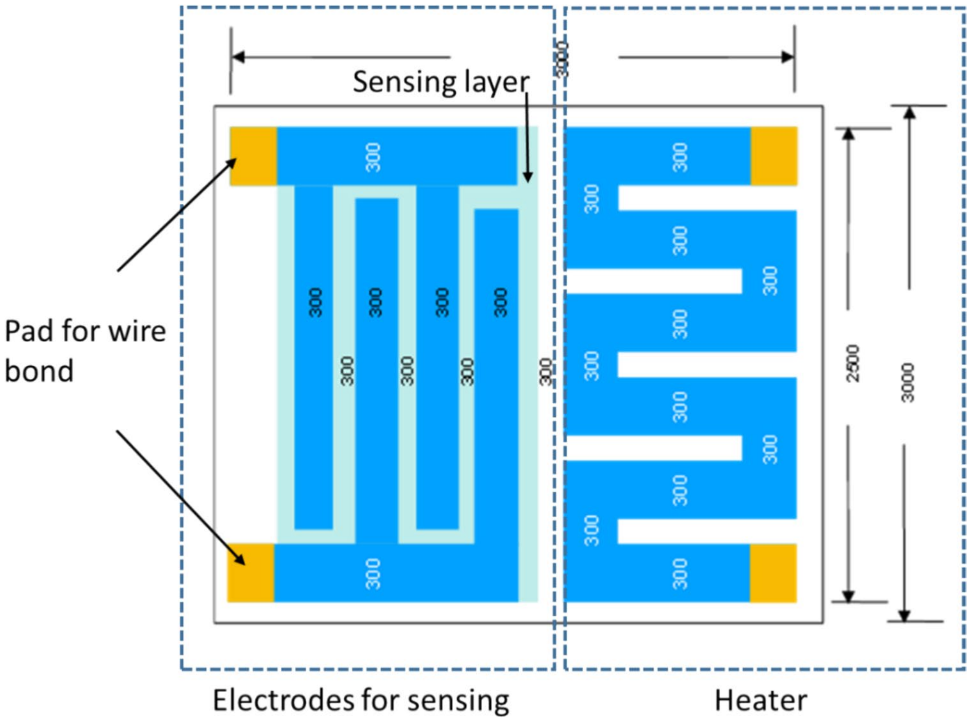

Fig. 1 Schematic and optical image of the MoS_2 gas sensor device showing the interdigitated electrodes used for resistance measurements and the integrated micro-heater for temperature control

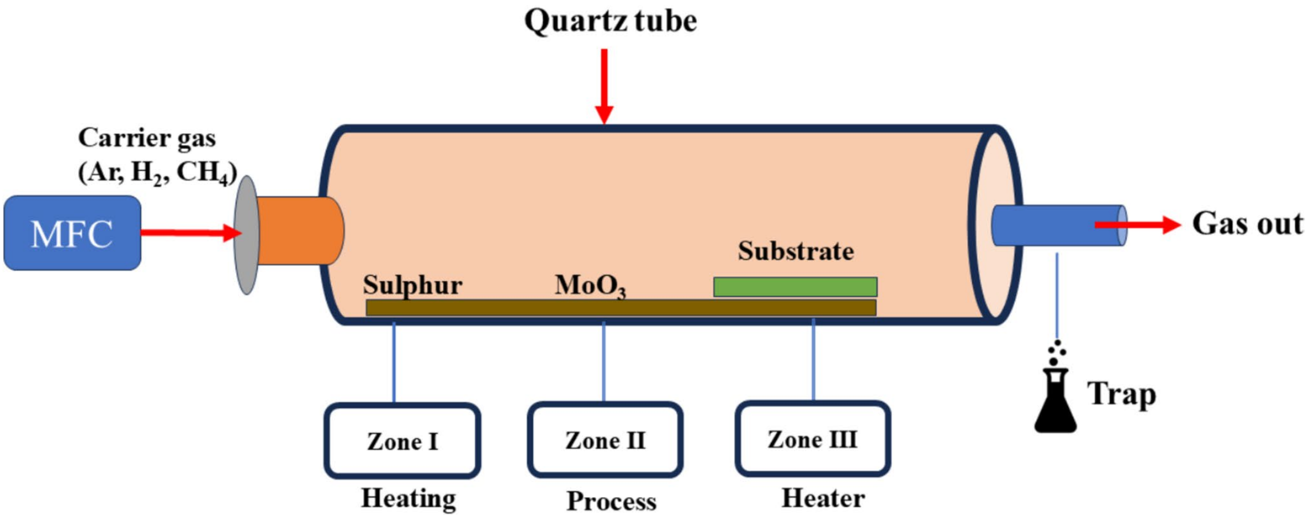

Fig. 2 Synthesis of MoS_2 films using three-zone chemical vapor deposition (CVD) technique

MoS_2's surface shape and elemental analysis were assessed using ZEISS EVO 40 energy dispersive spectroscopy (EDS) and scanning electron microscopy (SEM). NTMDTNTEGRA-prima instrument was used to perform atomic force microscopy (AFM) for the roughness measurements of thin-film surface.

3 Results and discussion

3.1 Structural analysis

X-ray diffraction (XRD) technique was used to determine the degree of crystallinity of the MoS_2 thin film deposited on the alumina substrate. Figure 3a shows the XRD pattern of the MoS_2 thin film. The XRD peaks appeared at the 2-theta values of 14.3°, 25.4°, 39.0°, and 58.4°, which correspond to values at (002), (004), (103), and (110) planes as confirmed from the JCPDS

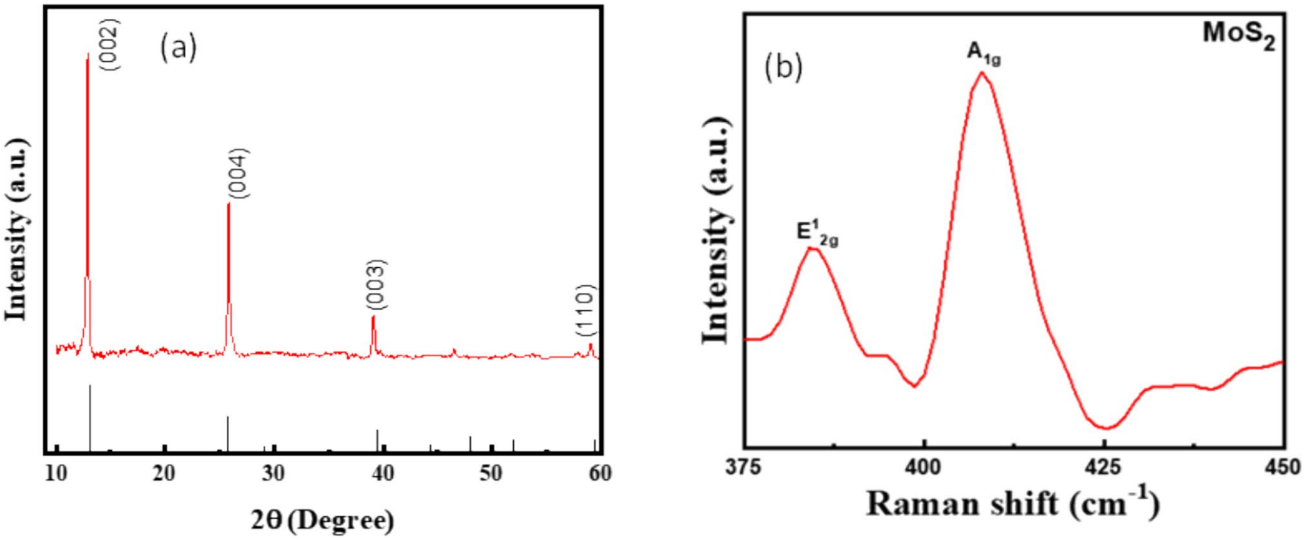

Fig. 3 **a** XRD pattern and **b** Raman spectrum of MoS_2 thin films having 20 nm thickness grown by CVD

No: 75–1539. This clearly confirms the synthesis of impurity-free polycrystalline MoS_2 phase.

To probe the short-range ordering in the MoS_2 thin films, the Raman spectroscopy technique is considered the most suitable tool. Figure 3b displays the Raman spectrum of the MoS_2 thin films. It exhibits the distinctive signal of 2H-MoS_2, with no observable evidence of carbon or oxide contamination. The characteristic peak appeared at the wavenumber of 385 cm^{-1}, corresponding to $E^1{}_{2g}$ due to in-plane vibrational modes of the MoS_2 lattice, where another peak appeared at the wavenumber of 405 cm^{-1}, representing the out-of-plane vibrations of the MoS_2 layers. The well-matched unique peaks clearly show the formation of impurity-free single-phase MoS_2.

3.2 Micro-structural analysis

The surface morphology of the MoS_2 thin film (20 nm) was assessed using scanning electron microscopy (SEM). Figure 4a displays a typical SEM picture of the MoS_2 thin film deposited using the CVD technique on alumina substrate. It shows that the MoS_2 nanosheets were evenly distributed throughout the substrate, giving the impression that there is no topographical contrast and that the surface is uniform. Initially, MoS_2 thin film grew as nanoparticles until it reached a threshold thickness. The nucleation sites merged, forming MoS_2 thin films. The nucleation sites in the favored curved direction progressively changed into vertically developed structures, resulting in a MoS_2 flower-like structure as shown in Fig. 4a. It may be noted that the film-like surface morphology of chemical vapor-deposited MoS_2 films differs significantly from films made using exfoliation or sputtering processes, which could improve gas sensing capability. Energy dispersive spectroscopy (EDS) was used to examine the composition of MoS_2 thin films, as shown in Table 1. This shows that Mo, O, S, and Al elements make up the majority of the MoS_2 thin film, according to the element distribution. The alumina substrate also contributes to the presence of the additional aluminum and oxygen element. The particle size distribution histogram, shown in Fig. 4b, provides an estimate of the average particle size of 0.63 ± 0.15 µm.

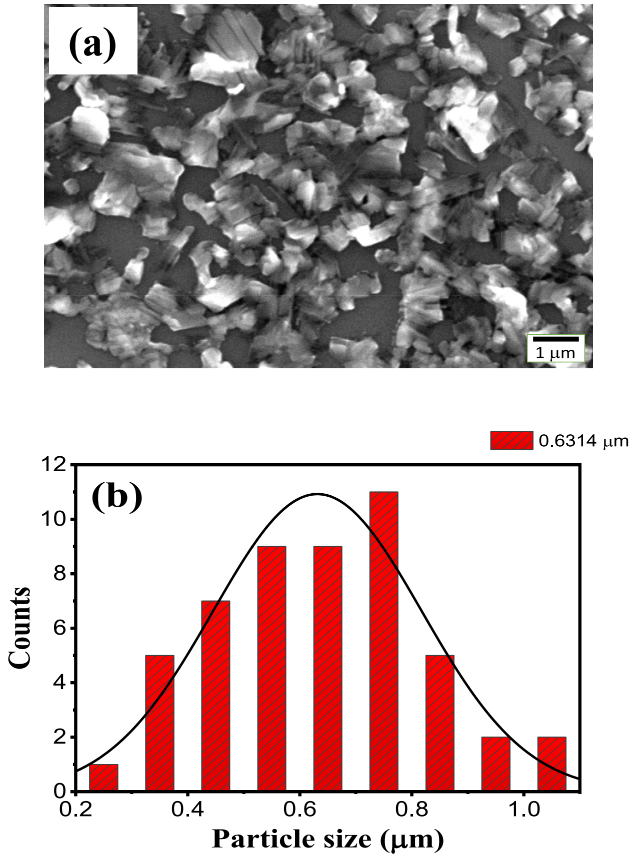

Fig. 4 **a** SEM micrograph and **b** size distribution plot of the as-synthesized MoS_2 thin films

Figure 5 shows AFM images of MoS_2 thin films synthesized using chemical vapor deposition (CVD) method. The surface roughness of film was calculated using Nasoscope analysis 1.5 software. It shows that thickness of film is 20 nm, and the roughness was found 4.2 nm.

3.3 Sensing characteristics of MoS_2 thin films

The sensing performance of MoS_2 thin film was determined by electrical transport properties studies and measuring the response time, recovery time, and sensitivity on the exposure to sensing gas. The predominant carrier in the sensing material and the kind of gas in the environment determine the change in the electrical resistance on the exposure to the NO_2 gas.

Table 1 Elemental composition obtained through EDS analysis of MoS_2 deposited on alumina substrate

Element	Line	Mass (%)	Atom (%)
O	K	25.18 ± 0.43	39.52 ± 0.67
Al	K	63.89 ± 0.54	57.12 ± 0.49
S	K	0.95 ± 0.19	0.74 ± 0.15
Mo	L	9.98 ± 0.60	2.61 ± 0.16

Fig. 5 AFM image of the as-grown MoS_2 thin films

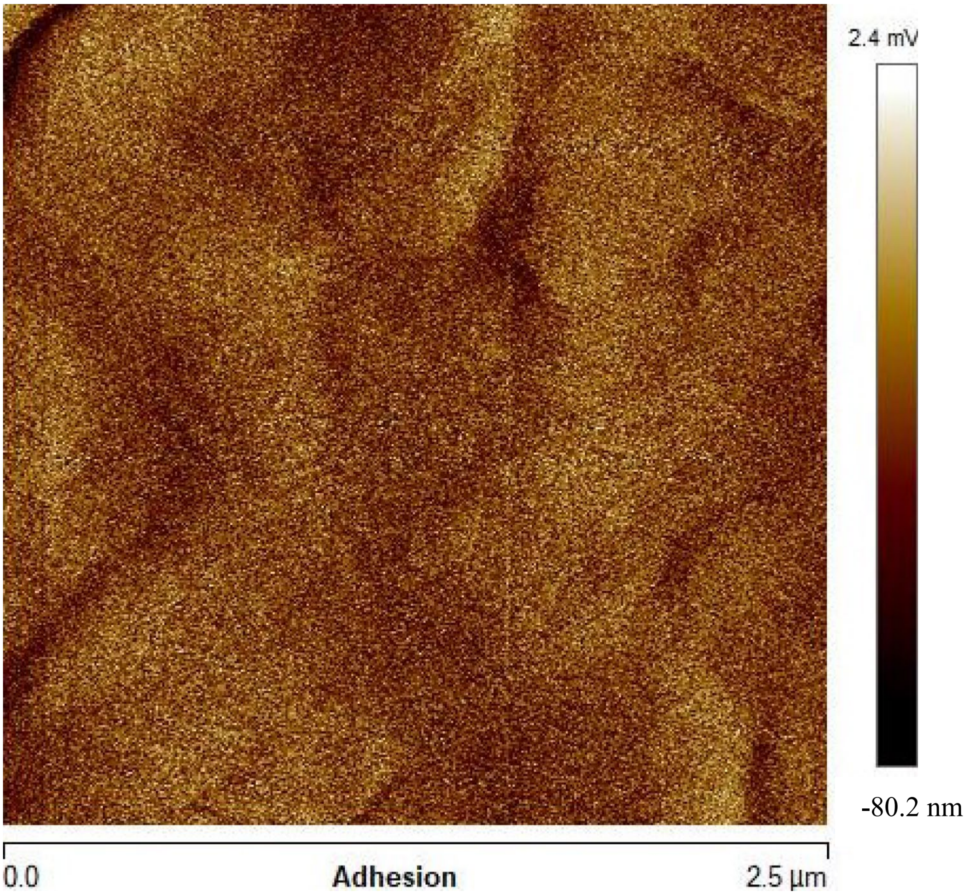

Although NO_2 is hazardous even at trace concentrations, the concentration range investigated in this work was intentionally selected to clearly resolve temperature-dependent sensing trends, response magnitude, and response–recovery kinetics under controlled laboratory conditions. The emphasis of this study is on understanding how operating temperature governs sensing behavior and performance trade-offs in pristine MoS_2 sensors, rather than on demonstrating trace-level detection limits. It has been reported that oxidizing gases act as acceptors, increasing resistance in n-type materials, whereas reducing gases act as donors, decreasing resistance in n-type materials [17]. In the case of p-type materials, the opposite pattern is observed. In the present study, the n-type MoS_2 sensor displays an increase in the electrical resistance of the MoS_2 thin film due to an oxidizing gas (NO_2). For the MoS_2–Al_2O_3 sample, electrical measurements were performed in two probe geometries to validate the MoS_2 film's behavior. Using a planar contact arrangement, I–V characteristics were measured. The two contacts were taken from interdigital electrodes. MoS_2's n-type semiconducting behavior is confirmed by the rectifying behavior displayed by the I–V characteristic. The response of the sensor is defined as.

$\text{Response}(\%) = \frac{Rg-Ra}{Ra}100$,where R_a and R_g are the electrical resistance of sensors in dry air and oxidizing gas atmosphere, respectively. Figure 6a shows the relative response of MoS_2 films toward NO_2 gas taken at different temperatures ranging from 50 °C, 75 °C, 100 °C, 125 °C to 150 °C at 20 ppm. This plot indicates that the relative response of MoS_2 films increases with an increase in the temperature. The highest response of 14.2% was observed for 20 ppm concentration at 150 °C temperature. When the sensing gas is removed, then the value of relative response decreased. The value of the relative response after removal of the sensing gas is highest at 50 °C. This is reduced when the temperature is increased from 50 °C to 100 °C. However, the minimum value of the relative response remained identical for 100 °C, 125 °C, and 150 °C temperatures. This indicates that some permanent structural defects were created in the film which were not removed even when the temperature was increased above 100 °C. In addition to temperature, the concentration of the sensing gas also plays an important role in the determination of the sensing properties of gas. Figure 6b exhibits the electrical resistance versus time plot for NO_2 gas sensing performed at 150 °C by exposing to the sensing gas at various concentrations starting from 1 to 100 ppm at concentrations of 1 ppm, 10 ppm, 20 ppm, 50 ppm, and 100 ppm. The maximum value of the electrical resistance is the same for all the values of the concentration but the time required to attain the maximum value depends upon the concentration. The minimum value of resistance after unloading the sensing gas is continuously decreasing as the concentration increases. The lowest value is achieved for the sample exposed to the highest concentration (100 ppm) of the sensing gas. Figure 6c displays the relative response of NO_2 gas at various concentrations starting from 1 to 100 ppm at concentrations of 1 ppm, 10 ppm, 20 ppm, 50 ppm, and 100 ppm performed at 150 °C. The relative response of NO_2 gas is increased as the concentration is increased from 1 to 100 ppm. The variation in the relative response for 20 ppm concentration at 150 °C is shown in Fig. 6 d. Figure 6e shows the repeatability of 20 ppm concentration sensing at the same temperature, and further, the response and recovery times of the as-prepared gas sensor were calculated for the sensing peak of 20 ppm and 150 °C. The calculated values of the response time and recovery time are 102 s and 94 s, respectively, as shown in Fig. 6f. The response time is defined as the duration required to reach 90% of the total resistance change upon NO_2 exposure, whereas the recovery time corresponds to 90% restoration of the baseline resistance after gas removal. The comparatively faster recovery arises from temperature-assisted desorption processes, which enhance the release of adsorbed NO_2 molecules from the MoS_2 surface. This kind of response is better than the early reported MoS_2 gas sensor for NO_2 gas sensing as depicted in Table 2 as well. In addition, baseline drift is also observed during repeated sensing cycles, particularly at elevated operating temperatures. This arises from slow desorption kinetics and partial irreversible adsorption of NO_2 molecules at defect-rich or edge sites of MoS_2. This behavior is characteristic of 2D material-based chemiresistive sensors exposed to oxidizing gases and primarily affects the absolute baseline rather than the relative sensing response.

Response and recovery periods for a 20-nm-thick MoS_2 sensor at 150 °C were measured for different NO_2 concentrations. These data reveal that when NO_2 gas concentrations increase, so do response and recovery times. As the quantity of exposed gas increases, then the number of gas molecules can interact with the detecting surface. Increased gas molecule adsorption increases response time while also increasing the electron concentration for exchange between sensing material and gas molecules. Many molecules must be desorbed from the surface during recovery, which increases the time required for the surface to restore its original resistance. As a result, the interaction kinetics of gas molecules at varied concentrations on the sensor surface generate varying response and recovery durations. Response and recovery time plot for NO_2 concentration is shown in Fig. 7. This clearly shows that response and recovery times are increasing with an increase in the concentration of the NO_2 gas. It is worth mentioning here that the sensor temperature was controlled using a variable voltage controller, while a constant 3 V bias was applied to the contact pad. The sensing performance was evaluated by monitoring resistance variations upon exposure to target gases NO_2 at a concentration of 1%. During sensing measurements, the temperature and relative humidity (RH) within the sensing chamber were continually monitored and adjusted using a digital hygrometer (HTC instrument HT-306) [18]. Relative response of MoS_2 for NO_2 gas at different concentration with error bars is shown in Fig. 8.

The limit of detection (LOD) may be estimated using the standard relation $LOD = 3\sigma/S$, where σ represents the standard deviation of the baseline resistance noise and S denotes the slope of the calibration curve in the low-concentration regime. This approach provides an estimate of the sensor's capability for detecting lower NO_2 concentrations. The calculated value of the limit of detection is 0.067 ppm.

In MoS_2 films, the sulfur vacancies and other flaws in the MoS_2 film serve as the gas molecules active sites. Initially, partial oxidation of the MoS_2 top layer is caused by oxygen gas molecules in the environment through the chemisorption at the surface of the sensing film and forming oxygen species. Conduction band electrons are extracted from the MoS_2 film by these ions acting as electron trap centers. Thus, initially, the electrical resistance of the sensor increases as the concentration of free electrons in the conduction band begins to drop. A significant factor in altering the sensing material's initial electrical resistance was the chemisorption of oxygen gas molecules.

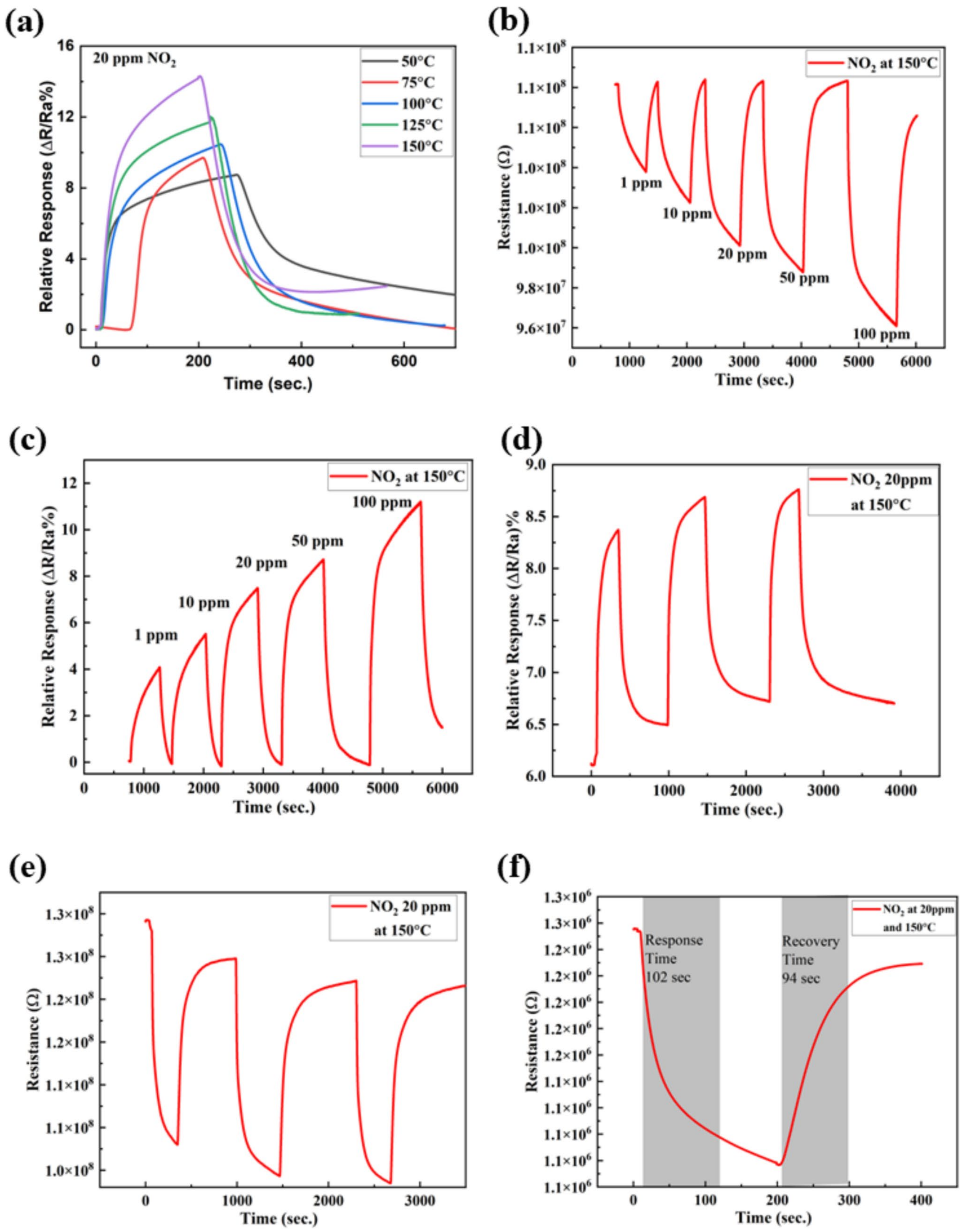
(a)
20 ppm NO_2
50°C
75°C
100°C
125°C
150°C
Relative Response (ΔR/Ra%)
Time (sec.)
(b)
NO_2 at 150°C
1 ppm
10 ppm
20 ppm
50 ppm
100 ppm
Resistance (Ω)
Time (sec.)
(c)
NO_2 at 150°C
1 ppm
10 ppm
20 ppm
50 ppm
100 ppm
Relative Response (ΔR/Ra%)
Time (sec.)
(d)
NO_2 20ppm at 150°C
Relative Response (ΔR/Ra)%
Time (sec.)
(e)
NO_2 20 ppm at 150°C
Resistance (Ω)
Time (sec.)
(f)
NO_2 at 20ppm and 150°C
Response Time 102 sec
Recovery Time 94 sec
Resistance (Ω)
Time (sec.)

◂**Fig. 6** Sensing response of NO_2 as **a** the relative response at different temperatures at 20 ppm concentration, **b** the resistance versus time plot at 150 °C with varying concentrations, **c** the relative response at 150 °C with varying concentrations, **d** the repeatability of response at 20 ppm, **e** its corresponding resistance plot, and **f** the calculations of response and recovery times

$$O_2(\text{gas}) \rightarrow O_2(\text{ads})$$

$$O_2(\text{ads}) + e^-_{\text{MoS2}} \rightarrow O_2(\text{ads})$$

When MoS_2 film is exposed to NO_2 gas, then the electrons from the MoS_2 conduction band are transferred to the NO_2 molecules and get adsorbed on the film surface [18]. Conversely, NO_2 gas creates NO_2 ions by reaction with oxygen ions (O_2). This procedure raises the gas sensor's overall electrical resistance while lowering the concentration of electrons in the detecting material. Figure 9 shows the mechanism for the sensing of NO_2 gas with MoS_2.

$$NO_2(\text{gas}) + e_{\text{MoS2}} \rightarrow NO_2(\text{ads})$$

$$NO_2(\text{ads}) + O_2(\text{ads}) \rightarrow NO_2(\text{gas}) + 2O(\text{ads})$$

During the recovery process, NO_2 ions react to O_2 ions in the sensing chamber to release NO_2 gas into the environment when the flow of NO_2 gas stops. Oxygen ions once more approach the active surface to create native oxide. The sensor resistance returns to its starting value when the electrons that NO_2 had trapped are released back into the MoS_2 conduction band.

The adsorption and desorption of oxygen are also affected by the operating temperature. At relatively low operating temperatures, molecularly adsorbed oxygen species dominate the surface, whereas increasing temperature promotes the formation of more reactive oxygen species with enhanced electron withdrawal capability. This temperature-dependent evolution of surface oxygen species contributes to the observed enhancement in charge transfer and sensing response. Recent NO_2 sensing studies based on MoS_2 have employed diverse performance-enhancement strategies. UV-assisted heterostructure sensing in the $MoS_2/PtSe_2$ system has demonstrated high sensitivity toward NO_2 gas at room temperature under UV illumination [22]. Edge-engineered heterostructures, such as the $Mo2TiC_2Tx/MoS_2$ platform reported by Zhao et al. [23], exploit enriched edge sites and interfacial coupling to improve sensing performance. Electrocatalytic and radical-assisted approaches have been explored by Li et al. [24] through CoP/MoS_2 systems, where surface radical generation enhances the NO_2 response at room temperature. In addition, Bharathi et al. [25] reported edge-activated, solution-processed Ni–MoS_2 nanosheets, highlighting the role of edge activation in achieving high sensitivity. In contrast to these approaches, the present work focuses on pristine CVD-grown MoS_2 and systematically examines temperature-driven sensing behavior using an integrated micro-heater, providing complementary insight into performance tuning without additional material modification or external activation. The comparison of performance metrics for the MoS_2-based gas sensors from several investigations, including the present one, is shown in Table 2.

The performance metrics for MoS_2-based gas sensors from several investigations show that sensing response critically depends upon various factors such as the surface morphology, methods for the preparation of film, concentration of sensing gas, and operating temperature. If one compares the temperature-dependent sensing response of CVD-grown MoS_2 films, it is observed that the response decreases with increasing temperature. The response time improves significantly, decreasing from 678 s at room temperature to 102 s at 150 °C, confirming enhanced response speed at elevated temperatures. This clearly suggests that the operating temperature plays a decisive role in controlling adsorption–desorption kinetics and charge transfer processes at the MoS_2 surface. Increasing operating temperature enhances the interaction between adsorbed NO_2 molecules and the sensing layer, resulting in improved response magnitude and faster recovery, while simultaneously introducing a trade-off with baseline stability. These observations highlight the importance of temperature optimization for achieving balanced sensor performance. In spite of all excellent sensing performance of MoS_2 thin films at high temperature, it consumes higher power which can increase the cost of the device. Therefore, further research on the optimizing the operating temperature of MoS_2-based sensor without compromising sensor performance is required.

4 Conclusion

The effect of gas concentrations and temperatures on the sensing response of the CVD-grown MoS_2 thin films measured on exposure to NO_2 gas

Table 2 Literature review of MoS_2 nanostructures for NO_2 gas response

Material	Method	Morphology	NO_2 conc	T (°C)	Gas Response (%)	Response/recovery time	Ref
MoS_2	CVD	Flakes	100 ppm	100	21.56	71/310 s	[7]
MoS_2	One-step hydrothermal	Hollow sphere	20 ppb	150	40.3	79/225 s	[18]
n-MoS_2 p-MoS_2	Chemical exfoliation	Flakes	100 ppm	200	5.8 1.15	2460/2340 s 660/720 s	[19]
MoS_2	Mechanical exfoliation	Five layer	100 ppm	RT	–	180/600 s	[20]
MoS_2	CVD	Bilayer film	1 ppm	RT	2.6	678/318 s	[21]
MoS_2	CVD	Vertically aligned layers	800 ppb	RT	13	344/581 s	[22]
MoS_2	CVD	Flakes	50 ppm	RT	19.25	33.5/140.1 s	[23]
MoS_2	CVD	Nanosheet	100 ppm	RT	20	15/180 s	[24]
Ni-MoS_2	CVD	Flakes	200 ppm	RT	45.2	28/250 s	[25]
MoS_2	CVD	Film	100 ppm	150	14	102/94 s	This work

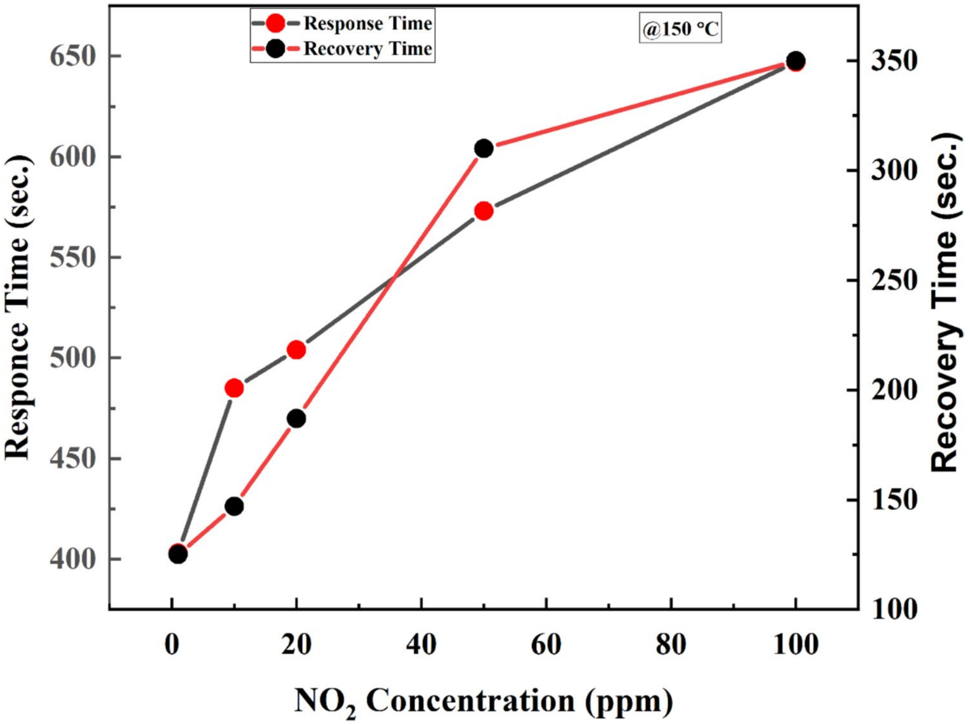

Fig. 7 Response and recovery time plot with respect to different gas concentrations (NO_2) at 150 °C temperature

displays excellent response for MoS_2 film thickness of 20 nm. The interdigitated contacts having improved shape were also used to increase the gas sensing response of the sensor. The as-prepared MoS_2 thin films were characterized using XRD, FESEM, EDS, AFM, and Raman spectroscopy techniques. XRD analysis showed the formation of polycrystalline phases of MoS_2. Structural and elemental analysis showed purity and uniformity of MoS_2. The MoS_2 sensor with a thickness of 20 nm results in reasonable responsivity (~ 14.2%), prompt response (~ 102 s.), and recovered (~ 94 s.) to 20 ppm NO_2 in dry air at 150 ℃. The sensing response is dominated by surface adsorption-induced charge

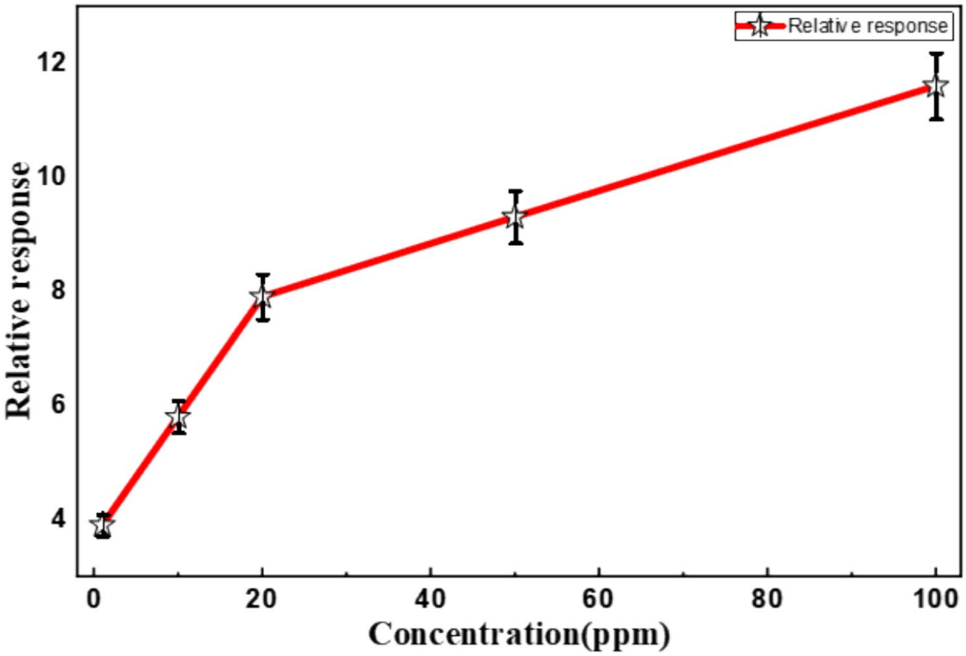

Fig. 8 Relative response of MoS_2 for NO_2 gas at different concentrations

transfer between NO_2 molecules and MoS_2, consistent with a surface-controlled chemiresistive mechanism. The sensor exhibited stable and repeatable responses over multiple consecutive sensing cycles, indicating reliable short-term operational stability under the tested conditions. The sensing response of MoS_2-based gas critically depends upon various factors such as the surface morphology, methods for the preparation of the film, concentration of sensing gas, and operating temperature.

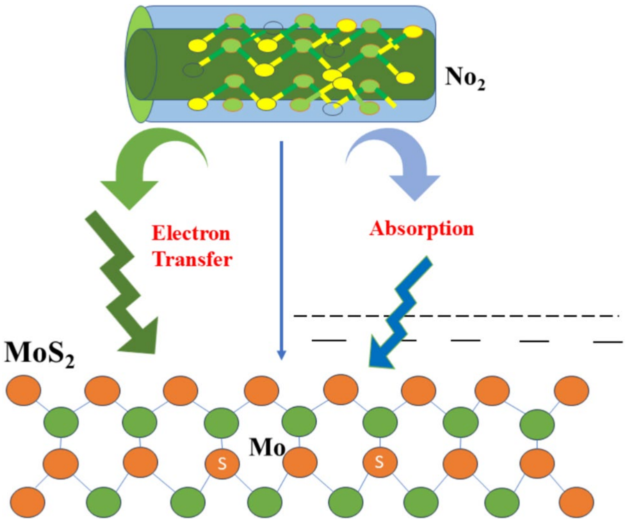

Fig. 9 Mechanism for the sensing of NO_2 gas with MoS_2

Acknowledgements

Ramesh Kumar is thankful to Delhi Technological University for providing resources and the Institute Research Fellowship for proper conduction of research.

Author contributions

Ramesh Kumar- Original manuscript writing, investigation, characterization, and synthesis. Jitendra Singh- Editing and drafting. Pawan K. Kulriya- Editing, Mahesh Kumar- Conceptualization, supervision, and validation. Vinod Singh- Resources, supervision, and validation.

Funding

The authors have not disclosed any funding.

Data availability

Data will be available on request.

Declarations

Conflict of interest The authors declare no competing interests.

References

1. S.J. McDonnell, R.M. Wallace, Atomically-thin layered films for device applications based upon 2D TMDC materials. Thin Solid Films **616**, 482–501 (2016)
2. S. Varghese, S. Varghese, S. Swaminathan, K. Singh, V. Mittal, Two-dimensional materials for sensing: graphene and beyond. Electronics **4**, 651–687 (2015)
3. A. Shokri, N. Salami, Gas sensor based on MoS_2 monolayer. Sens. Actuat. B Chem. **236**, 378–385 (2016)
4. A.A. Mane, A.V. Moholkar, Effect of solution concentration on physicochemical and NO_2 gas sensing properties of sprayed MoO_3 nanobelts. Thin Solid Films **648**, 50–61 (2018)
5. J. Guo, R. Wen, J. Zhai, Z.L. Wang, Enhanced NO_2 gas sensing of a single-layer MoS_2 by photogating and piezo-phototronic effects. Sci. Bull. **64**, 128–135 (2019)
6. W. Li, Y. Zhang, X. Long, J. Cao, X. Xin, X. Guan, J. Peng, X. Zheng, Gas sensors based on mechanically exfoliated MoS_2 nanosheets for room-temperature NO_2 detection. Sensors (Basel) **19**, 1–12 (2019)
7. R. Kumar, N. Goel, M. Kumar, UV-activated MoS_2 based fast and reversible NO_2 sensor at room temperature. ACS Sens. **2**, 1744–1752 (2017)
8. A. Kuc, T. Heine, A. Kis, Electronic properties of transition-metal dichalcogenides. MRS Bull. **40**, 577–584 (2015)
9. R. Sha, T.K. Bhattacharyya, Mos_2-based nanosensors in biomedical and environmental monitoring applications. Electrochim. Acta **349**, 136370 (2020)
10. J. Wang et al., Synthesis of MoS_2 and graphene composites as the anode materials for Li–ion batteries. Energy Technol. **6**(10), 1913–1920 (2018)
11. S. Palsaniya, H.B. Nemade, A.K. Dasmahapatra, Synthesis of polyaniline/graphene/MoS_2 nanocomposite for high performance supercapacitor electrode. Polymer **150**, 150–158 (2018)
12. L. Yu et al., Graphene/MoS_2 hybrid technology for large-scale two-dimensional electronics. Nano Lett. **14**(6), 3055–3063 (2014)
13. K. Roy et al., Graphene–MoS_2 hybrid structures for multifunctional photoresponsive memory devices. Nat. Nanotechnol. **8**(11), 826–830 (2013)
14. P. Dutta, G. Gupta, Environmental gas sensors based on electroactive hybrid organic–inorganic nanocomposites using nanostructured materials. Phys. Chem. Chem. Phys. **24**(47), 28680–28699 (2022)
15. M.E. Davila, L. Xian, S. Cahangirov, A. Rubio, G. LeLay, Germanene: anoveltwo-dimensionalgermanium allotrope akin to graphene and silicene. New J. Phys. **16**, 095002 (2014)
16. S. Kumar et al., A systematic review on 2D MoS_2 for nitrogen dioxide (NO_2) sensing at room temperature. Mater. Today Commun. **34**, 105045 (2023)
17. M. Donarelli, S. Prezioso, F. Perrozzi, F. Bisti, M. Nardone, L. Giancaterini, C. Cantalini, L. Ottaviano, Response to NO_2 exfoliated MoS_2 and other gases of resistive chemically -based gas sensors. Sens. Actuat. B Chem. **207**, 602–613 (2015)
18. B. Liu, L. Chen, G. Liu, A.N. Abbas, M. Fathi, C. Zhou, High-performance chemical sensing using schottky-contacted chemical vapor deposition grown monolayer MoS_2 transistors. ACS Nano **8**, 5304 (2014)
19. D.J. Late, Y.-K. Huang, B. Liu, J. Acharya, S.N. Shirodkar, J. Luo, A. Yan, D. Charles, U.V. Waghmare, V.P. Dravid, C.N.R. Rao, Sensing behavior of atomically thin-layered MoS_2 transistors. ACS Nano **7**, 4879–4891 (2013)
20. S.-Y. Cho, S.J. Kim, Y. Lee, J.-S. Kim, W.-B. Jung, H.-W. Yoo, J. Kim, H. Jung, Highly enhanced gas adsorption properties in vertically aligned MoS2. ACS Nano **9**, 9314 (2015)
21. T. Xu, Y. Pei, Y. Liu, D. Wu, Z. Shi, J. Xu, Y. Tian, X. Li, High-response NO gas sensor based on bilayer MoS_2 resistive grown by a new two-step chemical vapor deposition method. J. Alloys Compd. **725**, 253–259 (2017)
22. M.I. Rizu, D. Fadil, E. Llobet, UV-enhanced exfoliated MoS2/PtSe2 heterostructure for ultra-sensitive NO2 detection at room temperature. npj 2D Mater. Applicat. **9**(1), 28 (2025)
23. Q. Zhao, W. Zhou, M. Zhang, Y. Wang, Z. Duan, C. Tan, B. Liu et al., Edge-enriched Mo2TiC2Tx/MoS2 heterostructure with coupling interface for selective NO2 monitoring. Adv. Funct. Mater. **32**(39), 2203528 (2022)
24. X. Li, X. Wang, Z. Sun, F. Li, Y. Fu, K. Zhao, G. Zhao, C. Zhu, X. Xu, Surface free radicals activated CoP/MoS2 sensors through electrocatalytic water splitting for enhanced NO2 sensing at room temperatures. Chem. Eng. J. **495**, 153381 (2024)
25. P. Bharathi, S. Harish, G. Mathankumar, M.K. Mohan, J. Archana, S. Kamalakannan, M. Prakash, M. Shimomura, M. Navaneethan, Solution processed edge activated

Ni-MoS2 nanosheets for highly sensitive room temperature NO2 gas sensor applications. Appl. Surf. Sci. **600**, 154086 (2022)

Ramesh Kumar

(PhD – Applied Physics)
Nano fabrication lab (NFL), Department of Applied Physics, Delhi Technological University, IN-110042
Phone: +91-6375556848

E-mail: rameshkulariya1996@gmail.com
Google Scholar Link:
https://scholar.google.com/scholar?hl=en&as_sdt=0%2C5&q=ramesh+kumar+kulriya&oq=

Education

- **Ph.D. (Applied & Engineering Physics)** – Delhi Technological University, 2021 – 2026
  Thesis: **Development of 2D Molybdenum Disulfide Based NO$_2$ Gas Sensor**
- **M.Sc. in Physics (Materials Science)** –Saurashtra university, Rajkot 2018–2020 (68.45%)
- **B.Sc. in Physical Sciences** – Shekhawati PG college sikar, Rajasthan, 2015–2018 (59.85%)

Research Focus

- Development of advanced gas sensors with superior sensitivity and selectivity.
- Exploration of 2D nanomaterials (MoS$_2$) for tailored electronic properties.
- Integration of energy harvesting mechanisms for sustainable operation.
- Design of self-powered sensing systems through energy–sensor coupling.

Research Publications

[1] **Ramesh Kumar**, Jitendra Singh, Pawan K. Kulriya, Mahesh Kumar, Vinod Singh “Influence of Temperature and NO$_2$ Concentration on the Sensing Performance of Nanostructured MoS$_2$.” *Journal of Materials Science: Materials in Electronics* 37, no. 383 (2026).

[2] **Kumar, Ramesh**, Nitesh K. Chourasia, Pawan K. Kulriya, Mahesh Kumar, and Vinod Singh. "Investigation of MoS2-hydrogen interaction using in-situ X-ray diffraction studies." *Applied Physics A* 131, no. 1 (2025): 14.

[3] Chourasia, Nitesh K., Ankita Rawat, Ritesh Kumar Chourasia, Hemant Singh, **Ramesh Kumar Kulriya**, Vinod Singh, and Pawan Kumar Kulriya. "Unveiling the potential of Ti$_3$C$_2$T$_x$ MXene for gas sensing: recent developments and future perspectives." *Materials Advances* 4, no. 23 (2023): 5948-5973.

[4] Singh, Vinod, Pawan K. Kulriya, Ashok Kumar, **Ramesh Kumar**, Priya Pradeep Kumar, Umang Berwal, Jasveer Singh, Kailash Chandra, and Kedar Singh. "Hydrogen induced structural modifications in size selected Pd-Carbon core-shell NPs: Effect of carbon shell thickness, size and pressure." *International Journal of Hydrogen Energy* 47, no. 25 (2022): 12642-12652.

[5] Lehru, Rujuta, Jaydeep Radhanpura, **Ramesh Kumar**, Divyarajsinh Zala, V. S. Vadgama, Himanshu Dadhich, V. R. Rathod et al. "Studies on electrical properties of Fe doped ZnO nanostructured oxides synthesized by sol–gel method." *Solid State Communications* 336 (2021): 114415.

Teaching Experience

- **Teaching Assistant (2021–present), DTU –** Undergraduate & Postgraduate Labs:
- Physics Experimental Laboratory (2021–25)
- Condensed Matter Physics (M.Sc., 2024)
- Electronics & Microwave Experimental Labs (M.Sc., 2023–25)

- Engineering Physics Course (B.Tech, 2024)

Awards & Fellowships

- **Commendable Research Award** – DTU (2023)
- **Senior Research Fellowship (SRF)** – DTU (2023–2025)
- **Junior Research Fellowship (JRF)** – DTU (2021–2023)

Professional Activities & Service

- Organized invited talks and workshops at DTU (2023–2025)
- Ph.D. Coordinator, Applied Physics Department, DTU (2024)
- Represented DTU laboratories & documents handling during NBA accreditation visits

Technical Skills

- Data Analysis: Origin, MS Office, Excel
- Operating Systems: Linux, Windows

Conferences, Seminars, and Workshops

- **Ramesh Kumar**, Vinod Singh, Mahesh Kumar, "Synthesis and Characterization of MoS_2 Thin Films for Gas Sensing", International Conference on Advanced Functional Materials and Devices (AFMD-2025), at Department of Physics, ARSD College, University of Delhi 3th– 5th March 2025. (Oral Talk)

- **Ramesh Kumar**, Vinod Singh, Mahesh Kumar, "MoS_2 - hydrogen interaction using in-situ X-ray diffraction studies", International Conference on Atomic, Molecular, Material, Nano and Optical Physics with Applications (ICAMNOP-2023), Department of Applied Physics, Delhi Technological University, Delhi 20th – 22th Dec 2022. (POSTER)

- Attended a one-day national seminar on "National Science Day (NSD-2023)" held at Delhi Technological University, Delhi, India on 28th Feb 2023.

- Attended a one-day national seminar on "Implementation of NEP-2020 in Special Reference to Innovation and Entrepreneurship" organized by Department of Applied Physics at Delhi Technological University (DTU), Delhi on 24th Feb 2023.

- Attended a one-day national workshop on "Ascertaining a Skill Centre for Glass and Glazing (ASCGG-2023) (Bringing Industry and Academia Together)" organized by the Department of Applied Physics at Delhi Technological University (DTU), Delhi on 11thAug 2023.

- Participated in the "National Science Day (NSD-2023)" Quiz, organized by Human Resource Development Centre (HRDC) in association with Institution", Innovation Council (IIC) & Department of Applied Physics, held at Delhi Technological University, Delhi, India on 28th Feb 2023.

- Attended a one-day national seminar on “Recent Advancement in Semiconductor Devices and Materials (RASDM-2023)” organized by Department of Applied Physics at Delhi Technological University (DTU), Delhi on 30th Jan 2023.
- Attended a one-day national seminar on “Recent Trends in Applied Physics and Engineering (RTAPE-2020)” by Shanti Swarup Bhatnagar (SSB) Awardees at Delhi Technological University (DTU), Delhi on 10th Feb 2020.

References

- **Prof. Vinod Singh** – Professor ***(Ph.D. Advisor)***
  Department of Applied Physics, DTU, New Delhi, India (110042) | ✉ vinodsingh@dtu.ac.in
- **Prof. Pawan Kumar Kulriya**– Professor
  Department of School of physical science, JNU, New Delhi, India (110042) | ✉ pawaniuac@gmail.com